MOLECULAR MECHANISMS OF THERAPEUTIC RESISTANCE IN CANCER

by

Hanxiao Wang

A dissertation submitted in partial fulfillment
of the requirements for the degree of
Doctor of Philosophy
(Cellular and Molecular Biology)
in the University of Michigan
2015

Doctoral Committee:

Professor Alnawaz Rehemtulla, Chair
Professor Kathleen R Cho
Associate Professor Gary D Luker
Assistant Professor Marina Pasca Di Magliano
Professor Brian Dale Ross
Professor Yi Sun

DEDICATION

This thesis is dedicated to the memory of my father, who believed in me, supported me and loved me.

ACKNOWLEDGEMENTS

This thesis work would not have been possible without the combined efforts of many talented individuals. First, my mentor, Dr. Alnawaz Rehemtulla deserves much credit for guiding me through my thesis research. He provided me the right amount of guidance and freedom to solve scientific problems and learn how to think like a scientist. It will be a great fortune for me forever.

I am grateful to all the members of my dissertation committee: Dr. Kathleen Cho, Dr. Gary Luker, Dr. Marina Pasca Di Magliano, Dr. Brian Ross and Dr. Yi Sun. Their thoughtful and constructive suggestions deepened my understanding of science and helped me avoid many potential detours in research. I would like to thank Dr. Ross and Dr. Cho. Dr. Ross provided great help on all the imaging studies, which were integral in my research. Dr. Cho's expertise in ovarian cancer helped me complete my very first scientific paper. It was an enjoyable and fruitful collaboration.

I want to thank Dr. Stefanie Galban. She has been a great mentor from the first day I joined the lab. My first project would not have gone so smooth without her day-to-day help. I also want to thank Dr. Brittany Bowman. She is such a kind-hearted person and great companion throughout my graduate school. I am very lucky to know them and became friends with them.

I would like to acknowledge all the members in Center for Molecular Imaging (CMI), especially Kevin Heist, Carlos Espinoza and Mallika Kumar. They helped me image, treat, implant countless animals, which made the research as solid as it is now. I also would like to thank CMI administer, Tania Cunningham, who keep the lab well organized. Most importantly, her enthusiasm always brings positive energy to the lab and cheers me up.

I thank all my collaborators. Dr. Rong Wu helped me complete the 2nd chapter of this thesis. Wajd Al-Holou dedicated numerous hours to the 3rd chapter of this thesis. Dr. Roeland Verhaak, Dr. Hoon Kim and Kathy Hu from MD Anderson Cancer Center provided insightful suggestions on the bioinformatics analysis. Dr. Tom Mikkelsen and Dr. Ana C. deCarvalho from Henry Ford hospital supplied precious materials for the 3rd chapter of the thesis.

Many undergraduate students also contributed greatly to this thesis, including Amanda Witte, Katrin Vetter, Michael Lafferty and Parker Latshaw. They make me feel old but they have been great help for my research. They spent hours genotyping and imaging animals, as well as making buffers, which probably is only thing I hate doing in the lab. I appreciate all their efforts and wish them a bright future.

I would like to extend my appreciation to my home department, Cellular and Molecular Biology program. It was an educational and inspiring environment with many talented scientists and young trainees. I am very lucky and proud to be CMB alumni.

Last but not the least, I am sincerely gracious for the support from my families. They might not quite understand signaling pathways or molecular imaging but they are always very proud of their little girl. This makes the support even more precious. I would like to especially thank my fiancée, Sanjeev Kumar. His true grit encourages me to reach out for my goals. His emotional support lifted my spirits during the hardest time of my life over the past two years.

No words are adequate to express my appreciation to everyone who teaches me, helps me, supports me and loves me. I feel truly grateful for where I am now.

TABLE OF CONTENTS

LIST OF FIGURES

ABSTRACT

Molecular mechanisms of therapeutic resistance in cancer

Development of therapeutic resistance limits the efficacy of current cancer treatment. Understanding the molecular basis for therapeutic resistance should facilitate the identification of actionable targets and development of new combination therapies for cancer patients. Yet the understanding of therapeutic resistance still remains incomplete. In this thesis, clinically relevant mouse models coupled with systematic genomic and imaging technologies are used to identify mechanisms driving resistance, which also formulate novel therapeutic paradigms for patients with drug-resistant tumors.

In the first study, a genetically engineered mouse model of ovarian endometrioid adenocarcinoma (OEA) was utilized in combination with molecular imaging to understand mechanisms of chemoresistance in OEA. It was demonstrated that AKT signaling pathway was activated upon chemotherapy (cisplatin) administration, which protected cells from apoptosis and thereby leading to the development of resistance. In support of this observation, inhibition of AKT activity improved the efficacy of chemotherapy by enhanced induction of apoptosis.

A second study was undertaken to develop a new understanding of the mechanistic basis for therapeutic resistance in glioblastoma using a patient derived xenograft model. An integrated transcriptome analysis revealed that chemoradioresistance was associated with an increased expression of genes involved in the mesenchymal and stem cell phenotype as well as a decreased expression of genes involved in cell death. TGF-β signaling was identified to be central to each of the mesenchymal/stem phenotype and therefore a critical

player in modulating therapeutic resistance. In support, treatment with a TGF-β inhibitor partially restored the sensitivity to therapy in TMZ/IR resistant tumors.

Overall, this thesis demonstrated the importance of the AKT and TGF-β signaling pathways in therapeutic resistance in a subset of ovarian cancer and glioblastoma patients, which provides clinical guidance for applying new combination therapies. It also demonstrates the concept that the combination of clinically relevant mouse models, molecular imaging and systematic genomic analysis can be used to derive novel insights into the dynamic signaling processes involved with gain of resistance. Future studies are needed to investigate if targeting these resistance mechanisms delays or prevents the development of resistance in treatment-naïve patients.

CHAPTER I

Introduction

1.1 Therapeutic resistance in cancer

1.1.1 Overview

Cancer is the second leading cause of death in the United States. It is estimated that 1,665,540 new cancer cases will be diagnosed and 585,720 patients will succumb to cancer in 2014 [1]. Besides surgery, chemotherapy and radiotherapy are the most common treatment options across different types of cancer [2]. They can be used singularly or in combination with other treatments such as hormone therapy. The benefits of chemotherapy and radiotherapy include: 1) killing cancer cells at the primary sites or metastasizing sites (e.g. lymphoma& breast cancer) [3, 4]; 2) preparing patients for surgery (e.g. esophageal cancer) [5]; 3) shrinking tumor sizes to relive patients from pain caused by cancer (e.g. bone metastasis) [6].

While chemotherapy and/or radiotherapy remain as the major standard of care for cancer patients, the response to treatment varies substantially in different types of cancer, or even among patients with the same type of cancer. For example, chemotherapy is extremely successful in childhood acute lymphocytic leukemia (ALL) treatment [2], where over 95% of the patients attain remission and 91.7% of them survive over 5 years [7]. On the contrary, despite intensive combinatorial treatment of chemotherapy and radiotherapy, most glioblastoma patients suffer from tumor recurrence, where the median time to tumor progression is only about 6.9 months and the 5-year-survival rate is less than 10% [8]. In the case of triple negative breast cancer (negative for

estrogen receptors, progesterone receptors, and HER2), the pathologic complete response rates to neoadjuvant chemotherapy vary from 50% to 0% in basal-like 1 subtype and basal-like 2 subtype, respectively [9, 10]. The variations in treatment response suggest that intrinsic or acquired therapeutic resistance exists in a subset of cancer patients, which leads to treatment failures, disease progression, and eventually mortality. This pervasive barrier confounds the ultimate goal of curing or managing cancer in long term.

The increasing knowledge of key driver genes in cancer has accelerated the development of novel targeted therapeutic agents over the past few decades. Many targeted therapies, including small molecule inhibitors and monoclonal antibodies, have been developed to target essential pathways in tumorigenesis and maintenance. This new category of therapy has demonstrated superior efficacy in eliminating cancer cells while sparing normal cells, thus resulting in less toxicity. A successful representative of targeted therapies is the anti-HER2 antibody (Trastuzumab®). Human epidermal growth factor receptor 2 (HER2) is a crucial oncogenic pathway in breast cancer. HER2 is overexpressed in 15-20% invasive breast cancer, and is associated with worse outcomes in patients. Laboratory experiments proved that aberrant HER2 signaling pathway is oncogenic and necessary for cancer cell survival, which formulated the strategy of anti-HER2 therapy. Trastuzumab® is a humanized monoclonal antibody, which can bind to HER2 receptor and block HER2 signaling pathway [11]. Trastuzumab® in combination with chemotherapy has been shown to reduce the rate of tumor recurrence by half as well as decrease the mortality rate by a third among patients with HER2 positive breast cancer [12]. Additionally, Trastuzumab® does not show significant effect in HER2 negative patients, demonstrating the specificity of this therapy.

This particularly triumphal case demonstrates the power of targeted therapy. Similarly, identifying key regulatory pathways in therapeutic resistance will

likely inform rationally-designed targeted therapies that overcome this problem in cancer patients. Yet the knowledge of therapeutic resistance still remains highly incomplete. The primary objective of this thesis is to elucidate the mechanisms of therapeutic resistance in ovarian cancer and glioblastoma, where therapeutic resistance contributes significantly to poor prognosis. Clinically relevant mouse models coupled with systematic genomic and imaging technologies will be used to identify key regulatory pathways in therapeutic resistance and plausible therapeutic avenue to intercept them. This knowledge can be leveraged to facilitate the development of salvaging therapeutic modules for future cancer patients.

1.1.2 Chemoresistance in ovarian cancer

Ovarian cancer is a leading cause of cancer death among American women [1]. Currently, surgery and chemotherapy are the standard of care for ovarian cancer patients. Despite an initial response to chemotherapy, patients tend to develop chemoresistance over time, which leads to poor prognosis [13]. Understanding the molecular basis of chemoresistance will aid in identification of new targets for ovarian cancer treatment, which will eventually improve patient outcomes.

Platinum-based agents form the first-line chemotherapy for ovarian cancer patients. The molecular actions of these agents involve hydrolysis, drug transportation, formation of intra-/inter-strand crosslinks of DNA, and activation of apoptosis cascade if DNA damage is left unrepaired [14]. Alterations in any of these steps could lead to chemoresistance (Figure 1.1). Moreover, remodeling of the tumor microenvironment and tumor heterogeneity can further decrease chemosensitivity in cancer cells. In fact, numerous studies have explored each possibility and demonstrated their association with chemoresistance in ovarian cancer (reviewed in [15-17]). The following section will highlight some recent studies on chemoresistance in ovarian cancer with a

focus on novel regulatory mechanisms and clinical trials.

DNA damage repair proficiency is a determinant for sensitivity to platinum-based agents [16] (Figure 1.2). Poly (ADP-ribose) polymerase (PARP) is a key player in repairing DNA single strand break (SSB). Inhibiting PARP may result in accumulation of SSB, and DSB subsequently. Phase-II clinical trials showed that a PARP inhibitor improved the outcomes of recurrent ovarian cancer patients as a single agent, including those who are resistant to platinum therapy [18, 19].

Ovarian cancer stem cells were first documented in 2005. Since then, many studies have provided evidence of the existence and importance of this unique population in ovarian cancer [20-23]. Yet, the hunt for effective targets against ovarian cancer stem cells is still ongoing [24]. A recent study showed that the Notch signaling pathway is critical for regulation of cancer stem cells and resistance to platinum-based therapy in ovarian cancer. Combination of a Notch pathway inhibitor and cisplatin showed superior efficacy in inducing DNA damage, arresting cell cycle, enhancing apoptosis, reducing tumor burden, and finally prolonging survival in tumor bearing mice [25]. As Notch inhibitors are currently being evaluated in early clinical trials [26], this study may provide a rationale for testing the combination of Notch inhibitors and chemotherapy in chemoresistant ovarian cancer patients.

Ovarian cancer microenvironment contributes to tumor growth, angiogenesis, dissemination, and chemoresistance (reviewed in [27]). One of the critical factors in ovarian cancer microenvironment is vascular endothelial growth factor (VEGF), which is a key regulator of angiogenesis and is associated with poor prognosis, and chemoresistance [28-30]. Bevacizumab, a monoclonal antibody against VEGF, has been tested in platinum-resistant recurrent ovarian cancer as an adjuvant therapy with chemotherapy in a phase III clinical

trial. The combination therapy prolonged tumor progression free time even though it has not shown significant benefits in overall survival [31].

Previous research on chemoresistance in ovarian cancer has generated insights pertaining to DNA damage response, cancer stem cells, and tumor microenvironment. At the same time, limited clinical improvement indicates that this early work is still incomplete. One major drawback is that early resistance research often did not fully account for the spectrum of heterogeneity in ovarian cancer. Clinical and molecular findings suggest that ovarian cancer represents a group of heterogeneous neoplasms [32]. Currently there are no differences in treatment strategies among various types of ovarian cancer, however it is becoming evident that the inherent variances of ovarian cancer influence treatment efficacy and development of therapeutic resistance [33].

Epithelial tumors account for approximately 90% of primary malignant ovarian cancer. Historically, epithelial ovarian cancer is classified into four major subtypes based on cell type, which include serous, endometrioid, clear cell, and mucinous subtypes [34]. Next generation sequencing revealed that both high-grade serous ovarian carcinoma (HGS-OvCa) and endometriod carcinoma can be further divided into various groups according to gene expression profiles [35, 36]. Yet the genetic drivers and corresponding biological features have not been well characterized in these subgroups.

Previous molecular data suggests that the four major subtypes have distinct genetic alterations. For example, K-RAS gene mutations are found in about 85% mucinous ovarian adenocarcinomas, but are much less frequently observed in other subtypes of ovarian carcinoma [37-39]. The canonical Wnt signaling pathway is shown to be deregulated in 16%–38% of human ovarian endometrioid adenocarcinomas (OEAs) while inactivating mutations of the tumor suppressor gene PTEN have been reported in 14%–21% of OEAs, but

are rare in the other types of ovarian carcinomas. More interestingly, Cho *et al.* showed that the defects in Wnt and PTEN signaling often occur concomitantly in a subset of OEA patients. By inactivating *Apc* and *Pten* in ovarian surface epithelium in a murine model, Cho *et al.* successfully recapitulated the histological features and gene expression profiles of human OEAs [40]. This mouse model of OEA provides a preclinical platform to study the biology of OEA as well as evaluate efficacies of new therapeutic paradigms [41]. Meanwhile, Chemoresistance mechanisms has not been investigated in OEA specifically. This model provides a platform to understand chemoresistance mechanisms in OEA and developing new therapeutic modules specifically for OEA patients.

1.1.3 Chemoradioresistance in glioblastoma

Glioblastoma (GBM) is the most aggressive and lethal brain tumor in adults. The median survival time of GBM patients is only about 15 months in the presence of surgery, chemotherapy and radiotherapy treatment. The majority patients suffer from tumor recurrence, which is the primary cause of death [8]. Yet, no effective therapies have been discovered for patients with recurrent tumors so far.

Temozolomide (TMZ) is a widely used chemotherapy for glioblastoma treatment. It primarily mediates methylation of DNA at O^6-guanine, which causes mismatch during DNA replication, resulting in DNA double strand break and subsequent apoptosis [42]. The O^6-methyguanine-DNA methyltransferase (MGMT) is a suicide enzyme that can remove methyl-groups at O^6-guanine sites and thus counteracts the lethal effect of TMZ. Elevated MGMT expression has been demonstrated to mediate resistance to TMZ [43]. Meanwhile, as DNA methylation plays an important role in regulating MGMT expression, the methylation status of MGMT promoter has been established as a critical prognostic factor for glioblastoma patients [8, 44]. However, many

studies, including *in vitro*, *in vivo*, and clinical studies have shown that the methylation status of MGMT promoter or MGMT expression does not always correspond with TMZ sensitivity, suggesting that MGMT might not be the only mechanism of therapeutic resistance in GBM [45-48].

Numerous efforts have been invested to determine key regulators of therapeutic resistance in GBM. Yet heterogeneity, one hallmark of GBM, might have been underappreciated in previous studies. First, different populations of cancer cells exist in the same tumor [49-51], which might be responsible for partial or no response for single targeted agent treatment. Brain tumor stem cells are among the firstly identified cancer stem cells in solid tumors [52, 53]. A recent study demonstrated that TMZ eliminated proliferating tumor cells but a quiescent population remained after treatment, which led to tumor recurrence. It shows that the therapeutic resistant clones exist before treatment, which can survive treatment and eventually regenerate tumor mass [54]. Further studies are needed to characterize this specific population and identify potential therapeutic targets. Secondly, genomic profiling has demonstrated that subtypes with distinguished genomic alterations exist in GBM, which would result in differences in treatment response. For example, patients with the mesenchymal subtype have worse outcomes compared to patients in other groups, suggesting that patients with the mesenchymal subtype are likely to be chemoradioresistant [55]. Yet, few studies have investigated therapeutic resistance in a subtype specific manner.

The goal of the second part of this thesis is to depict a comprehensive picture of the molecular events leading to therapeutic resistance in a mouse model representing the heterogeneous disease. This knowledge will further guide research to pinpoint the master regulatory pathways and the subsequent development of targeted therapies for individual GBM patients.

1.2 Experimental approaches to study therapeutic resistance

1.2.1 Studies of therapeutic resistance in mouse models

As discussed earlier, one type of cancer can be further grouped into multiple genetically and morphologically distinctive groups, which has been proven in ovarian cancer as well as glioblastoma [56]. Moreover, patient outcomes and treatment response are associated with cancer subtypes, suggesting that the genetic signatures in each subtype influence the response to treatment. Therefore, individual genetic variances should be taken into account to fully understand mechanisms of therapeutic resistance.

In order to address this challenge, a clinically relevant model system is required to recapitulate the heterogeneity of cancer. Mice are excellent models in cancer research for multiple reasons [57]. Over 95% of the mouse genome is similar to human genome and mice have similar metabolism system to human, which makes the research highly translatable. Mice provide tumor microenvironment that cannot be recapitulated *in vitro*, such as angiogenesis and immune response. Finally, mice have several traits that make them efficient tools for experimental studies, such as a short reproduction cycle, accelerated life span and small body sizes.

Studies described in this thesis primarily utilized two types of cancer mouse models: genetically engineered mouse models and patient derived xenograft models. The advantages of each model, especially those related to therapeutic resistance research, are described below.

Genetically engineered mouse models (GEMMs)

GEMMs refer to mice with induced mutations, including transgenes, localized knockouts or knockins, or retroviral-, proviral- or chemical-induced mutations. GEMMs allow scientists to study the functions of specific genes as well as evaluate targeted therapeutic agents and treatment schedules. Various

GEMMs with alterations in oncogenes or tumor suppressors have been generated, which faithfully recapitulate human cancer genetically and pathologically [58]. With advanced technology, such as CRISPR/Cas-mediated genome engineering, it is becoming less time-consuming and technically challenging to generate GEMMs with multiple genetic manipulations, which overall makes GEMMs more appealing for cancer research [59].

GEMMs have multiple advantages compared to other mouse model systems. Firstly, most implanted cells/tumor specimens in xenograft models are from tumor masses at a detectable level, which usually happens much later after tumor initiation. GEMMs mimic the evolution of tumors from initiation to advanced stages, which provide the opportunity to study drug response at different stages of cancer progression. Secondly, GEMMs have uniform genetic background, which enable scientists to study one or more specific pathways simultaneously and thus eliminate interference from other potential genetic alterations. Inducible manipulation of oncogenes and tumor suppressor genes also allows scientists to differentiate molecular functions in tumor initiation and maintenance in cancer [60]. Lastly, GEMMs have fully functional immune systems and therefore can mirror tumor microenvironment, which plays a critical role in therapeutic response.

Patient derived xenograft (PDX) model

PDX models are renewable tumor models generated from tumor specimen of cancer patients. Tumor specimen (usually from surgery or biopsy) can be engrafted and propagated in immunodeficient mice directly. It can also be cultured briefly *in vitro* and then implanted into immunodeficient mice (Figure 1.3) [61]. PDX models have been established for a variety of cancers, including pancreatic cancer [62], prostate cancer [63], ovarian cancer [64], and glioblastoma [65, 66].

In comparison to traditional cell line derived xenograft models, PDX models retain the genomic alterations of primary tumors faithfully, which can be utilized to establish banks of PDX mice with different genetic background within the same type of cancer. This system closely resembles the heterogeneity in cancer patients and allows scientists to study evolution of therapeutic resistance in individual patient. Moreover, new therapies can be evaluated in PDX mice to determine the most effective treatment options. This personalized pre-clinical trial will ideally speed up the process of clinical trials [67].

Overall, GEMMs and PDX models represent state-of-the-art mouse models in cancer research, and provide clinically relevant platforms to investigate mechanisms of therapeutic resistance.

1.2.2 Genomic and molecular studies of therapeutic resistance

There are two overarching themes in therapeutic resistance research: 1) candidate driven research, where one gene or pathway is proposed to regulate therapeutic resistance and the hypothesis is tested experimentally; 2) unbiased studies, where large-scale genomic, transcriptomics, proteomic, or kinomic information is collected and analyzed to identify new mechanisms of therapeutic resistance [68].

This thesis explores both research themes. The PI3K/AKT signaling pathway is a critical oncogenic pathway in various types of cancer. It also has been shown to mediate chemoresistance in ovarian cancer cells by promoting cell survival, or escaping apoptosis [14]. However, the role of PI3K/AKT in chemoresistance has not been studied in OEA. By using molecular imaging tools, the role of AKT activity was evaluated in a clinically relevant mouse model of OEA in the first part of this thesis. In the second part of the thesis, an unbiased transcriptomic analysis was used to identify novel regulatory mechanisms of chemoradioresistance in glioblastoma. It has been demonstrated that cancer cells continuously divide, grow, invade, metastasize,

and avoid cell death through coordinated actions of oncogenes and tumor suppressor genes [69]. It is conceivable that tumor cells might survive treatment via multiple sophisticated therapeutic resistance pathways. This systematic analysis will shed lights to our understanding of key signaling networks and nodules for therapeutic resistance. Meanwhile, the role of key signaling pathways will be further pursued to validate their involvement in therapeutic resistance.

In order to pursue candidate-driven research and systematic genomic research, two major experimental tools, including molecular imaging and RNA sequencing, were used in this thesis research.

Molecular imaging

Molecular imaging provides a platform to monitor treatment response accurately and noninvasively in live animals. It exploits specific molecular probes as well as intrinsic tissue characteristics as a source of imaging contrast, which can be used to characterize and quantify biological processes [70]. Molecular imaging modalities include optical imaging (bioluminescence imaging (BLI) and fluorescence imaging), magnetic resonance imaging (MRI), ultrasound imaging, positron emission tomography (PET), single-photon emission computerized tomography (SPECT), and computed tomography (CT) [71]. It possesses several advantages over conventional biochemical assays, especially for research in animal models. Molecular imaging can be performed repetitively, non-invasively, and in a relatively short time in the same living animal. Therefore, it can reduce the number of animals required for research, which reduces cost while retaining the statistical power for longitudinal studies. Furthermore, molecular imaging can provide detailed spatial and temporal information of biological events in living animals, which sometimes is overlooked in studies with end-point assays. Lastly, some imaging techniques are clinically transferable, which can facilitate discovery and validation of new

imaging surrogates for diagnosis or treatment response. For example, apparent diffusion co-efficiency (ADC), a parameter that measures water diffusion rates via diffusion-weighted MRI, has been used as a surrogate for treatment response in both pre-clinical animal models and clinical settings [72, 73].

The two major imaging modules used in this thesis are BLI and MRI. BLI is based on the luciferin-luciferase enzymatic reaction, where visible light (bioluminescence) is generated as a by-product. The signal-to-noise ratio of BLI is excellent, thus generating high imaging sensitivity both *in vitro* and *in vivo*. As a part of the system, the luciferase gene is usually induced into cells or animals by transient transfection, virus-mediated transduction or genetic manipulation (e.g. homologous recombination). Luciferin can be delivered directly into cell culture or via injection in animals.

The luciferin-luciferase system has been utilized to reveal cell mobility, gene expression patterns and biological activities in live cells or animals. For example, since the luciferase gene can be propagated during cell proliferation, the intensity and locations of bioluminescence signals correlate with the number of cells and their spatial distributions, which can be utilized to quantify tumor burden and metastasis. In a recent study, a transgenic mouse model of lung cancer was used to evaluate the role of IKK2 and NF-κB in lung cancer development. The mouse model contains alleles of mutated KRAS oncogene and luciferase gene, which is activated in a tissue specific manner by cre-mediated recombination. The orthotropic tumor burden was measured by BLI repeatedly upon IKK2 inhibitor treatment, which generated a longitudinal treatment response profile [74]. Another study investigated the role of CXCR7 in regulating CXCR4+ cells metastasis by BLI. Tumor cells were labeled with luciferase gene and then implanted orthotopically. The bioluminescence intensity at various organ locations were monitored and used as an indication of metastasis capability [75].

Besides the direct fusion of luciferase, split luciferase complementation has been used to monitor various biological activities. A luciferase gene is split into two complement components and the physical proximity between the two parts determines reconstitution of luciferase activity. This versatile technique is used to measure apoptosis, kinase activities, and protein-protein interactions. For example, an apoptosis reporter was developed with split luciferase components linked by a DEVD sequence, which can be recognized by activated caspase-3. Upon activation of apoptosis, the DEVD sequence is cleaved, thus allowing reconstitution of the luciferase activity [76]. Since apoptosis is a key parameter to measure treatment efficacy, this reporter has been adapted in high-throughput pro-apoptotic compound screening in cell culture as well as optimization of therapeutic treatment in live animals [77-79]. To monitor AKT kinase activity, the split subunits of luciferase are linked by an AKT substrate peptide and a phospho-specific binding peptide, where the two parts of luciferase only reconstitute enzyme activity in the absence of AKT activation [80]. Similar kinase reporters also include a smad2/TGF-β reporter, a cMET reporter, an EGFR reporter and an ATM reporter [81-84]. Lastly, split luciferase complementation allows detection of protein-protein interactions. For example, a beetle red luciferase complementation reporter was recently developed by Luker *et al.*. This reporter measures CXCL12-dependent activation of CXCR4 both in cell culture and in live animals. More specifically, split luciferase fragments were fused to CXCL12 and β-arrestin 2 separately. Luciferase activity was determined by the interaction between CXCL12 and β-arrestin 2, which corresponded to CXCL12 signaling activity [85].

MRI is another major imaging modality used in this thesis. Unlike BLI, MRI does not require introduction of exogenous genes to create detectable contrast. It is based on the signals emitted by excited hydrogen atoms that are present in any tissue containing water molecules. The differences in water content among different tissues generate the contrast signals, which can be collected

and reconstructed into 3D images. To improve image quality, contrast agents, such as gadolinium, may be used. MRI serves a wide range of purposes in pre-clinical research. The most basic application of MRI is to generate 3D image atlases, which can be used to detect tumor locations, monitor tumor volumes, and characterize histology features. MRI can also track cells noninvasively with iron oxide- and 19F-based probes, which are used to monitor therapeutic delivery and immune response [86]. Some other advanced MRI techniques are developed to broaden MRI applications and improve cancer management clinically. For example, diffusion weighted MRI, which was mentioned earlier, has been applied in multiple areas, including tumor characterization, tumor grading, prognosis prediction, and treatment monitoring [87].

RNA sequencing

To identify the molecular basis underlying therapeutic resistance, a comprehensive approach is required to identify the genome-wide alterations responsible for therapeutic resistance. One such approach is RNA sequencing, which can reveal genome-wide gene expression patterns. RNA sequencing is derived from next generation sequencing (NGS); NGS technology deciphers DNA sequence by identifying fluorescence signals emitted from nucleotides that is incorporated into the DNA strand during double strand synthesis. This process is extended to billions of short DNA strands in parallel. In the case of RNA sequencing, RNA is first extracted from tissues or cells and then converted to cDNA by reverse transcription. Once cDNA is synthesized, it can be further fragmented into ideal sizes for NGS. Millions of short reads are obtained and assembled into transcriptome either by aligning reads to a reference genome or by *de novo* assembling without the genomic references [88]. High-throughput sequencing technology has drastically revolutionized the way scientists acquire genetic information [89].

Compared to microarrays, a commonly used hybridization-based approach for transcriptome quantifications, RNA sequencing possesses several advantages. First, no previous knowledge of candidates' genome is required. Microarrays rely on existing knowledge of gene sequences for probe design while RNA sequencing detects RNA from *de novo* sequencing, which allows detection of new RNA species or genomic events. For example, RNA sequencing identified novel recurrent transcript fusions in glioma, which revealed a new aspect of genomic alterations upon treatment [90]. Secondly, microarrays have limited sensitivity and require large amount of RNA materials whereas RNA sequencing has a much larger dynamic range and only needs a tiny amount of starting materials [91]. Currently, RNA sequencing can be adapted to single cell resolution, which has been utilized to configure the evolution map during tumorigenesis as well as development of therapeutic resistance [49, 92].

RNA sequencing has revealed multiple new insights into cancer biology since its debut. It allows detection of transcript fusions, splicing events as well as new RNA species, including long non-coding RNA (lncRNA) [90, 93, 94]. It can also map differentially expressed genes in two or more sample sets, identify prognostic or predictive gene signatures associated with outcomes, and pinpoint new regulatory pathways. For example, RNA sequencing of neuroendocrine prostate cancer (NEPC) and prostate adenocarcinoma (PCA) samples found that AURKA and MYCN genes are overexpressed in about 40% NEPC. Moreover, NEPC showed high sensitivity to Aurora kinase inhibitor, indicating that AURKA might be a potential target in at least a subset of NEPC [95].

Overall, both candidate-driven and discovery-oriented research are capable of informing new knowledge of therapeutic resistance. This thesis combines both research types via molecular imaging and RNA sequencing, which provides new insights into therapeutic resistance in ovarian cancer and glioblastoma.

1.3 Conclusion

Therapeutic resistance leads to treatment failures and mortality in patients. Yet the resistance mechanisms still remains incomplete. This thesis aims to decipher mechanisms of therapeutic resistance by using molecular imaging and high throughput sequencing technologies in clinically relevant mouse models. Actionable targets will be identified and evaluated in conjunction with the standard of care, which will provide a rationale for further investigation of such treatment regimens in clinical trials.

Figure 1.1

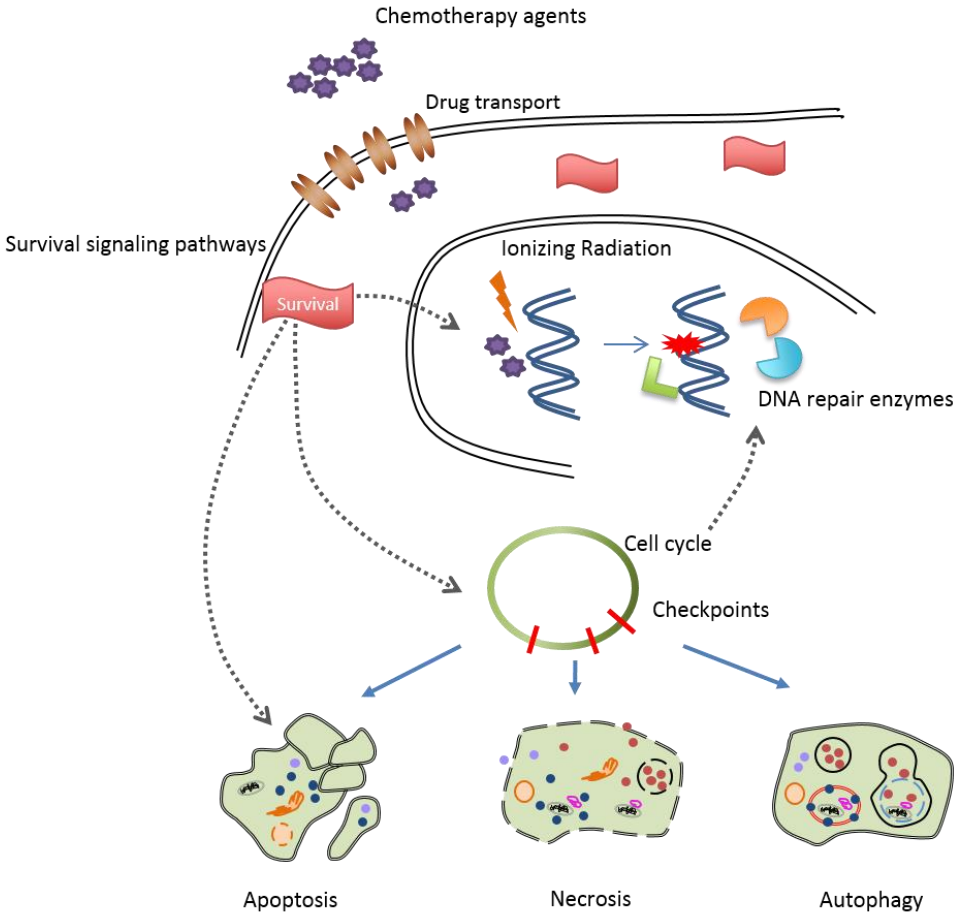

Figure 1.1 Mechanisms of action of chemotherapy and radiotherapy. Both chemotherapy and radiotherapy cause direct or indirect DNA damage, which triggers cell cycle arrest. DNA repair machinery attempts to repair the damage and allows cells to proceed into mitosis. If it fails to do so, cells will eventually undergo cell death, which could be apoptosis, necrosis, or autophagy. Cell survival signaling pathways influence the efficacy of chemotherapy and radiotherapy by regulating DNA repair pathways, cell cycle and cell death. Intracellular concentration of chemotherapeutic agents is regulated by membrane drug transporters.

Figure 1.2

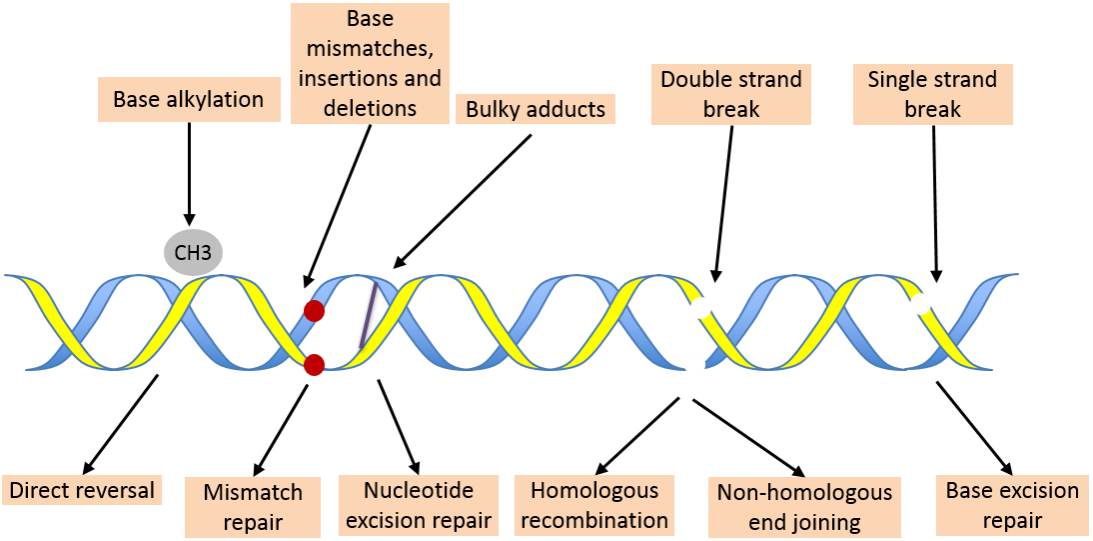

Figure 1.2 Overview of DNA damage and DNA repair mechanisms. Chemotherapy and radiotherapy induce various types of DNA damage, including base alkylation, base mismatches, base insertions, base deletions, bulky adducts, double strand breaks and single strand breaks. The major DNA repair pathways are direct reversal, base excision repair, nucleotide excision repair, mismatch repair, non-homologous end joining and homologous recombination.

Figure 1.3

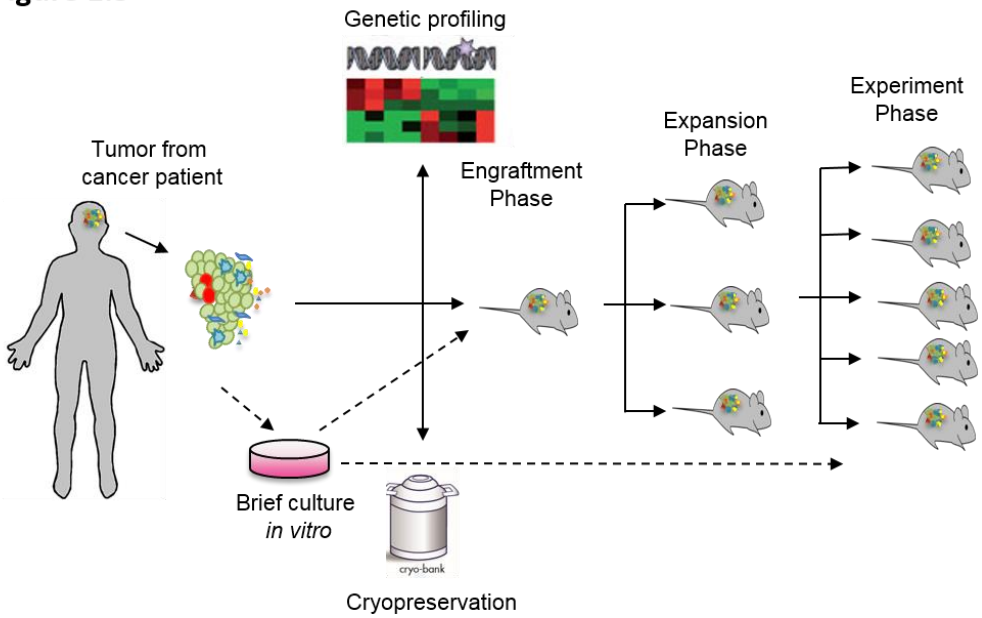

Figure 1.3 Schematic of patient derived xenograft models. Tumor specimens are collected from surgery or biopsy procedures in cancer patients. Tumor cells can be either engrafted and propagated in immunocompromised mice directly or cultured briefly *in vitro* and then implanted into mice. Ideally, genomic analysis and cryopreservation will be conducted before engraftment.

1.4 References

1. American Cancer Society, *Cancer facts & figures 2014.*
2. DeSantis, C.E., et al., *Cancer Treatment and Survivorship Statistics, 2014.* Ca-a Cancer Journal for Clinicians, 2014. **64**(4): p. 252-271.
3. Wilson, W.H., *Treatment strategies for aggressive lymphomas: what works?* Hematology-American Society of Hematology Education Program, 2013: p. 584-590.
4. Langlands, F.E., et al., *Breast cancer subtypes: response to radiotherapy and potential radiosensitisation.* British Journal of Radiology, 2013. **86**(1023).
5. Kato, H. and M. Nakajima, *Treatments for esophageal cancer: a review.* Gen Thorac Cardiovasc Surg, 2013. **61**(6): p. 330-5.
6. Vakaet, L.A. and T. Boterberg, *Pain control by ionizing radiation of bone metastasis.* Int J Dev Biol, 2004. **48**(5-6): p. 599-606.
7. Inaba, H., M. Greaves, and C.G. Mullighan, *Acute lymphoblastic leukaemia.* Lancet, 2013. **381**(9881): p. 1943-55.
8. Stupp, R., et al., *Effects of radiotherapy with concomitant and adjuvant temozolomide versus radiotherapy alone on survival in glioblastoma in a randomised phase III study: 5-year analysis of the EORTC-NCIC trial.* Lancet Oncol, 2009. **10**(5): p. 459-66.
9. Lehmann, B.D., et al., *Identification of human triple-negative breast cancer subtypes and preclinical models for selection of targeted therapies.* Journal of Clinical Investigation, 2011. **121**(7): p. 2750-2767.
10. Masuda, H., et al., *Differential Response to Neoadjuvant Chemotherapy Among 7 Triple-Negative Breast Cancer Molecular Subtypes.* Clinical Cancer Research, 2013. **19**(19): p. 5533-5540.
11. Burstein, H.J., *The distinctive nature of HER2-positive breast cancers.* New England Journal of Medicine, 2005. **353**(16): p. 1652-1654.
12. Romond, E.H., et al., *Trastuzumab plus adjuvant chemotherapy for operable HER2-positive breast cancer.* New England Journal of Medicine, 2005. **353**(16): p. 1673-1684.
13. Agarwal, R. and S.B. Kaye, *Ovarian cancer: Strategies for overcoming resistance to chemotherapy.* Nature Reviews Cancer, 2003. **3**(7): p. 502-516.
14. Siddik, Z.H., *Cisplatin: mode of cytotoxic action and molecular basis of resistance.* Oncogene, 2003. **22**(47): p. 7265-7279.
15. Chien, J., et al., *Platinum-sensitive recurrence in ovarian cancer: the role of tumor microenvironment.* Front Oncol, 2013. **3**: p. 251.
16. Galluzzi, L., et al., *Molecular mechanisms of cisplatin resistance.* Oncogene, 2012. **31**(15): p. 1869-1883.
17. Zhan, Q.L., C.M. Wang, and S. Ngai, *Ovarian Cancer Stem Cells: A New Target for Cancer Therapy.* Biomed Research International, 2013.

18. Gelmon, K.A., et al., *Olaparib in patients with recurrent high-grade serous or poorly differentiated ovarian carcinoma or triple-negative breast cancer: a phase 2, multicentre, open-label, non-randomised study.* Lancet Oncol, 2011. **12**(9): p. 852-61.
19. Audeh, M.W., et al., *Oral poly(ADP-ribose) polymerase inhibitor olaparib in patients with BRCA1 or BRCA2 mutations and recurrent ovarian cancer: a proof-of-concept trial.* Lancet, 2010. **376**(9737): p. 245-251.
20. Zhang, S., et al., *Identification and characterization of ovarian cancer-initiating cells from primary human tumors.* Cancer Res, 2008. **68**(11): p. 4311-20.
21. Alvero, A.B., et al., *Molecular phenotyping of human ovarian cancer stem cells unravels the mechanisms for repair and chemoresistance.* Cell Cycle, 2009. **8**(1): p. 158-66.
22. Szotek, P.P., et al., *Ovarian cancer side population defines cells with stem cell-like characteristics and Mullerian Inhibiting Substance responsiveness.* Proceedings of the National Academy of Sciences of the United States of America, 2006. **103**(30): p. 11154-11159.
23. Bapat, S.A., et al., *Stem and progenitor-like cells contribute to the aggressive behavior of human epithelial ovarian cancer.* Cancer Res, 2005. **65**(8): p. 3025-9.
24. Zhan, Q., C. Wang, and S. Ngai, *Ovarian cancer stem cells: a new target for cancer therapy.* Biomed Res Int, 2013. **2013**: p. 916819.
25. McAuliffe, S.M., et al., *Targeting Notch, a key pathway for ovarian cancer stem cells, sensitizes tumors to platinum therapy.* Proceedings of the National Academy of Sciences of the United States of America, 2012. **109**(43): p. E2939-E2948.
26. Andersson, E.R. and U. Lendahl, *Therapeutic modulation of Notch signalling - are we there yet?* Nature Reviews Drug Discovery, 2014. **13**(5): p. 359-380.
27. Thibault, B., et al., *Ovarian cancer microenvironment: implications for cancer dissemination and chemoresistance acquisition.* Cancer Metastasis Rev, 2014. **33**(1): p. 17-39.
28. Hollingsworth, H.C., et al., *Tumor angiogenesis in advanced stage ovarian carcinoma.* Am J Pathol, 1995. **147**(1): p. 33-41.
29. Ferrara, N., H.P. Gerber, and J. LeCouter, *The biology of VEGF and its receptors.* Nat Med, 2003. **9**(6): p. 669-76.
30. Vecchione, A., et al., *A microRNA signature defines chemoresistance in ovarian cancer through modulation of angiogenesis.* Proc Natl Acad Sci U S A, 2013. **110**(24): p. 9845-50.
31. Pujade-Lauraine, E., et al., *Bevacizumab combined with chemotherapy for platinum-resistant recurrent ovarian cancer: The AURELIA open-label randomized phase III trial.* J Clin Oncol, 2014. **32**(13): p. 1302-8.

32. Bast, R.C., Jr., B. Hennessy, and G.B. Mills, *The biology of ovarian cancer: new opportunities for translation.* Nat Rev Cancer, 2009. **9**(6): p. 415-28.
33. Verhaak, R.G., et al., *Prognostically relevant gene signatures of high-grade serous ovarian carcinoma.* J Clin Invest, 2013. **123**(1): p. 517-25.
34. Cho, K.R. and M. Shih Ie, *Ovarian cancer.* Annu Rev Pathol, 2009. **4**: p. 287-313.
35. Cancer Genome Atlas Research, N., *Integrated genomic analyses of ovarian carcinoma.* Nature, 2011. **474**(7353): p. 609-15.
36. Cancer Genome Atlas Research, N., et al., *Integrated genomic characterization of endometrial carcinoma.* Nature, 2013. **497**(7447): p. 67-73.
37. Ichikawa, Y., et al., *Mutation of K-Ras Protooncogene Is Associated with Histological Subtypes in Human Mucinous Ovarian-Tumors.* Cancer Research, 1994. **54**(1): p. 33-35.
38. Cuatrecasas, M., et al., *K-ras mutations in mucinous ovarian tumors - A clinicopathologic and molecular study of 95 cases.* Cancer, 1997. **79**(8): p. 1581-1586.
39. Enomoto, T., et al., *K-Ras Activation Occurs Frequently in Mucinous Adenocarcinomas and Rarely in Other Common Epithelial Tumors of the Human Ovary.* American Journal of Pathology, 1991. **139**(4): p. 777-785.
40. Wu, R., et al., *Mouse model of human ovarian endometrioid adenocarcinoma based on somatic defects in the Wnt/beta-catenin and PI3K/Pten signaling pathways.* Cancer Cell, 2007. **11**(4): p. 321-333.
41. Wu, R., et al., *Preclinical testing of PI3K/AKT/mTOR signaling inhibitors in a mouse model of ovarian endometrioid adenocarcinoma.* Clin Cancer Res, 2011. **17**(23): p. 7359-72.
42. Roos, W.P., et al., *Apoptosis in malignant glioma cells triggered by the temozolomide-induced DNA lesion O6-methylguanine.* Oncogene, 2007. **26**(2): p. 186-97.
43. Jiang, X.Y., et al., *O-6-methylguanine-DNA methyltransferase (MGMT) immunohistochemistry as a predictor of resistance to temozolomide in primary CNS lymphoma.* Journal of Neuro-Oncology, 2013. **114**(1): p. 135-140.
44. Hegi, M.E., et al., *MGMT gene silencing and benefit from temozolomide in glioblastoma.* N Engl J Med, 2005. **352**(10): p. 997-1003.
45. Carlson, B.L., et al., *Radiosensitizing Effects of Temozolomide Observed in Vivo Only in a Subset of O6-Methylguanine-DNA Methyltransferase Methylated Glioblastoma Multiforme Xenografts.* International Journal of Radiation Oncology Biology Physics, 2009. **75**(1): p. 212-219.

46. Kitange, G.J., et al., *Induction of MGMT expression is associated with temozolomide resistance in glioblastoma xenografts.* Neuro-Oncology, 2009. **11**(3): p. 281-291.
47. Park, C.K., et al., *The Changes in MGMT Promoter Methylation Status in Initial and Recurrent Glioblastomas.* Transl Oncol, 2012. **5**(5): p. 393-7.
48. Esteller, M., et al., *Inactivation of the DNA-repair gene MGMT and the clinical response of gliomas to alkylating agents.* N Engl J Med, 2000. **343**(19): p. 1350-4.
49. Patel, A.P., et al., *Single-cell RNA-seq highlights intratumoral heterogeneity in primary glioblastoma.* Science, 2014. **344**(6190): p. 1396-401.
50. Szerlip, N.J., et al., *Intratumoral heterogeneity of receptor tyrosine kinases EGFR and PDGFRA amplification in glioblastoma defines subpopulations with distinct growth factor response.* Proc Natl Acad Sci U S A, 2012. **109**(8): p. 3041-6.
51. Sottoriva, A., et al., *Intratumor heterogeneity in human glioblastoma reflects cancer evolutionary dynamics.* Proc Natl Acad Sci U S A, 2013. **110**(10): p. 4009-14.
52. Singh, S.K., et al., *Identification of a cancer stem cell in human brain tumors.* Cancer Res, 2003. **63**(18): p. 5821-8.
53. Singh, S.K., et al., *Identification of human brain tumour initiating cells.* Nature, 2004. **432**(7015): p. 396-401.
54. Chen, J., et al., *A restricted cell population propagates glioblastoma growth after chemotherapy.* Nature, 2012. **488**(7412): p. 522-6.
55. Verhaak, R.G.W., et al., *Integrated Genomic Analysis Identifies Clinically Relevant Subtypes of Glioblastoma Characterized by Abnormalities in PDGFRA, IDH1, EGFR, and NF1.* Cancer Cell, 2010. **17**(1): p. 98-110.
56. !!! INVALID CITATION !!!
57. Frese, K.K. and D.A. Tuveson, *Maximizing mouse cancer models.* Nature Reviews Cancer, 2007. **7**(9): p. 645-658.
58. Singh, M. and L. Johnson, *Using genetically engineered mouse models of cancer to aid drug development: An industry perspective.* Clinical Cancer Research, 2006. **12**(18): p. 5312-5328.
59. Wang, H.Y., et al., *One-Step Generation of Mice Carrying Mutations in Multiple Genes by CRISPR/Cas-Mediated Genome Engineering.* Cell, 2013. **153**(4): p. 910-918.
60. Sharpless, N.E. and R.A. DePinho, *Model organisms - The mighty mouse: genetically engineered mouse models in cancer drug development.* Nature Reviews Drug Discovery, 2006. **5**(9): p. 741-754.
61. Tentler, J.J., et al., *Patient-derived tumour xenografts as models for oncology drug development.* Nature Reviews Clinical Oncology, 2012. **9**(6): p. 338-350.

62. Rubio-Viqueira, B., et al., *An in vivo platform for translational drug development in pancreatic cancer.* Clinical Cancer Research, 2006. **12**(15): p. 4652-4661.
63. Lin, D., et al., *High Fidelity Patient-Derived Xenografts for Accelerating Prostate Cancer Discovery and Drug Development.* Cancer Research, 2014. **74**(4): p. 1272-1283.
64. Bankert, R.B., et al., *Humanized Mouse Model of Ovarian Cancer Recapitulates Patient Solid Tumor Progression, Ascites Formation, and Metastasis.* Plos One, 2011. **6**(9).
65. Cen, L., et al., *Efficacy of protracted temozolomide dosing is limited in MGMT unmethylated GBM xenograft models.* Neuro-Oncology, 2013. **15**(6): p. 735-746.
66. Wang, J., et al., *A reproducible brain tumour model established from human glioblastoma biopsies.* Bmc Cancer, 2009. **9**.
67. Siolas, D. and G.J. Hannon, *Patient-Derived Tumor Xenografts: Transforming Clinical Samples into Mouse Models.* Cancer Research, 2013. **73**(17): p. 5315-5319.
68. Garraway, L.A. and P.A. Janne, *Circumventing Cancer Drug Resistance in the Era of Personalized Medicine.* Cancer Discovery, 2012. **2**(3): p. 214-226.
69. Hanahan, D. and R.A. Weinberg, *Hallmarks of Cancer: The Next Generation.* Cell, 2011. **144**(5): p. 646-674.
70. Willmann, J.K., et al., *Molecular imaging in drug development.* Nature Reviews Drug Discovery, 2008. **7**(7): p. 591-607.
71. Massoud, T.F. and S.S. Gambhir, *Molecular imaging in living subjects: seeing fundamental biological processes in a new light.* Genes & Development, 2003. **17**(5): p. 545-580.
72. Galban, C.J., et al., *A Feasibility Study of Parametric Response Map Analysis of Diffusion-Weighted Magnetic Resonance Imaging Scans of Head and Neck Cancer Patients for Providing Early Detection of Therapeutic Efficacy.* Translational Oncology, 2009. **2**(3): p. 184-190.
73. Lemasson, B., et al., *Diffusion-Weighted MRI as a Biomarker of Tumor Radiation Treatment Response Heterogeneity: A Comparative Study of Whole-Volume Histogram Analysis versus Voxel-Based Functional Diffusion Map Analysis.* Translational Oncology, 2013. **6**(5): p. 554-561.
74. Xia, Y., et al., *Reduced cell proliferation by IKK2 depletion in a mouse lung-cancer model.* Nat Cell Biol, 2012. **14**(3): p. 257-65.
75. Luker, K.E., et al., *Scavenging of CXCL12 by CXCR7 promotes tumor growth and metastasis of CXCR4-positive breast cancer cells.* Oncogene, 2012. **31**(45): p. 4750-8.
76. Coppola, J.M., B.D. Ross, and A. Rehemtulla, *Noninvasive imaging of apoptosis and its application in cancer therapeutics.* Clin Cancer Res, 2008. **14**(8): p. 2492-501.

77. Weber, T.G., et al., *Noninvasive monitoring of pharmacodynamics and kinetics of a death receptor 5 antibody and its enhanced apoptosis induction in sequential application with doxorubicin.* Neoplasia, 2013. **15**(8): p. 863-74.
78. Weber, T.G., et al., *Apoptosis imaging for monitoring DR5 antibody accumulation and pharmacodynamics in brain tumors noninvasively.* Cancer Res, 2014. **74**(7): p. 1913-23.
79. Galban, S., et al., *Imaging proteolytic activity in live cells and animal models.* PLoS One, 2013. **8**(6): p. e66248.
80. Zhang, L., et al., *Molecular imaging of Akt kinase activity.* Nat Med, 2007. **13**(9): p. 1114-9.
81. Williams, T.M., et al., *Molecular imaging of the ATM kinase activity.* Int J Radiat Oncol Biol Phys, 2013. **86**(5): p. 969-77.
82. Nyati, S., et al., *Molecular imaging of TGFbeta-induced Smad2/3 phosphorylation reveals a role for receptor tyrosine kinases in modulating TGFbeta signaling.* Clin Cancer Res, 2011. **17**(23): p. 7424-39.
83. Khan, A.P., et al., *Molecular imaging of epidermal growth factor receptor kinase activity.* Anal Biochem, 2011. **417**(1): p. 57-64.
84. Zhang, L., et al., *Molecular imaging of c-Met tyrosine kinase activity.* Anal Biochem, 2011. **412**(1): p. 1-8.
85. Salomonnson, E., et al., *Imaging CXCL12-CXCR4 signaling in ovarian cancer therapy.* PLoS One, 2013. **8**(1): p. e51500.
86. Ahrens, E.T. and J.W.M. Bulte, *Tracking immune cells in vivo using magnetic resonance imaging.* Nature Reviews Immunology, 2013. **13**(10): p. 755-763.
87. Chenevert, T.L. and B.D. Ross, *Diffusion Imaging for Therapy Response Assessment of Brain Tumor.* Neuroimaging Clinics of North America, 2009. **19**(4): p. 559-+.
88. Ozsolak, F. and P.M. Milos, *RNA sequencing: advances, challenges and opportunities.* Nature Reviews Genetics, 2011. **12**(2): p. 87-98.
89. van Dijk, E.L., et al., *Ten years of next-generation sequencing technology.* Trends Genet, 2014. **30**(9): p. 418-426.
90. Bao, Z.S., et al., *RNA-seq of 272 gliomas revealed a novel, recurrent PTPRZ1-MET fusion transcript in secondary glioblastomas.* Genome Res, 2014.
91. Wang, Z., M. Gerstein, and M. Snyder, *RNA-Seq: a revolutionary tool for transcriptomics.* Nature Reviews Genetics, 2009. **10**(1): p. 57-63.
92. Yu, M., et al., *RNA sequencing of pancreatic circulating tumour cells implicates WNT signalling in metastasis.* Nature, 2012. **487**(7408): p. 510-3.
93. Eswaran, J., et al., *RNA sequencing of cancer reveals novel splicing alterations.* Scientific Reports, 2013. **3**.

94. Prensner, J.R., et al., *Transcriptome sequencing across a prostate cancer cohort identifies PCAT-1, an unannotated lincRNA implicated in disease progression.* Nature Biotechnology, 2011. **29**(8): p. 742-U134.
95. Beltran, H., et al., *Molecular Characterization of Neuroendocrine Prostate Cancer and Identification of New Drug Targets.* Cancer Discovery, 2011. **1**(6): p. 487-495.

CHAPTER II

Molecular Imaging Reveals a Role for AKT in Resistance to Cisplatin for Ovarian Endometrioid Adenocarcinoma

Summary

Ovarian cancer is the fifth leading cause of cancer deaths among American women. Platinum-based chemotherapy, such as cisplatin, represents the standard of care for ovarian cancer. However, toxicity and acquired resistance to cisplatin have proven challenging in the treatment of ovarian cancer patients. Using a genetically engineered mouse (GEM) model of ovarian endometrioid adenocarcinoma (OEA) in combination with molecular imaging technologies, we studied the activation of the AKT serine/threonine kinase in response to long-term cisplatin therapy. Treatment of cells in culture and tumor-bearing animals with cisplatin resulted in activation of AKT, a key mediator of cell survival. Based on these results we investigated the therapeutic utility of AKT inhibition in combination with cisplatin, which resulted in enhanced and prolonged induction of apoptosis and in significantly improved tumor control compared to either agent alone. These results provide an impetus for clinical trials using combination therapy. To facilitate these trials, we also demonstrate the utility of diffusion-weighted MRI as an imaging biomarker for evaluation of therapeutic efficacy in OEA.

2.1 Introduction

Among American women, ovarian cancer remains the fifth leading cause of cancer related deaths with an estimated 22,280 new cases for the year 2012 [1]. At diagnosis, nearly two thirds of women with ovarian cancer present with advanced stage disease, and their overall five-year survival is only 27% [2, 3]. The vast majority of ovarian cancers are epithelial (carcinomas) and can be classified into four major subtypes, including serous, endometrioid, clear cell, and mucinous carcinomas [4]. Recent efforts to better understand the genetic differences between these subtypes have shown that mutations predicted to dysregulate key signaling pathways characterize each subtype [5]. For example, mutations of genes in the Wnt/β-catenin and PI3K/Pten signaling pathways co-occur in a substantial fraction of ovarian endometrioid adenocaraciomas (OEAs) [6]. Although genetic differences in the subtypes of ovarian cancer have been recognized, surgical debulking followed by chemotherapy with taxanes and platinum-based drugs remains the first-line therapy for all subtypes [7]. Unfortunately, even though most patients initially respond to treatment, tumors eventually relapse due to acquired drug resistance [8, 9]. To overcome these hurdles, dose escalation studies have been explored but have been found intolerable due to toxicity and serious side-effects [10]. Therefore, a better understanding of the mechanisms leading to drug resistance is urgently needed for the development of novel treatment paradigms to improve length and quality of life for ovarian cancer patients.

The cisplatin-resistant phenotype of cancer cells may be due to a number of mechanisms, including alterations that affect the intracellular uptake of cisplatin or altered sigaling pathways that ultimately impact the execution of the apoptotic program [10]. The PI3K/AKT signaling pathway is important for cell survival, and plays a critical role in a number of other tumor-associated cellular processes, including cell growth, and cell cycle progression [11].

Moreover, a recent study in cultured cells suggested that chemoresistance is mediated by AKT activation through DNA dependent protein kinase (DNA-PK) [12]. However, limited work has been done to study the molecular basis of chemoresistance in a clinically relevant mouse model of ovarian cancer. We have previously described a genetically engineered mouse (GEM) model for OEA, which recapitulates the human disease more closely than traditionally utilized tumor xenograft models. In this model, simultaneous activation of canonical Wnt/β-catenin and PI3K/AKT signaling invariably leads to ovarian tumor development and is achieved by conditionally inactivating the *Apc* and *Pten* tumor suppressor genes in the ovarian surface epithelium of $Apc^{loxP/loxP}$;$Pten^{loxP/loxP}$ mice [6]. Tumors arise as early as three weeks post expression of Cre recombinase, and the utility of this model for testing novel therapies or treatment paradigms has been recently demonstrated [13].

Molecular imaging provides a unique opportunity to evaluate drug target interactions, induction of cell death, and tumor regression in a non-invasive and dynamic manner [14, 15]. Using a bioluminescence reporter for AKT activity [16] and caspase-3 proteolysis [17], we provide evidence in the mouse model that the activation of the PI3K/AKT cell survival signaling pathway in response to cisplatin treatment contributes to resistance to cisplatin-induced apoptosis. Simultaneously, we here describe a new modification of our genetically engineered mouse model for OEA, wherein tumor specific caspase-3-dependent apoptosis can be imaged over time in response to therapeutic intervention. We provide validation studies for the use of diffusion-weighted MRI (DW-MRI) as an imaging surrogate for treatment efficacy and identified cisplatin in combination with perifosine as a therapeutic paradigm for future clinical trials.

2.2 Materials and Methods

Cell culture

Murine OEA-derived tumor cell lines were established by mechanically dispersing ovarian tumor tissues with sterile scalpels followed by digestion at 37°C with 0.05% Trypsin-EDTA for 20 minutes. Cells were cultured for five passages in DMEM containing 10% FBS/1% Penicillin/Streptomycin (P/S)/1% Insulin-Transferrin-Selenium (Invitrogen) in an incubator with 3% O_2/5% CO_2 (Model NAPCO 8000WJ, Thermal Scientific, Asheville, NC). During the first five passages of primary culture, all non-adherent cells were discarded, and only adherent cells were passaged. Adherent mesenchymal cells were removed by differential trypsinzation to further enrich the epithelial cell population. The Apc-/Pten- OEA-derived tumor cell line W2532T, denoted hereafter as W25, was maintained in DMEM medium (Gibco, Gaithersburg, MD) supplemented with 10% fetal bovine serum (Gibco). W25 cells display epithelial (cobblestone) morphology by light microscopy, and express epithelial markers cytokeratin 8 and 19 by immunofluorescence[13]. Cre-mediated bi-allelic recombination of Apc and Pten in W25 cells was confirmed by PCR. To generate stable cell lines with bioluminescence reporters, W25 cells were transfected with plasmids (pEF apoptosis or AKT reporter) [16, 17] by using FuGENE 6 transfection reagent (Roche Diagnostics, Indianapolis, IN) following the manufacturer's instructions. Single clones stably expressing the reporters were maintained in DMEM medium with 10% FBS and 300μg/mL G418 (Invitrogen, CA).

Mouse Strains

Apc$^{loxP/loxP}$*;Pten*$^{loxP/loxP}$ mice have been previously described in detail [6]. The transgenic bioluminescence-apoptosis reporter (*Apoptosis reporter*$^{tg/+}$) mouse was generated by the transgenic core of the University of Michigan. In brief, the Elongation Factor-1(EF1) promoter, which is widely and constitutively expressed, drives the transcription of the tdTomato coding sequence (a derivative of red fluorescent protein). The presence of a transcription stop site

and poly-adenylation target site (pA) at the end of the tdTomato coding sequence results in termination of transcription such that only the tdTomato protein is expressed. In the presence of Cre recombinase, recombination of the loxP sequences results in deletion of the tdTomato coding sequence as well as the adjoining pA sequences. Cre recombination of the transgene results in transcription of the molecular imaging reporter as well as an internal ribosome entry site (IRES) and the renilla luciferase (rluc) coding sequence. A single mRNA from the transgene will express the reporter protein (apoptosis reporter) as well as the rluc protein.

Apc$^{loxP/loxP}$*;Pten*$^{loxP/loxP}$*;Apoptosis reporter*$^{tg/+}$ mice were generated by crossbreeding *Apc*$^{loxP/loxP}$*;Pten*$^{loxP/loxP}$ mice with *Apoptosis reporter*$^{tg/+}$ mice. All the animal experiments were done in accordance with protocols approved by University Committee on Use and Care of Animals of the University of Michigan (UCUCA protocol numbers 08669 and 09921).

Genotyping

Animals were genotyped using tail DNA. Genotyping primers used in this study are listed here: *Pten*$^{loxP/loxP}$ allele: forward primer 5'-CTCCTCTACTCCATTCTTCCC-3' and reverse primer 5'-ACTCCCACCAATGAACAAAC-3' [18]; *Apc*$^{loxP/loxP}$ allele: forward primer 5'-GTTCTGTATCATGGAAAGATAGGTGGT-3' and Reverse primer 5'-CACTCAAAACGCTTTTGAGGGTTGATTC-3' [19]; *Apoptosis reporter*$^{tg/+}$ allele: forward primer 5’-GAAGTATAGCAACAGAAGACGCCAAAAACATA-3’ and reverse primer 5’-CTAGAAATAGATCTCCCTCCTCCATCGACTTC-3’.

Western blot analysis

Cells were washed with phosphate-buffered saline (PBS) and lysed with NP-40 lysis buffer (1% NP40, 150 mM NaCl, and 25 mM Tris, pH 8.0) supplemented with protease inhibitors (Complete Protease Inhibitor Cocktail,

Roche) and phosphatase inhibitors (PhosSTOP, Roche). Tumor tissues were collected at indicated time points, snap-frozen in liquid nitrogen, and stored at -80^{o}C. Tissues were then homogenized in NP-40 lysis buffer supplemented with protease inhibitors and phosphotase inhibitors. Concentration of protein was determined using Lowry assays (Bio-Rad, Hercules, CA). Equal amount of protein was loaded in each lane and resolved by 4-12% gradient Bis-Tris gel (Invitrogen, CA). Proteins were transferred to 0.2 μm nitrocellulose membrane (Invitrogen, CA). Membranes were incubated overnight at 4^{o}C with primary antibodies after blocking, followed by incubation with appropriate HRP-conjugated secondary antibody at room temperature for one hour. ECL-Plus was used to detect the activity of peroxidase according to the manufacturer's protocol (Amersham Pharmacia, Uppsala, Sweden). Antibodies raised against PARP, pAKT (Serine473 and Thr308), total AKT, pH2A.X(Ser139) and total H2A.X were purchased from Cell Signaling Technology (Beverly, MA).

Immunohistochemistry

After drug treatment, all mice were euthanized and tumor tissues were collected, fixed in 10% (v/v) buffered formalin, and embedded in paraffin. Immunohistochemical (IHC) staining for Ki67 was completed by the Tissue Core of the University of Michigan Comprehensive Cancer Center using standard techniques. Images from two representative 600X fields in the most cellular areas of tumors were acquired by Olympus BX-51 upright light microscope and an Olympus DP-70 high resolution digital camera (Olympus Corporation of the Americas, Center Valley, PA). Ki67 positive cells and negative cells were counted by ImageJ software (Wayne Rasband, National Institutes of Health, MD).

Bioluminescence imaging of cell culture

Cells were seeded at 5,000 cells/well in a 96-well dish. 24 hours post seeding,

cells were incubated with indicated drugs for 20 hours prior to adding luciferin at a final concentration of 100 μg/ml. Luminescence was recorded by a luminometer (EnVision Xcite Multilabel Reader, PerkinElmer, Waltham, MA).

PI exclusion assay

Cell viability was determined by propidium iodide (PI) exclusion assay. PI was purchased from Invitrogen (Eugene, OR). Cells were seeded at 1 x 10^5 cells/ml. 24 hours post seeding, cells were incubated with indicated drugs for 48 hours prior to trypsinization and subsequently collection by centrifugation (400*g* for 3 minutes). PI staining solution was added at a final concentration of 0.1ug/ml. Percentage of PI positive cells was determined and recorded by BD FACSCanto^{TM} Flow cytometry (BD Biosciences, San Jose, CA).

Allograft Implantation

6-week-old athymic female mice (CD-1 nu/nu, Charles River Laboratory, Wilmington, MA) were inoculated subcutaneously (s.c.) with 1x10^7 W25 cells expressing the bioluminescence reporters (apoptosis or Akt) into the flank on each side. Injections were a total volume of 200 μl cell suspension in 50% DMEM mixed with 50% BD Matrigel Matrix (Becton, Dickinson and Company, NJ). Caliper measurements were performed weekly to determine tumor volumes using the formula V= (length/2)x(width^2) until s.q. tumors reached an approximate volume of 200 mm^3 at which time each animal was randomized into one of four treatment groups.

Intra-bursal injection

Replication-incompetent recombinant adenovirus expressing Cre recombinase (AdCre) under the control of the CMV promoter [20] was obtained from the University of Michigan's Vector Core. 5 x 10^7 plaque-forming units (p.f.u.) of AdCre were injected in a total volume of 5 μl containing 0.1% Evans blue (Sigma-Aldrich Inc., St. Louis, MO) into the right ovarian bursal cavity of 8- to

10-week-old female *Apc$^{loxP/loxP}$;Pten$^{loxP/loxP}$; Apoptosis reporter $^{tg/+}$* mice. Intrabursal injection was performed as previously described [21, 22]. Each mouse's left ovarian bursa was untreated, thereby serving as control.

Drug administration

Control and perifosine-treated animals received vehicle or 10 mg/kg perifosine by intraperitoneal injection (i.p.), respectively, five times a week for two weeks with two days off in between treatment weeks. Animals in the cisplatin group received 2.5 mg/kg or 5 mg/kg cisplatin by i.p. injection twice a week for two weeks. For combination groups, mice were treated with 2.5 mg/kg or 5 mg/kg cisplatin twice a week with co-administration of 10 mg/kg perifosine.

***In vivo* Bioluminescence imaging**

In vivo bioluminescence imaging was carried out by injecting tumor-bearing nude and genetically engineered mice intraperitoneally with 150 or 300 mg/kg of 40 mg/mL D-luciferin (Biosynth, Naperville, IL)/PBS solution, respectively, using an IVIS imaging system (Xenogen, Alameda, CA). Post injection mice were anesthetized with a 1–2% isoflurane/air mixture and serial images were acquired over 20-30 minutes to capture the peak photon emission for each animal. Regions of interest were drawn around the area of interest in each mouse and peak luminescence values of each series were used for analysis.

MR-Imaging

MR imaging on OEA mice was carried out on a 7T Agilent, Inc. (Palo Alto, CA) *Direct Drive* system with a quadrature mouse body volume coil (m2m Imaging Corp., Cleveland, OH). During all MRI procedures, animals were anesthetized with a 1–2% isoflurane/air mixture while maintaining body temperature using a heated air system (Air-Therm Heater, World Precision Instruments, Sarasota, FL). Anatomical MR images were acquired by a fast spin echo sequence with the following parameters: repetition time/echo time

(TR/TE) = 4000/15 ms, field of view (FOV)=40x30, matrix size=128x128, slice thickness=0.5 mm, echo train=8, echo spacing=15ms, and number of slices: 25~30. OEA mice were screened for tumor burden once per week from the fourth week post intra-bursal surgery. Mice were randomized into vehicle, cisplatin, perifosine or cisplatin plus perifosine group when their orthotopic tumor sizes reached approximately 50 mm^3. Mice were imaged by MRI twice weekly to follow tumor sizes during treatment.

DW-MR images were obtained from a diffusion-weighted spin-echo sequence, with the following parameters: TR/TE = 2000/32 ms, FOV = 30×30, matrix size = 128×64, slice thickness = 1.0 mm, 10 slices, 2 averages, b-values (diffusion weighting) of 128 and 795 s/mm^2. Respiratory gating was performed using a monitoring system (Small Animal Instruments, Inc., Stony Brook, NY) to eliminate motion artifacts from breathing. DW-MRI scans were performed before treatment and seven days post treatment initiation.

Image Reconstruction and Analysis

Volumes of interest (VOIs) were manually contoured around the enhancing rim of the tumors on the anatomical images for measurements of tumor volume. To determine the whole-tumor means of ADC (apparent diffusion coefficient), VOIs were manually contoured around the enhancing rim of the tumors on diffusion-weighted image slices at b=128 s/mm^2. ADC maps were calculated from the two diffusion weightings (b-values) using the following equation:

$$ADC = \ln\left(\frac{S_1}{S_2}\right) / (b_2 - b_1)$$

where S_1 and S_2 are the signal intensities at b-values b_1 and b_2, respectively. Voxels that exhibited insufficient signal, defined as <10*noise, in the low b-value image (b = 128 s/mm^2) were excluded from the analysis. Subsequently, mean ADC values were calculated over the entire tumor volume. All image

reconstruction and digital image analysis was accomplished using programs developed in Matlab (The Mathworks, Natick, MA, USA).

2.3 Results

2.3.1 Resistance to apoptosis in response to cisplatin is reversed by AKT inhibition

To study the mechanistic basis of cisplatin chemoresistance, we established a primary ovarian tumor cell line (W25) derived from our previously described murine OEA model [13]. To enable imaging of caspase-3 activation, a surrogate for apoptosis, we generated a stable cell line (W25-Apop) expressing a previously described bioluminescent apoptosis reporter [17] as illustrated in Figure 2.1A.

The induction of apoptosis was evaluated using cultured cells in response to cisplatin alone (20 μM) or in combination with perifosine (30 μM), a small molecule inhibitor of AKT activity [23]. As depicted in Figure 2.1B, combination therapy resulted in significantly elevated caspase-3 activation when compared to single agent as measured by an increase in bioluminescence signal. This finding was consistent with conventional western blot analysis for caspase-3 activity as measured by cleavage of PARP, which was only observed in response to combination therapy (Figure 2.1C). Additionally, we evaluated overall cell viability using PI exclusion assays (Figure 2.1D), wherein the combination therapy showed higher percentage of PI positivity compared to either agent alone.

To extend these studies *in vivo*, initial studies focused on following the treatment effects of subcutaneous W25-Apop tumors growing in athymic nude mice. Animals treated with vehicle, perifosine (10 mg/kg, 5 times a week), cisplatin (5 mg/kg, 2 times a week), or combination treatment of cisplatin (5 mg/kg, 2 times a week) and perifosine (10 mg/kg, 5 times a week) were

studied using the bioluminescence molecular reporters. The greatest induction of apoptosis as measured by bioluminescence was observed in the cohort of animals treated with the combination of cisplatin and perifosine (Figure 2.2A and 2.2B). Treatment of tumor-bearing animals with perifosine resulted in enhanced bioluminescence signals (5 fold) on each day of treatment during the first week over the control group. Perifosine as a single agent failed to induce apoptosis during the second week (days 8-12). The combination of cisplatin and perifosine induced apoptosis to a similar extent as perifosine alone in the first week of treatment (5-6 fold) but a significant increase in apoptosis (10 fold) was observed in the second week of treatment (Figure 2.2A). A significant degree of toxicity as measured by loss of weight was observed in mice treated with cisplatin at 5mg/kg, twice a week. To further evaluate the efficacy of cisplatin and perifosine, we used a lower dose of cisplatin (2.5mg/kg, twice a week). At these doses we observed a similar enhancement of bioluminescence in the combination group, compared to cisplatin alone after the first day of treatment (Figure 2.2C). Furthermore, by the end of two weeks of treatment both cisplatin and perifosine as single agents showed significantly increased tumor volumes over baseline measurements while the combination treatment prevented tumor growth during the treatment period (Figure 2.2D). Cisplatin alone had some anti-tumor effect, as tumors were smaller in cisplatin-treated mice than in mice treated with vehicle alone over the 2 week treatment period.

2.3.2 A role for AKT in resistance to cisplatin treatment.

To investigate the regulation of AKT activity in live cells and animals, we used our previously described bioluminescence AKT reporter (BAR, Figure 2.3A). The reporter is designed such that increased bioluminescence activity is observed upon inhibition of the AKT-kinase [16]. Using BAR-expressing W25 cells (W25-BAR) we evaluated AKT activity in response to cisplatin and/or perifosine. As expected, perifosine treatment resulted in a significant increase

of bioluminescence activity due to AKT inhibition. Unexpectedly, the combination of cisplatin and perifosine showed a six fold increase of bioluminescence, suggesting that cisplatin treatment elevated AKT kinase activity and that perifosine treatment resulted in a greater decrease in AKT activity (Figure 2.3B). This was confirmed by phospho-AKT western blot analysis which showed that both Ser473 and Thr308 phosphorylation was elevated upon cisplatin treatment in W25-BAR cells whereas perifosine treatment reversed AKT phosphorylation (Figure 2.3C). To investigate if this phenomenon was reproducible in tumors, AKT activity in response to therapies was evaluated in W25-BAR allografts. W25-BAR tumor-bearing animals were randomized into four groups consisting of control (vehicle), cisplatin (2.5 mg/kg, 2 times a week), perifosine (10 mg/kg, 5 times a week) or combination therapy when tumors reached 200mm^3 in volume. As shown in Figure 2.3D, treatment of s.q. tumor bearing mice with perifosine expectedly resulted in increased bioluminescence during treatment. In accordance with cell culture results, animals treated with the combination of cisplatin and perifosine showed a prolonged and enhanced increase in bioluminescence signal in the second week of treatment, indicative of enhanced AKT inhibition (and therefore activity). We hypothesized that repetitive cisplatin exposure during the first week of treatment elevated phospho-AKT levels in tumor allografts thereby allowed for increased bioluminescence signal to be detected due to simultaneous AKT inhibition. To test this hypothesis, tumor samples were collected following the first week (cycle) of therapy. Western blot analysis confirmed that cisplatin treatment resulted in an increase in AKT activation as measured by phospho-AKT. Combination treatment showed decreased levels of phospho-AKT compared to cisplatin alone indicating that perifosine treatment reversed the activation of AKT (Figure 2.3E).

AKT phosphorylation is regulated by various factors, including DNA damage caused by radiation and chemotherapies [12, 24]. In order to evaluate the DNA

damage response pathway following cisplatin treatment, phosphorylation of histone H2A.X levels were evaluated. As shown in Figure 2.3F, phospho-H2A.X was induced in cisplatin and combination treatment groups, indicating that cisplatin treatment resulted in DNA damage inducing AKT activation.

2.3.3 Imaging of apoptosis in a GEM model.

The tumor microenvironment - including adjacent normal tissue, stromal cells, vasculature, lymph and immune cells - impacts the response of tumor cells to therapeutic intervention [25, 26]. For the purpose of imaging apoptosis non-invasively in an ovarian cancer animal model, we generated a new reporter mouse by pronuclear microinjection of a transgene containing the apoptosis reporter into fertilized eggs obtained from FVB/N females. The schematic diagram shown in Figure 2.4A depicts the transgene apoptosis reporter construct. *Apoptosis reporter* $^{tg/+}$ transgenic animals were crossed with *Apc*$^{loxP/loxP}$*; Pten*$^{loxP/loxP}$ mice to generate *Apc*$^{loxP/loxP}$*; Pten*$^{loxP/loxP}$*; Apoptosis reporter* $^{tg/+}$ mice for use in subsequent experiments.

In this new OEA model with the built-in apoptosis imaging reporter, Cre-expression resulted in the deletion of both copies of *Apc* and *Pten* and expression of the apoptosis reporter in transformed ovarian surface epithelial cells. Mice injected with AdCre are referred hereafter as *Apc*$^{-/-}$*; Pten*$^{-/-}$*; Apopreporter*$^{+}$, indicating successful Cre-mediated recombination. Representative images of bioluminescence activity in *Apc*$^{-/-}$*; Pten*$^{-/-}$*; Apopreporter*$^{+}$ mice with ovarian tumors before and following one day of treatment are shown in Figure 2.4B. Bioluminescence signals were only detected in the right abdomen, indicative of tissue-specific activation of the apoptosis reporter upon AdCre injection into the right ovary. Consistent with our previous data obtained in cell culture and allografts, bioluminescence activity increased following combination therapy indicating activation of

caspase-3 had occurred. Tumor progression in *Apc*$^{-/-}$*; Pten*$^{-/-}$*; Apopreporter*$^{+}$ animals was followed over time using MRI beginning at four weeks post AdCre injection. Once tumor volumes reached approximately 50mm^3, animals were randomized into four treatment groups: vehicle, perifosine, cisplatin and combination therapy. Following treatment initiation, bioluminescence imaging was performed 6 hours post treatment on days 1, 5, 8 and 12. Apoptosis reporter activation was normalized to tumor volume changes by performing MRI at the same time points in which bioluminescence imaging was performed. As demonstrated in Figure 2.4C, the combination treatment of perifosine and cisplatin resulted in the highest and most sustained induction of bioluminescence when compared to vehicle treated or single agent treated animals, indicating maximum apoptotic cell kill was achieved. Similar to the data obtained from the allograft study, we observed an increase in the level of apoptosis in perifosine treated animals 6 hours post treatment initiation. As mentioned above, the initial surge in cell death upon phospho-AKT inhibition might be due to the cells' addiction to activated PI3K/AKT pathway. In fact, inhibition of the PI3K/AKT pathway in cancer cells has been shown to induce apoptosis [23]. Although no caspase-3 activation upon single agent cisplatin treatment was observed using bioluminescence imaging, tumor growth was inhibited as assessed by MRI (Figure 2.4E) indicative of caspase-3 independent cytotoxicity due to the high dose of cisplatin which was also observed in our allograft study (Figure 2.2A). Quantitative analysis of the MRI data show tumor volumes were significantly reduced in the combinatorial treatment over all other treatment groups (Figure 2.4E), thus confirming our previous results using the OEA tumor allografts. Target inhibition by drug was confirmed by western blotting against phospho-AKT(Ser473) and total AKT of tumor tissues obtained from animals treated with perifosine. As depicted in Figure 2.4F, perifosine treatment resulted in a decrease in phospho-AKT levels at 3 hours post-treatment initiation.

DW-MRI can be used to measure changes in cellular density within tumor tissue and has been established as a clinically relevant surrogate imaging biomarker for treatment response assessment in cancer patients [27, 28]. We performed DW-MRI on tumor-bearing mice in order to evaluate the effects the treatment as well as the ability of DW-MRI to detect and differentiate the effectiveness of each treatment. As shown in Figure 2.5A and Figure 2.5B, we observed a decrease in ADC values in vehicle and perifosine-treated animals after two weeks of treatment suggesting that perifosine alone is not efficacious in inducing cell death. The observed decrease in ADC values in vehicle and perifosine groups suggested that cells were undergoing active proliferation resulting in increased tumor cellularity over this time period. This finding was further supported by immunohistochemical analysis of tumors obtained from these animals one week after treatment initiation. Ki67 staining, indicative of cell proliferation, increased in vehicle and perifosine-treated animals as shown in Figure 2.5C and Figure 2.5D. However, cisplatin and combination treated animals showed increased ADC values (Figure 2.5A and Figure 2.5B) and decreased Ki67 staining (Figure 2.5D), which suggested that increased cell death was the likely cause of the resultant tumor regression as demonstrated in Figure 2.4E.

In summary, these studies revealed that combination treatment of cisplatin and perifosine was more efficacious than either drug alone in inducing apoptosis, and thereby tumor regression, by utilizing our new reporter mouse model of OEA in conjunction with non-invasive imaging modalities.

2.4 Discussion

Ovarian cancer patients treated with the chemotherapeutic agent, cisplatin, usually show an initial response yet ultimately succumb to their disease due to the development of resistance [10]. Regulation of cellular drug uptake, increased DNA damage repair, and inhibition of apoptosis have been proposed

to cause cisplatin resistance [29]. The development of strategies for chemosensitization and prevention of therapeutic resistance remains a major goal with important clinical implications. Although a large body of work has been conducted towards this aim, the model systems typically employ cultured cells and/or immunocompromised mice bearing subcutaneous xenografts. In addition, analyses of molecular events in these model systems involves resection of tumor cells for *ex vivo* assays and thus provide only a non-quantitative snapshot of a dynamically changing and highly interactive cascade of signaling events following therapeutic intervention. The present study utilizes recent advances in genetically engineered mouse ovarian cancer models as well as the development of molecular imaging biomarkers which enable quantitative, non-invasive and temporal imaging of dynamic molecular events in living animals. Combining our tumor model systems with anatomical and molecular imaging approaches provided an opportunity to gain novel insights into the roles of PI3K/AKT signaling and the apoptotic machinery in the development of therapeutic resistance to cisplatin.

Our initial study utilized a mouse OEA cell line derived from an ovarian tumor which was engineered to express the apoptosis reporter. This line was subcutaneously implanted allowing for detection of caspase-3 activation in perifosine treated animals using bioluminescence imaging. While the imaging signal increased during the first week, a significant decline was observed during the second week of treatment. We reasoned that the cells' dependency on the PI3K/AKT pathway leads to an initial induction of apoptosis upon inhibition of AKT activity by perifosine, which may later be compensated by activation of alternate survival signaling pathways. In support, we and others have previously reported that AKT inhibition results in activation of compensatory signaling through MEK/ERK or other signaling pathways [13, 30]. This finding may provide additional rationale for the simultaneous targeting of PI3K/AKT and MEK/ERK signaling pathways, but remains to be

investigated for the treatment of OEA. Intriguingly, the caspase-3 reporter allowed us to determine that cell death and tumor regression induced by cisplatin in cell culture and in allografted or transgenic animals, respectively appeared to be largely caspase-3 independent. This is not surprising since cisplatin has been shown to exert its effects by inducing DNA damage, cell cycle arrest and ultimately necrotic cell death [31, 32] which serves to further validate the use of these molecular imaging reporters in the context of pre-clinical drug optimization studies.

Initial response to platinum-based therapies in the treatment of patients afflicted with ovarian cancer is usually high, yet most patients relapse due to acquired resistance. Recent studies by Stronach *et al.* comparing cisplatin-resistant and cisplatin-sensitive cell lines revealed a significant increase in phosphorylated AKT upon cisplatin treatment. AKT inhibition sensitized resistant cells to cisplatin, whereas inhibition of AKT in cisplatin sensitive lines had little effect on caspase-3/7 induction [12]. With the ability to image and thus quantify AKT and caspase-3 activity in live tumor-bearing animals dynamically over time, our results support the concept that activation of AKT contributes to cisplatin resistance and likely results from prior exposure to the agent.

Activation of AKT is regulated by various factors, including insulin and the DNA damage response. Several reports have thus far demonstrated that AKT's complete activation depends on its phosphorylation at Ser473 and Thr308. Interestingly, Thr308 is phosphorylated by 3-phosphoinositide-dependent kinase 1 (PDK1) [33] whereas Ser473 is likely regulated by mammalian target of rapamycin complex 2 (mTORC2) [34], DNA-PK [35] and ATM [36]. Here we present data indicating that cisplatin alone or in combination with perifosine induced similar DNA damage, yet single agent treatment with cisplatin induced AKT activation and resistance to apoptosis. These findings suggest that AKT activation by cisplatin may be mediated by the DNA damage response.

Supporting these findings are the results of a recent study, which demonstrated DNA-PK dependent regulation of AKT phosphorylation upon cisplatin treatment [12]. However, since ATM is also activated following DNA double strand breaks and has been implicated in radiation-induced AKT activation [24], the possibility remains that ATM may also play a role in regulating AKT phosphorylation which should be the subject of further investigations.

The PI3K/AKT pathway plays an important role in the cell survival pathway. The enhanced effect which we observed following cisplatin and perifosine treatments suggests that cisplatin activates the PI3K/AKT pathway thereby preventing apoptosis. Simultaneous inhibition of AKT activity by perifosine treatment can overcome this effect resulting in apoptosis. In fact, previous studies have shown that AKT through the modulation of p53 activity as well as activation of various apoptotic factors can lead to resistance to apoptosis [37-39].

Genetically engineered OEA mouse models closely recapitulate the human disease, thereby providing an excellent opportunity to study this subtype of ovarian cancer and optimize therapeutic paradigms for future clinical investigation [13]. We have recently shown that the OEAs arising in our model system are inhibited by the mTOR inhibitor rapamycin, two mechanistically distinct AKT inhibitors (perifosine and API-2), as well as cisplatin plus paclitaxel [13], but combinations of conventional with targeted therapies have not been evaluated in our model system until now. Though we have not yet tested effects of cisplatin and perifosine in GEM models of serous carcinoma, we note that a substantial fraction of high grade serous carcinomas also have activated PI3K/AKT signaling, often on the basis of amplification *PIK3CA, AKT1*, or *AKT2*[5]. Hence our finding that cisplatin plus perifosine is more effective than either agent alone, may apply to other ovarian cancer subtypes besides the subset of endometrioid carcinomas with activated PI3K/AKT

signaling. We also note that other chemotherapeutic agents used to treat ovarian cancers, including paclitaxel, have also been shown to activate PI3K/AKT signaling [40]. In addition, inhibition of PI3K has been shown to increase efficacy of paclitaxel in ovarian cancer model systems [41]. Even more recently, perifosine plus docetaxel were used to treat patients with platinum and taxane resistant or refractory ovarian carcinomas in a Phase I clinical trial [42]. Interestingly, all four (of 21) patients who achieved partial remission or stable disease had either endometrioid or clear cell carcinomas, and two had mutations predicted to activate PI3K/AKT signaling. Clearly, more work is required to determine whether activation of AKT by cisplatin or paclitaxel is a drug-specific or more general effect, and to define the tumor subsets most likely to respond to therapeutic regimens including PI3K/AKT pathway inhibitors.

Monitoring tumor progression and molecular events in intra-abdominal tumors usually involves sacrificing large number of animals for traditional biochemical assays. In order to enable the detection of molecular events within tumors longitudinally, we utilized our previously developed bioluminescence reporters along with anatomical- and DW-MR imaging. The use of the bioluminescence reporters provided for the ability to quantify the extent of apoptosis and AKT activation over time. We demonstrated *in vivo* that repeated cycles of cisplatin treatment resulted in AKT activation, thus revealing molecular mechanisms that contribute to the development of cisplatin resistance. The combination of cisplatin and perifosine was able to inhibit AKT activity and overcome resistance to cisplatin through apoptotic induction and therefore may present a more effective therapeutic paradigm for the treatment of ovarian patients.

Although bioluminescence imaging represents a vital tool for imaging molecular events in animal models, it has its limitations in the clinical settings. In order to develop an imaging biomarker that can be clinically translated for use with ovarian cancer patients, we evaluated the application of DW-MRI as a

surrogate for detection of treatment associated loss of tumor cellularity. DW-MRI has shown promise as a surrogate biomarker of therapeutic response with correlations to survival outcomes in cancer patients [27, 43, 44]. In our study, DW-MRI revealed that both high doses of cisplatin and in combination with perifosine, significant loss of tumor cellularity occurs in contrast to treatment using perifosine alone which was found to have a minimal effect on reducing tumor cell density.

In summary, animal models with defined mutations in key signaling pathways are powerful tools to provide a better understanding of therapeutic efficacy of single agents and to explore the efficacy of combination therapeutic strategies. Molecular imaging technologies such as bioluminescence imaging of mouse models as well as MRI in pre-clinical and clinical studies not only provide an accurate and non-invasive measure of tumor burden and efficacy, but can also enable validation of drug target interactions and acquired drug resistance. Results described here provide an impetus for initiation of clinical studies with integrated DW-MRI biomarker readouts to evaluate pharmacological inhibition of the PI3K/AKT survival signaling pathway when combined with cisplatin to prevent the development of therapeutic resistance and thus significantly impact overall survival in women with OEA.

Figure 2.1

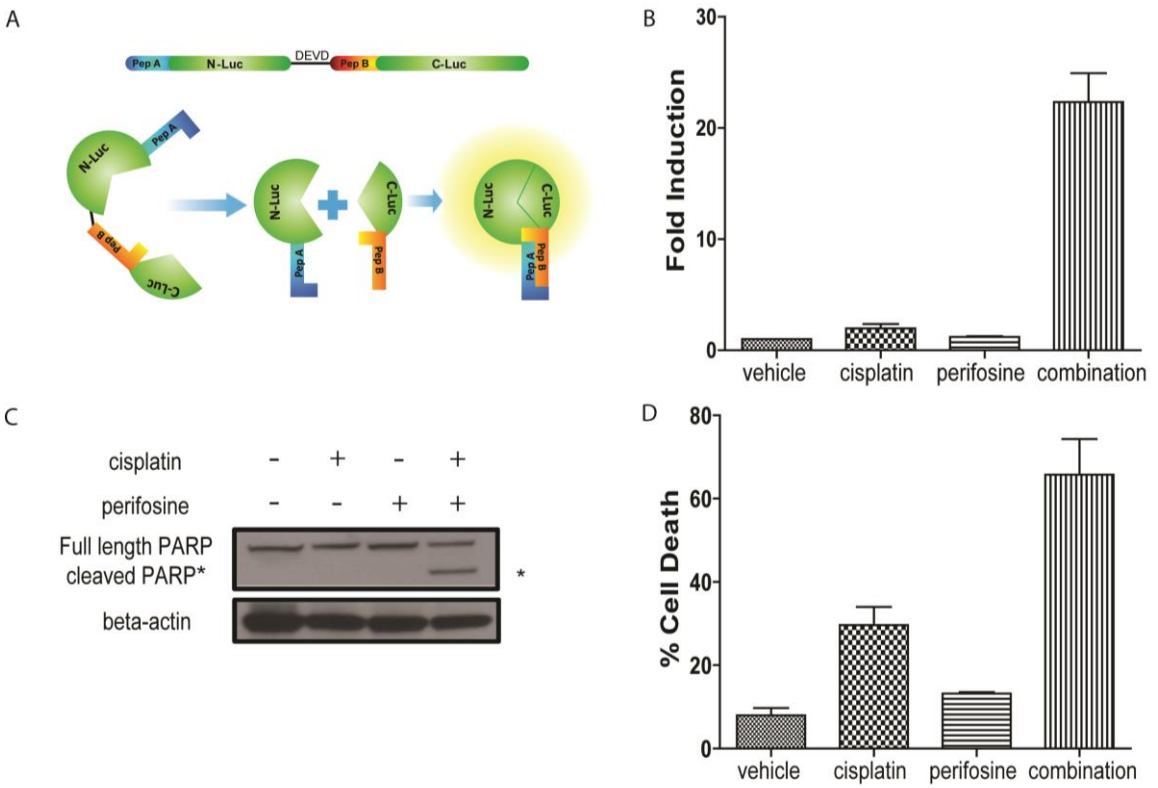

Figure 2.1 Perifosine sensitizes ovarian tumor cells to cisplatin-induced apoptosis. (A) Schematic of bioluminescent apoptosis reporter molecule. Wildtype luciferase was separated into two peptides, N-terminal luciferase (N-luc) and C-terminal luciferase (C-luc). The two termini were separated by a linker region and the DEVD sequence, a recognition- and cleavage site of activated caspase-3. Two strong interacting peptides, namely peptide A and peptide B were fused to N-luc and C-luc, respectively. Upon cleavage at DEVD, peptide A and peptide B overcome the hindrance created by the linker region and reconstitute wildtype luciferase activity by bringing N-luc and C-luc in proximity. **(B)** Bioluminescence assay in W25-Apop cells post 20 hours treatment with PBS, cisplatin [20 µM], perifosine [30 µM] or both of perifosine and cisplatin. Fold induction of bioluminescence signals in each group was calculated at indicated time points by normalizing bioluminescence signals to the values of vehicle group. Three independent experiments were performed and data ± SEM is depicted. **(C)** Representative western blot for PARP in W25-Apop cells treated by cisplatin and/or perifosine for 20 hours. Cleaved PARP (89 kDa) was only observed in cells treated with combination of cisplatin and perifosine. **(D)** Percent cell death was assessed by PI exclusion assay of W25-Apop cells treated for 48 hours with PBS, cisplatin [20 µM], perifosine [30 µM] or both (perifosine and cisplatin). Data was obtained from three independent experiments and represent mean ± SEM.

Figure 2.2

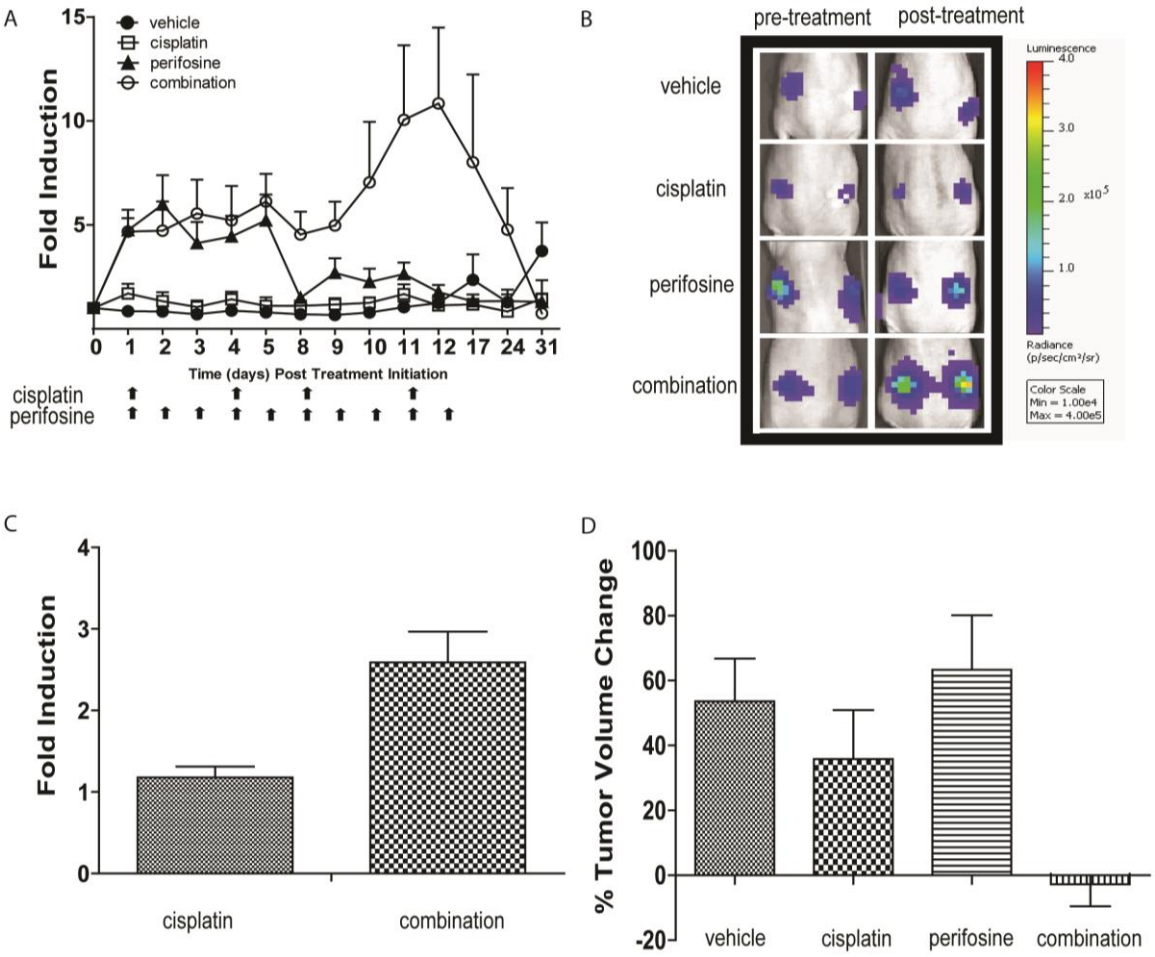

Figure 2.2 Induction of apoptosis in tumor allograft by combination treatment. (A) Bioluminescence imaging of W25-Apop allografts. When tumors reached ≥ 200 mm^3, animals were randomized into four treatment groups: vehicle, perifosine (10 mg/kg 5 times a week), cisplatin (5 mg/kg 2 times a week) and combination group which were treated with 5 mg/kg cisplatin 2 times a week and 10 mg/kg perifosine 5 times a week. Arrows indicate days of treatment for cisplatin and perifosine. Bioluminescence signals were normalized to tumor volumes and pre-treatment values at each time point. Mean fold induction is plotted ± SEM. **(B)** Representative BLI images pre- and post-treatment of each treatment group are shown. **(C)** Bioluminescence imaging of W25-Apop allografts at lower cisplatin doses (2.5mg/kg) at one time point (6 hours post treatment). Bioluminescence signals were normalized to pre-treatment values at each time point. Mean fold induction is plotted ± SEM. **(D)** Percent change of tumor volumes two weeks post treatment initiation. Tumor volumes were measured by caliper pre- and post- treatment. Data represent mean ± SEM.

Figure 2.3

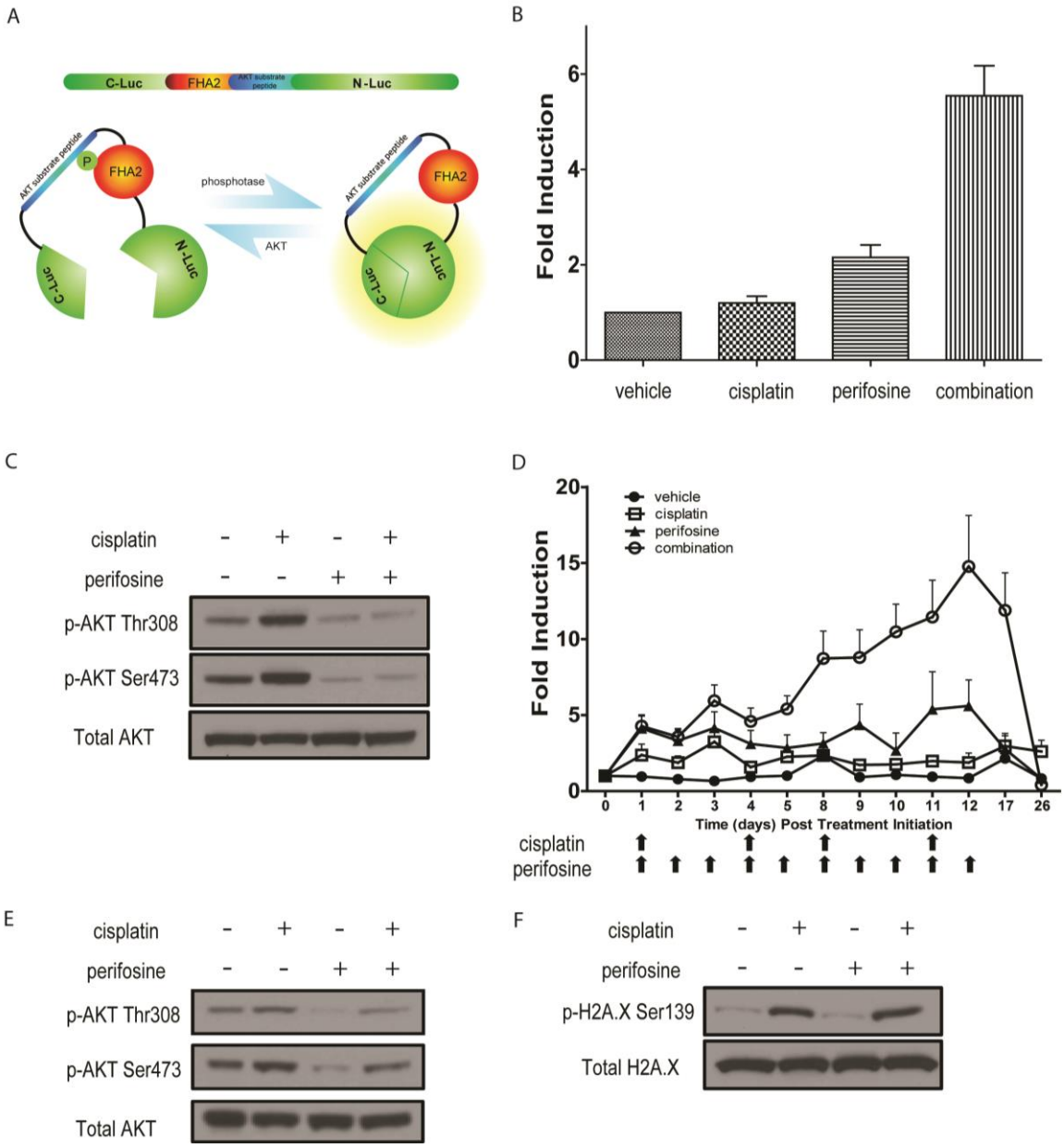

Figure 2.3 Cisplatin induces increase in AKT phosphorylation. (A) Schematic of Bioluminescence AKT Reporter (BAR). **(B)** Bioluminescence assay in W25-BAR cells post 20 hours treatment with vehicle, cisplatin [40 μM], perifosine [30 μM] or both of perifosine and cisplatin. Fold induction of bioluminescence signals in each group was calculated at indicated time points by normalizing bioluminescence signals to the values of vehicle group. Three independent experiments were performed and mean ± SEM is depicted. **(C)** Representative western blot of W25 cell lysates from vehicle-, cisplatin [40μM]-, perifosine [30μM]- or both treated cells. Antibodies against pAKT Ser473, pAKT Thr308 and total AKT were used. **(D)** Bioluminescence imaging of W25-BAR reporter allografts. When tumors reached ≥ 200 mm^3, animals were randomized into four treatment groups: vehicle, perifosine (10 mg/kg 5 times a

week), cisplatin (2.5 mg/kg 2 times a week) and combination group which are treated with 2.5 mg/kg cisplatin 2 times a week and 10 mg/kg perifosine 5 times a week. Arrows indicate days of treatment for cisplatin and perifosine. Bioluminescence signals were normalized to tumor volumes and pre-treatment values at indicated time points. Mean fold induction is plotted ± SEM. **(E)** Representative images of western blot analysis of tumor tissue derived from OEA transgenic at one week post cisplatin treatment. Antibodies against pAKT Ser473, pAKT Thr308 and total AKT were used. **(F)** Representative images of western blot analysis from W25 cells treated with vehicle, cisplatin [40 µM], perifosine [30 µM] or both. pH2A.X Ser139 and total H2A.X were detected by specific antibodies.

Figure 2.4

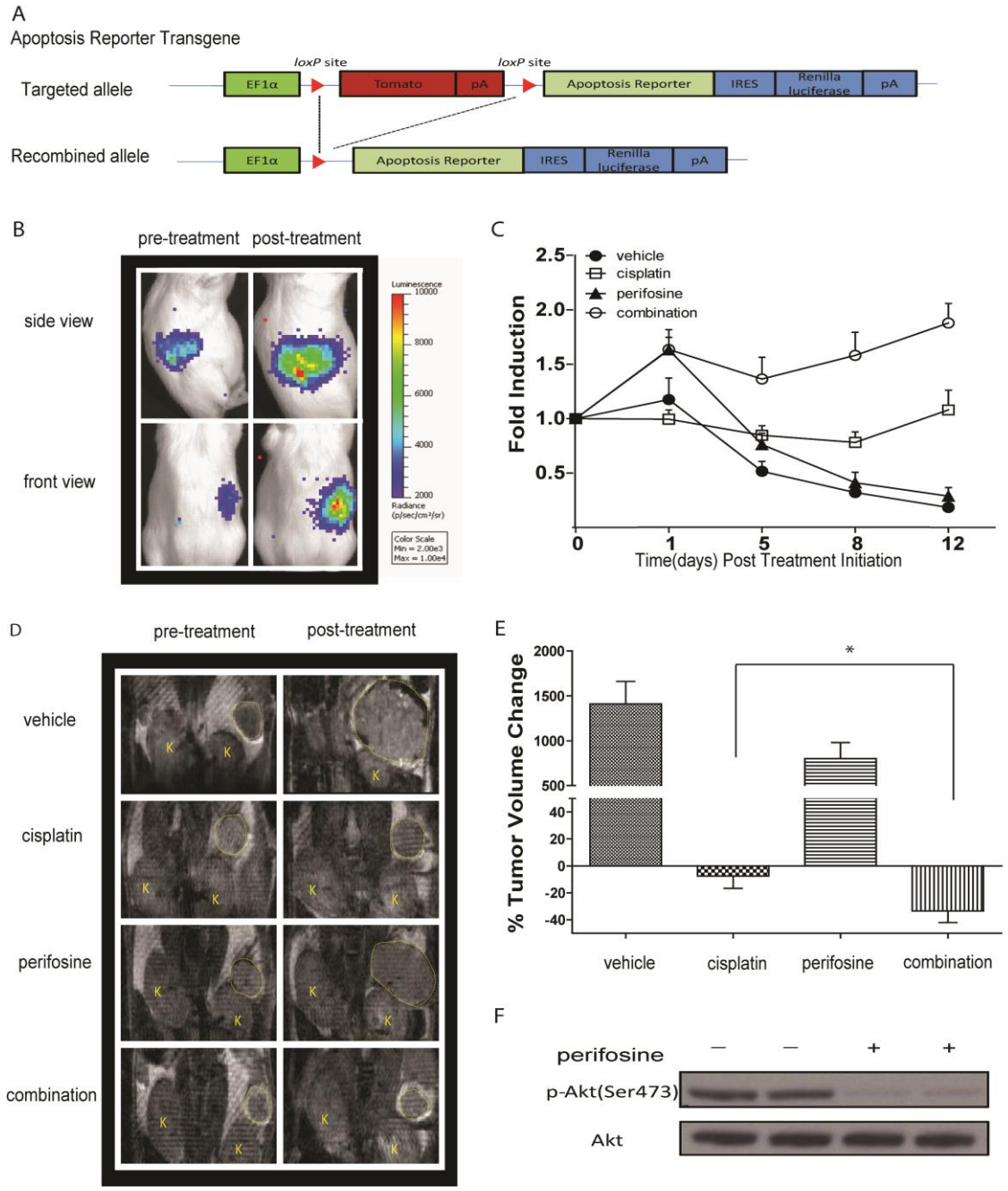

Figure 2.4 Inhibition of AKT activity potentiates the efficacy of cisplatin in a genetically engineered mouse model of OEA. (A) Schematic of the bioluminescence apoptosis reporter transgene. EF-1 alpha drives expression of floxed fluorescence protein tdTomato, which is removed upon tissue specific Cre recombination. Conditional Cre recombination leads to transcription of the bioluminescent apoptosis reporter and IRES dependent renilla luciferase expression. **(B)** Representative bioluminescence images from *Apc*$^{-/-}$, *Pten* $^{-/-}$, *Apopreporter*$^{+}$ animals before treatment and one day after treatment. Bioluminescence signal is detected in the right but not left ovaries of animals. **(C)** When tumor size reached ≥ 50 mm^3 animals were randomized into four

treatment groups and BL- and MR- imaging was performed before treatment and on day1, day 5, day 8 and day 12 post treatment initiation. Fold induction was calculated by normalizing bioluminescence signals to tumor volumes acquired by MRI and pre-treatment values at each time point. Data represents mean ± SEM. **(D)** Representative MR images of animals in each group pre- and two weeks post treatment. **(E)** Percent change in tumor volume as measured by MR imaging. Data represents mean ± SEM. Statistical significance was assessed at a $p<0.05$ (*) using an unpaired Student's t-test. **(F)** Representative images of western blotting analysis for total AKT and pAKT (Ser473) 3 hours post treatment with perifosine of tumors obtained from *Apc*$^{-/-}$, *Pten* $^{-/-}$, *Apopreporter*$^{+}$ animals.

Figure 2.5

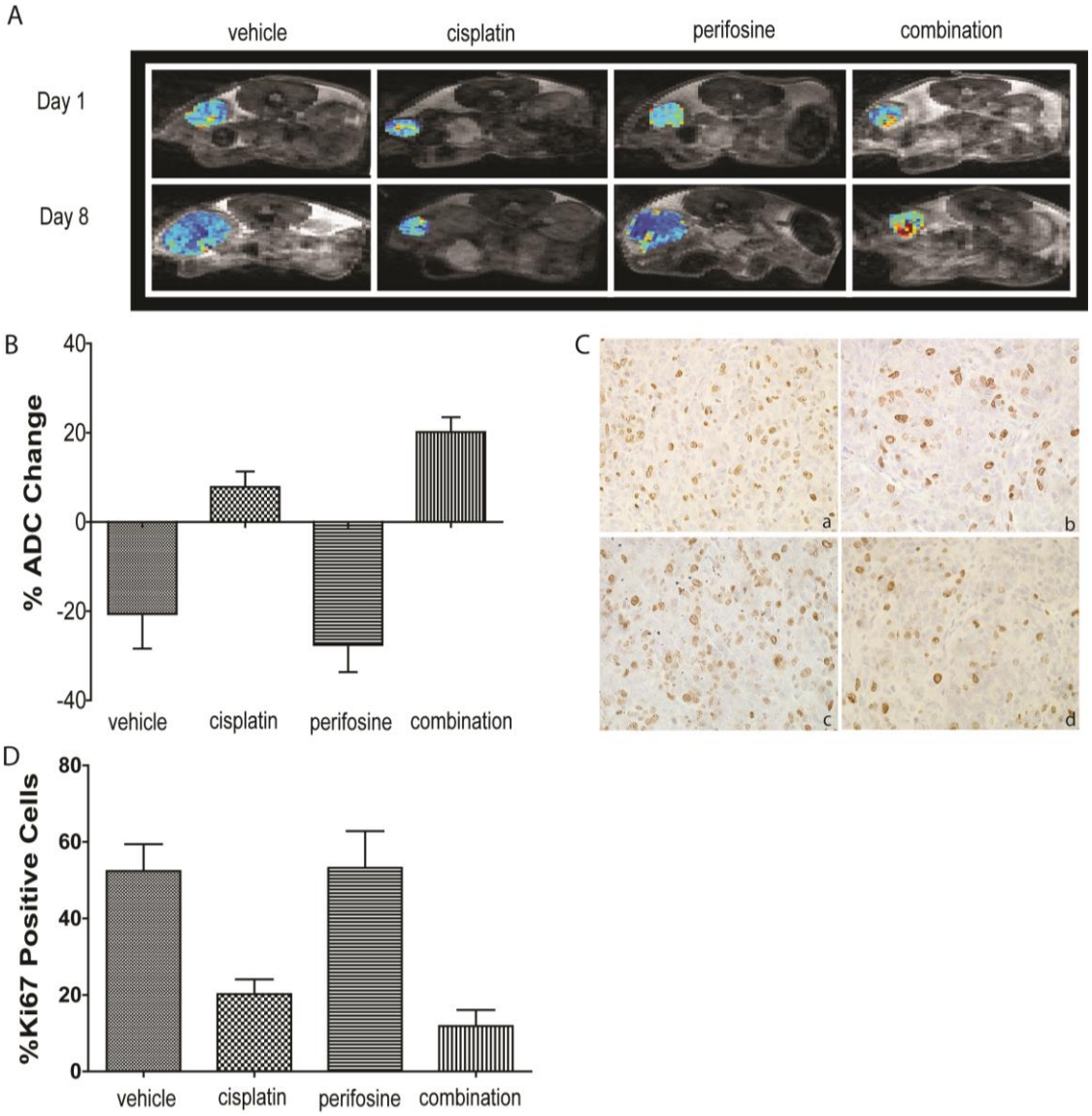

Figure 2.5 Diffusion-weighted MRI serves as an imaging surrogate for treatment response in OEA. (A) Representative ADC maps of tumor bearing *Apc*$^{-/-}$, *Pten* $^{-/-}$, *Apopreporter*$^{+}$ animals treated with vehicle, cisplatin, perifosine or combined treatment before treatment and one week after treatment. **(B)** Percent change of ADC values and statistical analysis of each treatment group after one week of treatment. Mean is plotted± SEM. **(C)** Representative images of Ki67 staining of tumor tissues from each treatment group after one week of treatment: (a) vehicle, (b) cisplatin, (c) perifosine and (d) combination. **(D)** Percent change of Ki67 stained cells of each treatment group with statistical analysis. Mean is plotted ± SEM.

2.6 References

1. Siegel, R., D. Naishadham, and A. Jemal, *Cancer Statistics, 2012.* Ca-a Cancer Journal for Clinicians, 2012. **62**(1): p. 10-29.
2. Jemal, A., et al., *Cancer statistics, 2010.* CA Cancer J Clin, 2010. **60**(5): p. 277-300.
3. Seidman, J.D., et al., *The histologic type and stage distribution of ovarian carcinomas of surface epithelial origin.* International Journal of Gynecological Pathology, 2004. **23**(1): p. 41-44.
4. Rosen, D.G., et al., *Ovarian cancer: pathology, biology, and disease models.* Front Biosci, 2009. **14**: p. 2089-102.
5. *Integrated genomic analyses of ovarian carcinoma.* Nature, 2011. **474**(7353): p. 609-15.
6. Wu, R., et al., *Mouse model of human ovarian endometrioid adenocarcinoma based on somatic defects in the Wnt/beta-catenin and PI3K/Pten signaling pathways.* Cancer Cell, 2007. **11**(4): p. 321-33.
7. Bast, R.C., Jr., B. Hennessy, and G.B. Mills, *The biology of ovarian cancer: new opportunities for translation.* Nat Rev Cancer, 2009. **9**(6): p. 415-28.
8. Kelland, L., *The resurgence of platinum-based cancer chemotherapy.* Nature Reviews Cancer, 2007. **7**(8): p. 573-584.
9. Agarwal, R. and S.B. Kaye, *Ovarian cancer: strategies for overcoming resistance to chemotherapy.* Nat Rev Cancer, 2003. **3**(7): p. 502-16.
10. Siddik, Z.H., *Cisplatin: mode of cytotoxic action and molecular basis of resistance.* Oncogene, 2003. **22**(47): p. 7265-7279.
11. Cheng, J.Q., et al., *The Akt/PKB pathway: molecular target for cancer drug discovery.* Oncogene, 2005. **24**(50): p. 7482-7492.
12. Stronach, E.A., et al., *DNA-PK mediates AKT activation and apoptosis inhibition in clinically acquired platinum resistance.* Neoplasia, 2011. **13**(11): p. 1069-80.
13. Wu, R., et al., *Preclinical testing of PI3K/AKT/mTOR signaling inhibitors in a mouse model of ovarian endometrioid adenocarcinoma.* Clin Cancer Res, 2011. **17**(23): p. 7359-72.
14. Gross, S. and D. Piwnica-Worms, *Molecular imaging strategies for drug discovery and development.* Current Opinion in Chemical Biology, 2006. **10**(4): p. 334-342.
15. Galban, C.J., et al., *Applications of molecular imaging.* Prog Mol Biol Transl Sci, 2010. **95**: p. 237-98.
16. Zhang, L., et al., *Molecular imaging of Akt kinase activity.* Nat Med, 2007. **13**(9): p. 1114-9.
17. Coppola, J.M., B.D. Ross, and A. Rehemtulla, *Noninvasive imaging of apoptosis and its application in cancer therapeutics.* Clin Cancer Res, 2008. **14**(8): p. 2492-501.
18. Suzuki, A., et al., *T cell-specific loss of Pten leads to defects in central*

and peripheral tolerance. Immunity, 2001. **14**(5): p. 523-34.
19. Shibata, H., et al., *Rapid colorectal adenoma formation initiated by conditional targeting of the Apc gene.* Science, 1997. **278**(5335): p. 120-3.
20. Anton, M. and F.L. Graham, *Site-specific recombination mediated by an adenovirus vector expressing the Cre recombinase protein: a molecular switch for control of gene expression.* J Virol, 1995. **69**(8): p. 4600-6.
21. Dinulescu, D.M., et al., *Role of K-ras and Pten in the development of mouse models of endometriosis and endometrioid ovarian cancer.* Nat Med, 2005. **11**(1): p. 63-70.
22. Flesken-Nikitin, A., et al., *Induction of carcinogenesis by concurrent inactivation of p53 and Rb1 in the mouse ovarian surface epithelium.* Cancer Res, 2003. **63**(13): p. 3459-63.
23. Kondapaka, S.B., et al., *Perifosine, a novel alkylphospholipid, inhibits protein kinase B activation.* Molecular Cancer Therapeutics, 2003. **2**(11): p. 1093-1103.
24. Bozulic, L., et al., *PKB alpha/Akt1 acts downstream of DNA-PK in the DNA double-strand break response and promotes survival.* Molecular Cell, 2008. **30**(2): p. 203-213.
25. Frese, K.K. and D.A. Tuveson, *Maximizing mouse cancer models.* Nat Rev Cancer, 2007. **7**(9): p. 645-58.
26. Becher, O.J. and E.C. Holland, *Genetically engineered models have advantages over xenografts for preclinical studies.* Cancer Res, 2006. **66**(7): p. 3355-8, discussion 3358-9.
27. Hamstra, D.A., A. Rehemtulla, and B.D. Ross, *Diffusion magnetic resonance imaging: a biomarker for treatment response in oncology.* J Clin Oncol, 2007. **25**(26): p. 4104-9.
28. Galban, S., et al., *DW-MRI as a biomarker to compare therapeutic outcomes in radiotherapy regimens incorporating temozolomide or gemcitabine in glioblastoma.* PLoS One, 2012. **7**(4): p. e35857.
29. Galluzzi, L., et al., *Molecular mechanisms of cisplatin resistance.* Oncogene, 2012. **31**(15): p. 1869-1883.
30. Stommel, J.M., et al., *Coactivation of receptor tyrosine kinases affects the response of tumor cells to targeted therapies.* Science, 2007. **318**(5848): p. 287-90.
31. Sancho-Martinez, S.M., et al., *Necrotic concentrations of cisplatin activate the apoptotic machinery but inhibit effector caspases and interfere with the execution of apoptosis.* Toxicol Sci, 2011. **122**(1): p. 73-85.
32. Yip, H.T., et al., *Cisplatin-induced growth arrest of head and neck cancer cells correlates with increased expression of p16 and p53.* Arch Otolaryngol Head Neck Surg, 2006. **132**(3): p. 317-26.
33. Alessi, D.R., et al., *Characterization of a 3-phosphoinositide-dependent protein kinase which phosphorylates and activates protein kinase*

Balpha. Curr Biol, 1997. **7**(4): p. 261-9.
34. Sarbassov, D.D., et al., *Phosphorylation and regulation of Akt/PKB by the rictor-mTOR complex.* Science, 2005. **307**(5712): p. 1098-101.
35. Feng, J., et al., *Identification of a PKB/Akt hydrophobic motif Ser-473 kinase as DNA-dependent protein kinase.* J Biol Chem, 2004. **279**(39): p. 41189-96.
36. Viniegra, J.G., et al., *Full activation of PKB/Akt in response to insulin or ionizing radiation is mediated through ATM.* Journal of Biological Chemistry, 2005. **280**(6): p. 4029-4036.
37. Abedini, M.R., et al., *Akt promotes chemoresistance in human ovarian cancer cells by modulating cisplatin-induced, p53-dependent ubiquitination of FLICE-like inhibitory protein.* Oncogene, 2010. **29**(1): p. 11-25.
38. Yang, X., et al., *Akt-mediated cisplatin resistance in ovarian cancer: modulation of p53 action on caspase-dependent mitochondrial death pathway.* Cancer Res, 2006. **66**(6): p. 3126-36.
39. Fraser, M., et al., *p53 is a determinant of X-linked inhibitor of apoptosis protein/Akt-mediated chemoresistance in human ovarian cancer cells.* Cancer Research, 2003. **63**(21): p. 7081-7088.
40. Le, X.F., et al., *Paclitaxel induces inactivation of p70 S6 kinase and phosphorylation of Thr(421) and Ser(424) via multiple signaling pathways in mitosis.* Oncogene, 2003. **22**(4): p. 484-497.
41. Hu, L.M., et al., *Inhibition of phosphatidylinositol 3 '-kinase increases efficacy of paclitaxel in in vitro and in vivo ovarian cancer models.* Cancer Research, 2002. **62**(4): p. 1087-1092.
42. Fu, S.Q., et al., *Perifosine plus docetaxel in patients with platinum and taxane resistant or refractory high-grade epithelial ovarian cancer.* Gynecologic Oncology, 2012. **126**(1): p. 47-53.
43. Chenevert, T.L., et al., *Diffusion magnetic resonance imaging: an early surrogate marker of therapeutic efficacy in brain tumors.* Journal of the National Cancer Institute, 2000. **92**(24): p. 2029-2036.
44. Sala, E., et al., *Advanced Ovarian Cancer: Multiparametric MR Imaging Demonstrates Response- and Metastasis-specific Effects.* Radiology, 2012. **263**(1): p. 149-159.

CHAPTER III

Coevolution of Mesenchymal and Stem Cell Signatures Promotes Therapeutic Resistance in Glioblastoma

Summary

Glioblastoma (GBM) represents the most aggressive malignant primary brain tumor. Radiation (IR) with concomitant and adjuvant temozolomide (TMZ) after surgical resection is the standard of care for newly diagnosed GBM patients. Despite an initial response, most patients succumb to the disease due to the development of resistance such that the median survival is only 15 months. In an effort to delineate the mechanistic basis for resistance to TMZ and IR, we utilized a patient derived intracranial xenograft mouse model coupled with MRI-guided stereotactic biopsy and RNA sequencing. Gene expression profiling of pre-treatment and recurrent tumor biopsy samples revealed a common signaling network underlying therapeutic resistance. The dominant feature of this network was an increased expression of genes involved in the mesenchymal and stem cell phenotype and a decreased expression of genes involved in cell death. TGF-β signaling was identified to be central to each of the mesenchymal/stem cell phenotype and therefore a key player in modulating therapeutic resistance. In support, treatment of tumor bearing animals with a TGF-β inhibitor partially restored the sensitivity to therapy in TZM/IR resistant tumors. This study provides a rationale for clinical trials wherein TGF-β inhibitors can be used in combination with chemoradiotherapy in GBM patients.

3.1 Introduction

Glioblastoma (GBM) is the most aggressive and common malignant glioma [1]. The median survival of GBM patients is only around 15 months, and less than 10% of patients survive beyond 5 years [2]. Current treatment for GBM patients includes surgery followed by temozolomide (TMZ) and radiation (IR) [3]. Although the extent of surgical resection has a strong effect on overall survival and progression free survival [4-6], most GBM patients will go through subsequent radiation and chemotherapy treatment. Yet, a majority of patients experience tumor recurrence in the presence of continued therapy [2], indicating the development of resistance to TMZ and/or IR.

Numerous efforts have been undertaken to delineate the mechanisms of TMZ/IR resistance. Some studies have focused on testing specific hypotheses, such as defects in DNA repair pathways. One prominent factor in TMZ resistance is O^6-methylguanine-DNA methyltransferase (MGMT). MGMT is a crucial member in repairing alkylating DNA damage and has often been identified as a predictor of treatment resistance in GBM [7]. However, evidence from *in vivo, in vitro*, and clinical studies has shown that MGMT expression does not always correspond with TMZ sensitivity, suggesting that MGMT is not the sole mechanism of treatment resistance [8-11]. Other studies have utilized genomic data and bioinformatics tools to identify genes associated with poor patient outcomes or treatment response [12-14], which could be potential mediators of TMZ/IR resistance. While these studies identified various predictive or prognostic gene signatures, the role of each individual gene or group of genes is unclear. Consequently, the mechanisms of therapeutic resistance still remain elusive. There is an urgent need to combine systematic genomic profiling and functional analysis to understand the mechanisms of TMZ/IR resistance, which will facilitate identification of actionable therapeutic targets in GBM.

In this study, we performed RNA sequencing in pre-treatment and recurrent tumor biopsy samples from a patient derived xenograft mouse model, where we identified a fine-tuned network underlying therapeutic resistance. In all recurrent cases, the expression of mesenchymal and stem cell genes was upregulated while the expression of cell death genes was downregulated. Inhibiting TGF-β signaling reduced the expression of both mesenchymal and stem cell genes and partially

restored TMZ/IR sensitivity. These findings establish TGF-β signaling as a promising therapeutic target against TMZ/IR resistance.

3.2 Methods

Patient derived primary neurosphere culture

Low passage, patient derived primary GBM neurosphere cells have been previously described [15], and were maintained in neurosphere medium composed of DMEM/F12 medium (#11320-033, Life Technologies, Carlsbad, CA) plus N2 supplement(#17502-048, Life Technologies, Carlsbad, CA), 0.5mg/ml BSA (#A4919, Sigma-Aldrich Co., St. Louis, MO), 25μg/ml Gentamicin (#15750-060, Life Technologies, Carlsbad, CA), 0.5% antibiotic/antimycotic (#15240-096, Life Technologies, Carlsbad, CA), 20ng/ml bFGF and 20 ng/ml EGF (#100-15 and #100-18B, PeproTech, Rocky Hill NJ).

Intracranial Implantation

Cultured neurosphere cells were dissociated and suspended in DMEM/F12 medium, and implanted intracranially into five-week-old Athymic Nude Foxn1^{nu} mice (Harlan Laboratories, Indianapolis, IN). Mice were anesthetized with a ketamine/xylazine (0.1/0.02mg/kg) mixture and the head surface was prepared with topical antiseptic solution (70% ethanol). A 1cm incision was made 2mm to the right of the midline and 1 mm retro-orbitally. The skull was exposed with a cotton-tip applicator and a handhold drill was used to drill a hole 1.5 mm anterior to bregma and 0.5 mm right to the midline. A 1ul cell suspension of 3x10^5 cells was injected using a 30-gauge needle attached to a Hamilton syringe and a stereotactic fixation device (Stoelting, Wood Dale, IL) at a depth of 1.5 mm underneath the skull surface. The hole was covered using bonewax (#W810, Ethicon, Somerville, NJ) and the incision was sealed using Vetbond (#1469SB, Vetbond, 3M, Saint Paul, MN). 100ul of Carprofen was subcutaneously injected following the surgical procedure as pain reliever. Mice were monitored and retained in the study until they displayed any physical or neurological symptoms due to tumor burden.

Xenograft implantation

Five-week-old five-week-old Athymic Nude Foxn1^{nu} mice were inoculated subcutaneously with 5 × 10^6 dissociated neurosphere cells into the flank on each side. Each injection contained a total volume of 200 μL cell suspension in 50%

MEM/F12 medium mixed with 50% BD Matrigel™ Basement Membrane Matrix (#356234, Becton, Dickinson and Company, East Rutherford, NJ). Caliper measurements were conducted weekly to determine tumor volumes using the formula V = (length/2) × (width2).

Magnetic resonance imaging (MRI)

MRI scans were performed on a 9.4T, 16 cm horizontal bore (Agilent Technologies, Inc., Santa Clara, CA) Direct Drive system with a mouse surface receive coil (m2m Imaging, Corp., Cleveland, OH) actively decoupled to a whole-body volume transmit coil (Rapid MR International, LLC., Columbus, OH). 50ul of 0.5M gadolinium-DTPA (Magnevist; Bayer Healthcare Pharmaceuticals, Montville, NJ) was injected intraperitoneal to each mouse 5 minutes before the mouse was anesthetized with a 1-2% isoflurane/air mixture. During MRI, a heated air system (Air-Therm Heater, World Precision Instruments, Sarasota, FL) was used to maintain animal body temperature. T1-weighted images were acquired for each animal with the following parameters: repetition time/echo time = 510/15ms, field of view = 20 x 20mm^2, matrix size = 128 x 128, slice thickness = 0.5mm, 25 slices, and two averages. Mice were screened for tumor burden every week starting the six week post intracranial implantation. Mice are randomized into different treatment groups when tumor sizes reached approximately 20-30 mm^3. Weekly MRI was continued during treatment.

Image reconstruction and analysis

Image reconstruction was completed by an in-house software. Tumors are manually contoured along the enhancing rim on the T1-weighted images, from which tumor volume was calculated.

Stereotactic biopsy

Coordinates for MRI-guided biopsy were determined by a fiducial markers attached to the whole-body volume transmit coil and VnmrJ software (Agilent Technologies, Inc., Santa Clara, CA). The mouse was moved to a stereotactic station along with the whole-body volume transmit coil. A 1cm incision was made and the skull was exposed with cotton-tip applicators. After biopsy location was recovered using the fiducial markers, a burr hole was drilled and a 22GA x 3 7/8” needle (#54722, Inrad, Kentwood, MI) attached to a vacuum syringe was inserted into the tumor. Biopsy tissues were dissociated and cultured in NMGF medium immediately. Holes covered

using bonewax and incisions were sealed using Vetbond. 100ul of Carprofen was subcutaneously injected following the surgical procedure.

Treatment

For mice bearing intracranial tumors, animals were randomized into treatment groups once their tumor volume reached 20-30mm^3 by MRI evaluation. Temozolomide (LKT Laboratories, St Paul, MN) was suspended in Ora‐Plus suspending vehicle (#0574-0303-16, Rotterdam, Netherlands) and administered to animals (66mg/kg) orally daily for five days per week. Cranial irradiation was carried out one hour post temozolomide treatment. Mice were restrained in a home-made plastic restraining device. A lead shield was used so that only the head was exposed to radiation using a Kimtron INC-320 orthovoltage irradiator (Kimtron Medical, Oxford, CT). A total of 20Gy radiation was delivered to each animal at 2 Gy/day for ten days. Maintenance temozolomide was delivered orally three times week every other week from the third week till animals reach moribund. For mice with subcutaneous flank tumors, animals were randomized into study groups when subcutaneous tumors reached an approximate volume of 300 mm^3. Temozolomide and radiation were delivered via similar administration routes and treatment schedules as described above. Radiation was targeted at local tumor sites with a lead shield. LY2109761 (AbMole, Houston, TX) was reconstituted using Ora‐Plus suspending vehicle and delivered to animals twice per day for five days every week for two weeks. For animals treated with temozolomide, LY2109761 and radiation, LY2109761 was administered one hour before radiation along with TMZ and six hours post radiation treatment.

RNA sequencing and data analysis

Pre-treatment and post-recurrence tumor biopsies were collected and cultured in NMGF medium for 3 passages. Neurosphere cells (1x10^5) were used for RNA extraction. Total RNA was extracted using TRIzol (#10296010, Life Technologies, Carlsbad, CA) and ethanol precipitated per manufacturer's instructions. RNAseq library preparation and sequencing were completed by the DNA sequencing core at the University of Michigan. Specifically, 30~45 million 50nt-single-end reads were obtained from each sample with an estimated 20~30x sequencing depth. Sequencing reads were aligned to a human reference genome (hg19) using Tophat

2.0 and the transciptome was assembled by cufflinks 2.1.1 [16, 17]. Differential expression analysis was performed using the EdgeR 3.0 package in R 3.0.3 [18-21]. Genes with FDR < 0.05 were chosen for further pathway enrichment analysis using David Bioinformatics Resources program and GENEmania [22-24].

Western Blot

Cells were lysed with NP-40 lysis buffer (1% NP40, 150 mmol/L NaCl, and 25 mmol/L Tris, pH 8.0) supplemented with protease inhibitors (#11697498001, Complete Protease Inhibitor Cocktail, Roche, Basel, Switzerland) and phosphatase inhibitors (#04906845001, PhosSTOP, Roche, Basel, Switzerland). Concentration of protein was determined using DC Protein Assay Kit II (#500-0112, Bio-Rad, Hercules, CA). Equal amount of protein was loaded in each lane and resolved by 4% to 12% gradient or 10% NuPAGE Bis-Tris gels (#NP0322BOX, #WG1202BOX, Life Technologies, Carlsbad, CA). Proteins were transferred to 0.2-μm nitrocellulose membrane (#162-0112, Bio-Rad, Hercules, CA Membranes were incubated overnight at 4°C with primary antibodies after blocking, followed by incubation with appropriate horseradish peroxidase (HRP)–conjugated secondary antibody at room temperature for 1 hour. Amersham ECL Prime Western Blotting Detection Reagent (#RPN2236, GE Healthcare&Life Sciences, Fairfield, CT) was used to detect the activity of peroxidase according to the manufacturer's protocol. Antibodies raised against Cdk6, Thy1, Sox2, Gli2 were purchased from Cell Signaling Technology (#3136, #9798, #2748, #2585, Beverly, MA). ZEB2 antibody was purchased from Santa Cruz (#sc-48789, Dallas, Texas) and VCAN, GAPDH-HRP conjugated antibodies were purchased from Abcam (#ab19345, #ab9385 Cambridge, England).

qRT-PCR

Total RNA from neurosphere cells was extracted as described in RNA sequencing session. 2.5ug RNA was subjected to reverse transcription using SuperScript® III First-Strand Synthesis System (#18080-051, Life Technologies, Carlsbad, CA). qPCR was performed in triplicates using the SYBR Premix Ex Taq II (Tli RNase H Plus)(# RR820L, Clontech, Mountain View, CA) and Mastercycler ep realplex^2 (Eppendorf, Hamburg, Germany). The qPCR program comprised 95°C for 60s and 40 cycles of 95°C for 5s, 60°C for 30s. Relative mRNA expression was calculated

based on Comparative C Method (ΔΔC Method) embedded in the Eppendorf Realplex software. The list of primers is included in the table 3.1.

3.3 Results

Recurrence of GBM in the presence of IR/TMZ treatment

Low-passage neurosphere cells were implanted intracranially into immunodeficient mice. MR imaging was performed weekly to monitor tumor growth. Once tumor volumes reached 20mm^3, animals were randomized into three study groups. In addition to a control group, mice were treated with TMZ (5 days/week at 66mg/kg, orally) and IR (5 days/week at 2Gy/day) for two weeks (TMZ/IR). In a third group, mice received the same treatment, but were given adjuvant TMZ every other week (3 days/week at 66mg/kg, orally) after completion of TMZ/IR treatment (TMZ/IR+TMZ, summarized in Figure 3.1A). TMZ/IR was effective in inducing a substantial therapeutic response during the first two weeks of treatment wherein control animals exhibited a significant increase in tumor volume. Despite an initial response, all animals had recurrence with or without adjuvant TMZ. Compared to the TMZ/IR group, adjuvant TMZ resulted in a significantly delayed tumor recurrence (10 weeks compared to 6 weeks, Figure 3.1B and C).

An MRI-guided stereotactic intracranial biopsy procedure was used to obtain pre-treatment tumor tissue when tumor volumes reached 20mm^3 (Figure 3.6). Additionally, viable tumor tissue was also obtained from moribund animals that exhibited tumor recurrence. In order to expand tumor tissue and to eliminate contaminating normal mouse brain tissue, samples were cultured as neurospheres for less than three passages and used for subsequent molecular analysis.

Recurrent tumors are resistant to TMZ/IR treatment

To confirm the therapeutic resistant phenotype of recurrent tumors, pre-treatment and recurrent biopsy tumor cells were implanted into the flanks of immunodeficient mice. Animals were treated with two-week concomitant TMZ/IR followed by adjuvant TMZ. As shown in Figure 3.2A, tumors derived from pre-treatment biopsy cells (named as pre-treatment tumors hereinafter) and tumors derived from recurrent tumor cells (named as recurrent tumors hereinafter) grew at a similar rate in the absence of treatment. In response to treatment, pre-treatment tumors demonstrated

a significant delay in tumor growth while recurrent tumors exhibited relative resistance to TMZ/IR treatment wherein pre-treatment tumors exhibited a 50% decrease in tumor volume, while recurrent tumors exhibited a 750% increase in tumor volume (Figure 3.2A). To confirm these findings in the appropriate tumor microenvironment, intracranial tumors were established using pre-treatment biopsy cells or recurrent tumor cells. Mice were enrolled into an untreated control group or a treatment group (TMZ/IR + TMZ) (Figure 3.2B). In agreement with the results from flank tumors, intracranial recurrent tumors were more resistant to the combination therapy than pre-treatment tumors, wherein the mean tumor volume was 106.7mm^3 in recurrent tumors compared to 30.1 mm^3 in pre-treatment tumors after two-week treatment of TMZ/IR. Median survival of mice bearing pre-treatment tumors was 11.9 weeks in response to TMZ/IR+TMZ treatment (Figure 3.2C). In contrast, mice with recurrent tumors had a decreased median survival of 7 weeks in response to treatment, further confirming that these samples were inherently resistant to the combination therapy.

RNA sequencing reveals functional gene clusters in recurrent tumors

In order to delineate the mechanistic basis for the observed resistance to therapy in recurrent samples, the gene expression profiles of three independent pre-treatment biopsies and four recurrent samples were evaluated using RNA sequencing. 1159 genes were found to be significantly differentially expressed between the two groups (FDR<0.05, Figure 3.3A). Among the 1159 differentially expressed genes, 645 genes were upregulated in recurrent tumor samples while 514 genes were downregulated. Unsupervised clustering analysis showed that each of the independent replicate pre-treatment biopsies and recurrence samples had a similar gene expression pattern (Figure 3.3A). Moreover, the gene expression profiles of each pre-treatment sample closely resembled that of the original patient derived neurospheres (Figure 3.7), demonstrating that gene expression profiles did not drift significantly during *in-vitro* expansion or upon intracranial tumor growth.

We then used David functional annotation analysis to identify common cellular events that underlie these changes in gene expression. Twenty functional clusters within the upregulated genes and thirteen functional clusters in downregulated genes were identified (FDR<0.05). Consolidation of clusters having the same genes under

different functional annotations yielded ten upregulated gene clusters and seven downregulated gene clusters (Figure 3.3B). Of the seven downregulated clusters, six were associated with apoptosis and cell death (Figure 3.3B). Functional clusters involved in cell adhesion, neuronal differentiation/development, and cellular morphogenesis were dominant in the upregulated genes (Figure 3.3B).

To evaluate the clinical significance of these differentially expressed genes, a metagene score was created based on the average gene expression level of 54 cell adhesion genes. We selected GBM patients treated with TMZ and IR from TCGA (the Cancer Genome Atlas) database and ranked them based on their metagene scores. Overall survival and tumor-progression-free days were evaluated in the patients with a high metagene score (upper 1/3 total selected patients) and those with a low metagene score (lower 1/3 of total selected patients). As shown in figure 3.3D, patients with a high cell adhesion metagene score had worse clinical outcome, both in terms of survival days and tumor-progression-free days, supporting the experimental mouse derived results that an increase in a cell adhesion signature correlates with a therapeutic resistant phenotype.

Mesenchymal and stem cells markers are enriched in TMZ/IR resistant tumors

Within the cluster of genes involved in cell adhesion, many, including THY1, ZEB2, VCAN and CDK6, have been implicated in driving cells into a mesenchymal phenotype [14]. There is mounting evidence for the role of signaling pathways that impart a mesenchymal phenotype in mediating therapeutic resistance in GBM [25, 26]. To investigate the significance of these genes in the development of therapeutic resistance, we first conducted studies to validate the RNA sequencing findings. RT-qPCR as well as western blot analysis confirmed an upregulation of a mesenchymal signature (ZEB2, VCAN, THY1 and CDK6) in recurrent tumor samples (Figure 3.4A and 3.4B).

The epithelial to mesenchymal transition has been associated with phenotypic properties of stem cells [27]; hence we investigated the expression of stem cell markers in recurrent tumors. Genes associated with a neuronal stem cell phenotype were also upregulated in recurrent tumors, including Sox2 and Gli2. RT-qPCR and western blot analysis (Figure 3.4C and 3.4D) confirmed increased expression of these two stemness markers. Expression of CD133 has been associated with

stemness in glioblastoma; hence we investigated its expression using FACS analysis. Two of the four recurrent tumors exhibited an enrichment of CD133-positive population compared to pre-treatment samples (Figure 3.4E).

TGF-β signaling mediates expression of mesenchymal/stem cell genes and resistance to TMZ/IR

TGF-β signaling plays a key role in epithelial to mesenchymal transition (EMT) and in maintaining stem-like cell populations [28-31]. Signaling network and protein interaction analysis found that 21/63 genes within the cell adhesion cluster were associated with the TGF-β signaling pathway (Figure 3.5A). We utilized LY2109761, an inhibitor of TGF-β signaling, to investigate the role of TGF-β signaling in modulating mesenchymal phenotype and an associated stem cell phenotype in GBM.

Animals bearing flank pre-treatment tumors and recurrent tumors were randomized into four groups:: a untreated group, a TMZ/IR group where mice were treated with TMZ (5 days/week at 66mg/kg) and IR (5 days/ week at 2Gy) for two weeks followed by TMZ (3 days/week at 66mg/kg) every other week, a LY2109761 group where mice received 50mg/kg LY2109761 twice every day (5 days/week for the first two weeks followed by 3 days/week every other week), and a TMZ/IR/LY2109761 group where the animals were treated with a combination of the three aforementioned treatment modules. As shown in Figure 3.5B, western blotting of treated recurrent tumor tissues showed that LY2109761 significantly decreased the expression levels of ZEB2, VCAN, THY1, CDK6, SOX2 and GLI2, even in the presence of TMZ/IR, demonstrating the key role of the TGF-β signaling pathway in regulating mesenchymal and stem cells markers. Furthermore, as a single agent, LY2109761 failed to show a significant benefit in preventing tumor progression in both pre-treatment and recurrent tumors. Combination of TMZ/IR with LY2109761 did not show significantly enhanced efficacy compared to TMZ/IR alone in tumors derived from pre-treatment samples. In contrast, recurrent tumors exhibited partially enhanced response to TMZ/IR/LY2109761 treatment, compared to either LY2109761 or TMZ/IR treatment alone (Figure 3.5C).

3.4 Discussion

Resistance to TMZ/IR is the leading cause of treatment failures in GBM. In this study, we investigated the mechanisms of therapeutic resistance in GBM using RNA sequencing and biochemical assays in a clinically relevant mouse model. By comparing the gene expression patterns in pre-treatment tumor biopsy samples and recurrent tumor samples, we identified a mutual network underlying TMZ/IR resistance. This network is dominated by an elevated expression of mesenchymal/stem cell markers and a decreased expression of genes related to cell death. We showed that the TGF-β signaling pathway played a critical role in orchestrating the expression of mesenchymal/stem cell markers and inhibition of the TGF-β signaling pathway partially reversed TMZ/IR resistance.

In order to recapitulate the genomic complexity of GBM, we utilized a patient derived xenograft model that preserves key genetic alterations in the original tumors [32]. A MRI-guided stereotactic biopsy procedure was established to minimize non-therapy-induced variations in pre-treatment and recurrent samples. We found that all samples from the pre-treatment or recurrent biopsy tumors exhibited similar gene expression patterns within the same group, which demonstrated the great consistency of the mouse model and the biopsy procedure.

TMZ and IR are the standard of care for GBM patients. Most of the current studies focus on understanding the molecular basis of therapeutic resistance in GBM utilizing either IR or TMZ. Although, it is important to understand the effect of individual treatments [26, 33, 34], these studies do not mimic the emergence of resistance in clinical settings; thus we selected a combination approach according to the clinical standard. We showed that adjuvant TMZ prolonged the overall survival from 7 weeks to 13 weeks, which demonstrated that adjuvant TMZ was effective in exerting selective pressure against tumor recurrence. In addition, TMZ alone and TMZ/IR induced resistant tumors exhibited distinct gene expression patterns (Figure 3.7), suggesting that TMZ/IR and TMZ alone resulted in different treatment response. These data demonstrated that the expression pattern in recurrent tumor indeed reflected effects caused by both TMZ and IR.

By RNA sequencing, our study revealed multiple gene clusters associated with TMZ/IR resistance. Cell death related clusters were dominant in downregulated genes, implying that evading cell death is a critical step in developing TMZ/IR

resistance. Among the upregulated gene clusters, the prevalent clusters were associated with cell adhesion, extracellular matrix organization, and cell morphogenesis. Cell adhesion and extracellular structure organization are essential for physical connections, communication, and mobility of cells [35]. Mesenchymal transition is a process where cells acquire mesenchymal phenotypes, including decreased cell adhesion, enhanced migratory capacity, and remodeling of extracellular matrix [36]. Besides the functional resemblances between mesenchymal transition and the top upregulated gene clusters, we also found enrichment for mesenchymal markers in recurrent tumors, suggesting that the mesenchymal phenotype might be involved in GBM recurrence. In fact, a few studies have suggested that the mesenchymal phenotype is associated with poor outcomes and therapeutic resistance to both conventional therapies and targeted therapies in glioma [14, 26, 37, 38]. For example, Mao *et al.* showed that radiation induced proneural-to-mesenchymal transition in glioma sphere like cultures and the mesenchymal signature was associated with radiation resistance [25]. However, the mechanistic relationship between mesenchymal phenotype and therapeutic resistance is still unclear.

Some studies found that mesenchymal signature genes modulate DNA repair pathways, which might lead to chemoradioresistance. ZEB1 and ZEB2 are two EMT master transcription factors, which are regulated by the TGF-β pathway. ZEB2, which was upregulated in TMZ/IR resistant samples, has been shown to affect ATM/ATR functions in response to DNA damage [39]. ZEB1 promotes radioresistance in breast cancer by regulating stability of CHK1. It also regulates TMZ sensitivity via regulation of MGMT in glioblastoma [40, 41]. These data suggests that mesenchymal transcription factors contribute to TMZ/IR resistance by modulating DNA damage response.

Mesenchymal transition is associated with generation of cancer stem-like cells. Weinberg *et al.* demonstrated that cancer cells possessed high plasticity and epithelial to mesenchymal transition (EMT) generated cancer stem-like cells [27, 42]. THY1, a candidate gene identified in our study, is among the top upregulated membrane proteins during EMT and cells with high expression of THY1 presented stem-like properties [43]. Interestingly, the second top enriched gene cluster in recurrent tumors is related to neuron differentiation, suggesting that neuron stem cell

genes might be involved in therapeutic resistance. Indeed, we identified neural stem cell transcription factors with elevated expression in recurrent tumors, including Sox2. Sox2 is one of the four core transcription factors that are capable of reprogramming differentiated GBM cells into stem-like tumor-propagating cells (TPCs), which drive tumor progression and therapeutic resistance [44]. Meanwhile, our study showed that the fraction of cells expressing CD133, a putative cancer stem-like cell marker, also increased in recurrent tumor samples. Enrichment for a CD133 positive population was shown to promote radioresistance via preferential activation of DNA damage response [45]. Taken together, our findings suggest that the population of stem-like cells was capable of surviving TMZ/IR treatment, which led to tumor recurrence.

The TGF-β signaling pathway is a master regulator of EMT and cancer stem-like cells. It can induce EMT through a number of transcription factors, including Snail, Slug, ZEB1, ZEB2, Twist, Goosecoid, and FOXC2 [36]. These transcription factors execute EMT reprogramming and grant cells mesenchymal phenotypes. Meanwhile, TGF-β signaling plays a critical role in maintaining cancer stem cell population in various types of cancer, including breast cancer, leukemia, and glioblastoma [28-30, 46]. Two groups have independently demonstrated that inhibition of TGF-β pathway caused decreased expression of stem cell markers, compromised neurosphere initiation capability, as well as delayed tumor growth in mice [29, 30]. Here we found that the TGF-β signaling pathway regulated the expression of mesenchymal and stem cell markers and modulated sensitivity to TMZ/IR treatment.

Besides changes at the transcription level, other alterations might also take place at the post-transcription level while developing therapeutic resistance. The methylation status and expression level of MGMT have been implicated in TMZ resistance in multiple studies. Here we found that the MGMT promoter was unmethylated in both the original patient derived neurosphere cells and pre-treatment tumor cells. Not surprisingly, the MGMT promoter of recurrent tumor cells remained unmethylated in recurrent tumor cells (Figure 3.8A). However, MGMT mRNA was moderately upregulated while the protein level increased substantially in recurrent tumor cells (Figure 3.8B&3.8C). Since MGMT participates in repairing TMZ induced DNA alkylation, the elevated level of MGMT protein might contribute to TMZ/IR resistance.

It also suggests that besides MGMT promoter methylation, there might be other mechanisms of MGMT regulation to be discovered.

Overall, we identified a network underpinning therapeutic resistance in GBM, which is dominated by an increased expression of mesenchymal/ stem cell genes and a decreased expression of genes involved in cell death. We also demonstrated that TGF-β signaling regulated mesenchymal/stem phenotype and partially restored the sensitivity to TMZ/IR treatment in GBM. This study provides a rational for clinical investigation of combining TGF-β inhibitors and TMZ/IR in GBM patients. Other potential mechanisms of resistance, including post-transcriptional regulation and regulation of apoptosis, should be investigated and exploited to fully re-sensitize TMZ/IR resistant tumors.

Figure 3.1

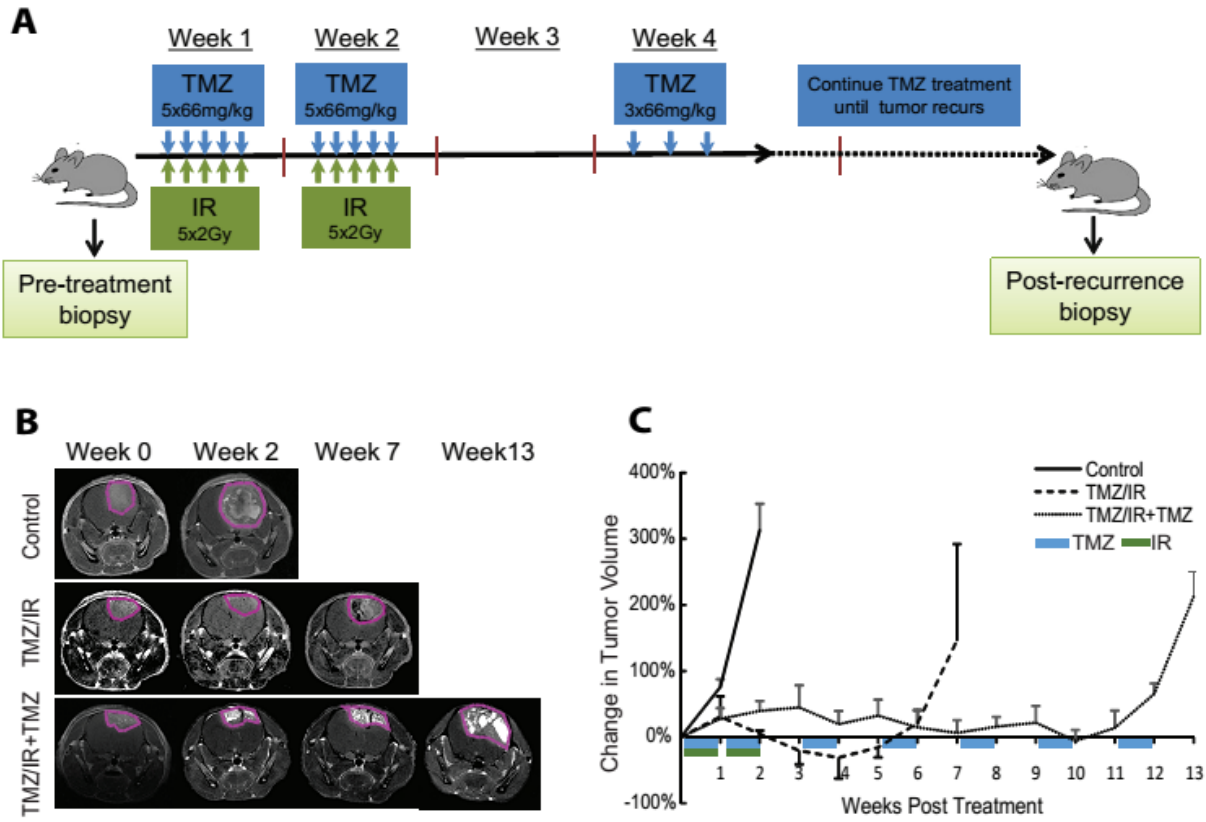

Figure 3.1. Recurrence of GBM in the presence of IR/TMZ treatment. (A) Schematic of experiment design. Mice bearing intracranial tumors were randomized into three groups once the tumor sizes reached about 20mm^3. Besides untreated group (control), one group of mice were treated with concomitant TMZ (5 times/week at 66mg/kg/day) and IR (5 times/week at 2Gy/day) for two weeks followed by adjuvant TMZ every other week (3 times/week at 66mg/kg/day) till animals reached moribund (TMZ/IR+TMZ). A third group only received concomitant TMZ and IR for the first two weeks (TMZ/IR). MRI was performed weekly to monitor tumor growth. Tumor biopsies were obtained pre-treatment and post-recurrence. **(B)** Representative MR images from control, TMZ/IR and TMZ/IR+TMZ groups at week0, week2, week7 and week13. Tumors were contoured along the enhancing rim with purple lines. **(C)** Treatment response quantified by percentage change in tumor volume in untreated, TMZ/IR and TMZ/IR+TMZ groups. Mean+/- SEM was plotted.

Figure 3.2

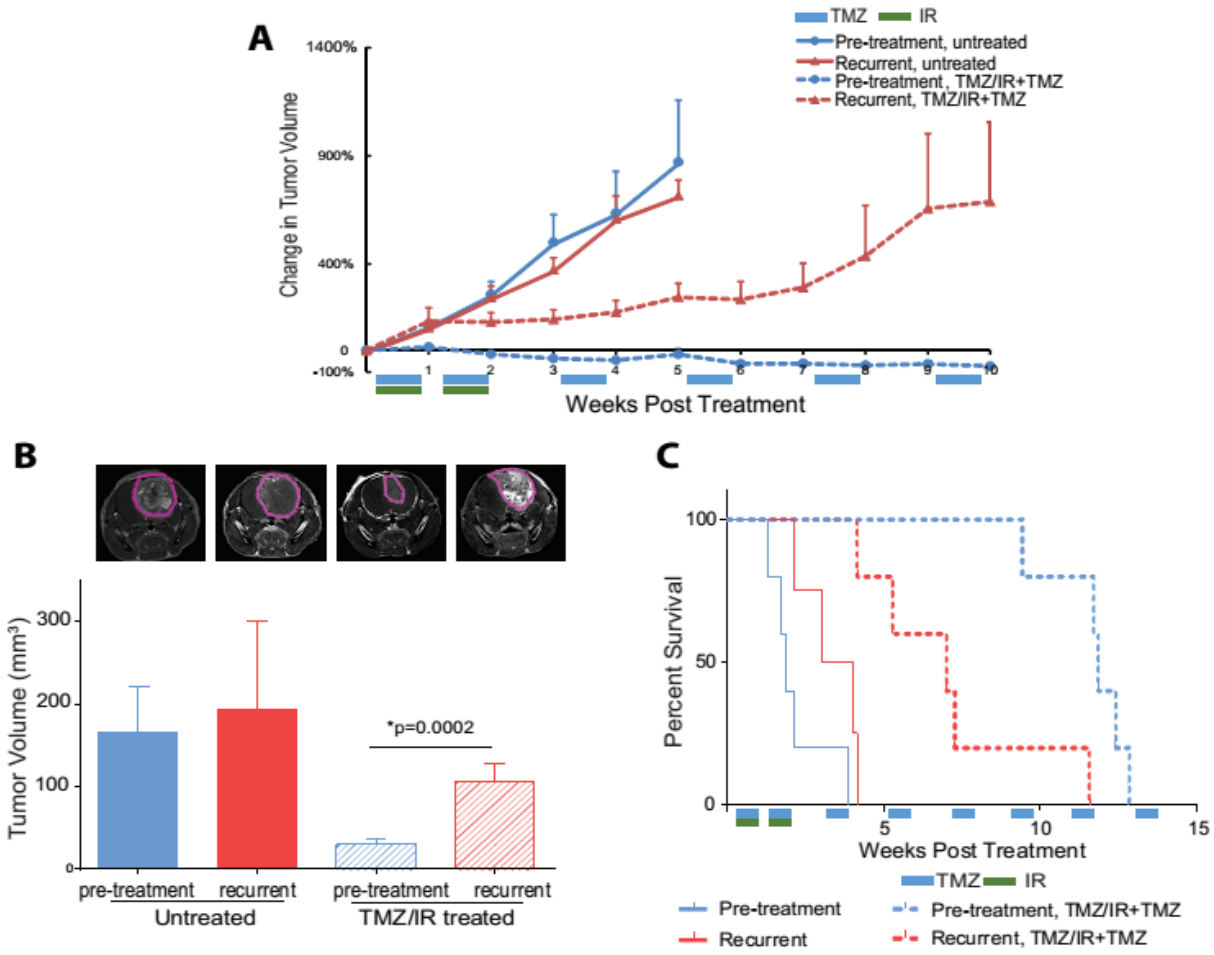

Figure 3.2. Recurrent tumors are resistant to TMZ/IR treatment. (A) Tumor response to TMZ/IR+IR treatment in mice bearing subcutaneous pre-treatment and recurrent tumors. Pre-treatment and recurrent tumor cells were implanted into left and right flanks of immunodeficient mice, respectively. Animals were randomized into untreated group and TMZ/IR+TMZ group where mice were treated with TMZ (5 days/week at 66mg/kg) and IR (5 days/ week at 2Gy) for two weeks followed by TMZ (3 days/week at 66mg/kg) every other week. Color bars indicate treatment modules. Tumor volumes were measured by caliper every week. Data represents mean+/-SEM of percentage change in tumor volume. **(B)** Tumor response to TMZ/IR+IR treatment in mice bearing intracranial pre-treatment and recurrent tumors. Mice were randomly grouped into an untreated group and a treated group where they received TMZ (5 days/week at 66mg/kg) and IR (5 days/ week at 2Gy) followed by TMZ (3 times/week at 66mg/kg) every other week. Tumor growth was monitored by weekly MR imaging. Data represents mean+/-SEM of tumor volumes after two weeks of treatment (lower panel). Representative MR images of corresponding tumors are shown in the upper panel. Tumors were contoured along the enhancing rim with purple lines. **(C)** Kaplan-Meier survival curve of mice bearing intracranial pre-treatment and recurrent tumors with or without TMZ/IR+TMZ treatment. Color bars indicate treatment modules.

Figure 3.3

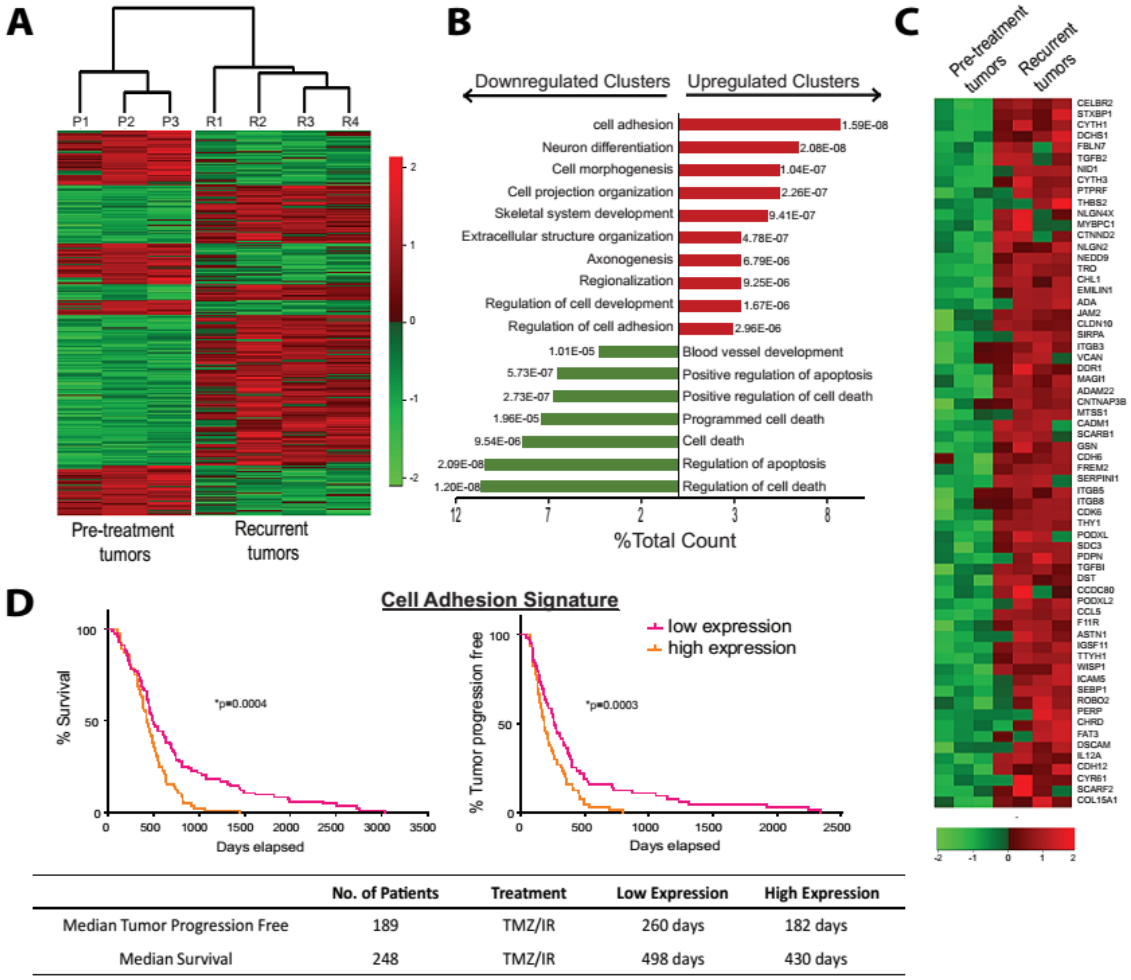

	No. of Patients	Treatment	Low Expression	High Expression
Median Tumor Progression Free	189	TMZ/IR	260 days	182 days
Median Survival	248	TMZ/IR	498 days	430 days

Figure 3.3. RNA sequencing reveals functional gene clusters in recurrent tumors. (A) Heatmap of differentially expressed genes in pre-treatment (P1,P2,P3) and recurrent tumors (R1,R2,R3,R4). **(B)** Functional gene clusters of upregulated and downregulated genes in recurrent tumors. Bar graph represents % total count, which indicates the number of genes in each cluster compared to the total number of upregulated or downregulated genes. P-value of each cluster was labeled next to its column. **(C)** Heatmap of upregulated cell adhesion genes in pre-treatment and recurrent tumor cells. **(D)** Upper panel depicts overall survival (Left) and tumor-progression-free (Right) of GBM patients with high and low expression level of cell adhesion genes. Lower panel shows characteristics of patients and median survival days/tumor-progression-free days in patient groups with high and low expression level of cell adhesion genes.

Figure 3.4

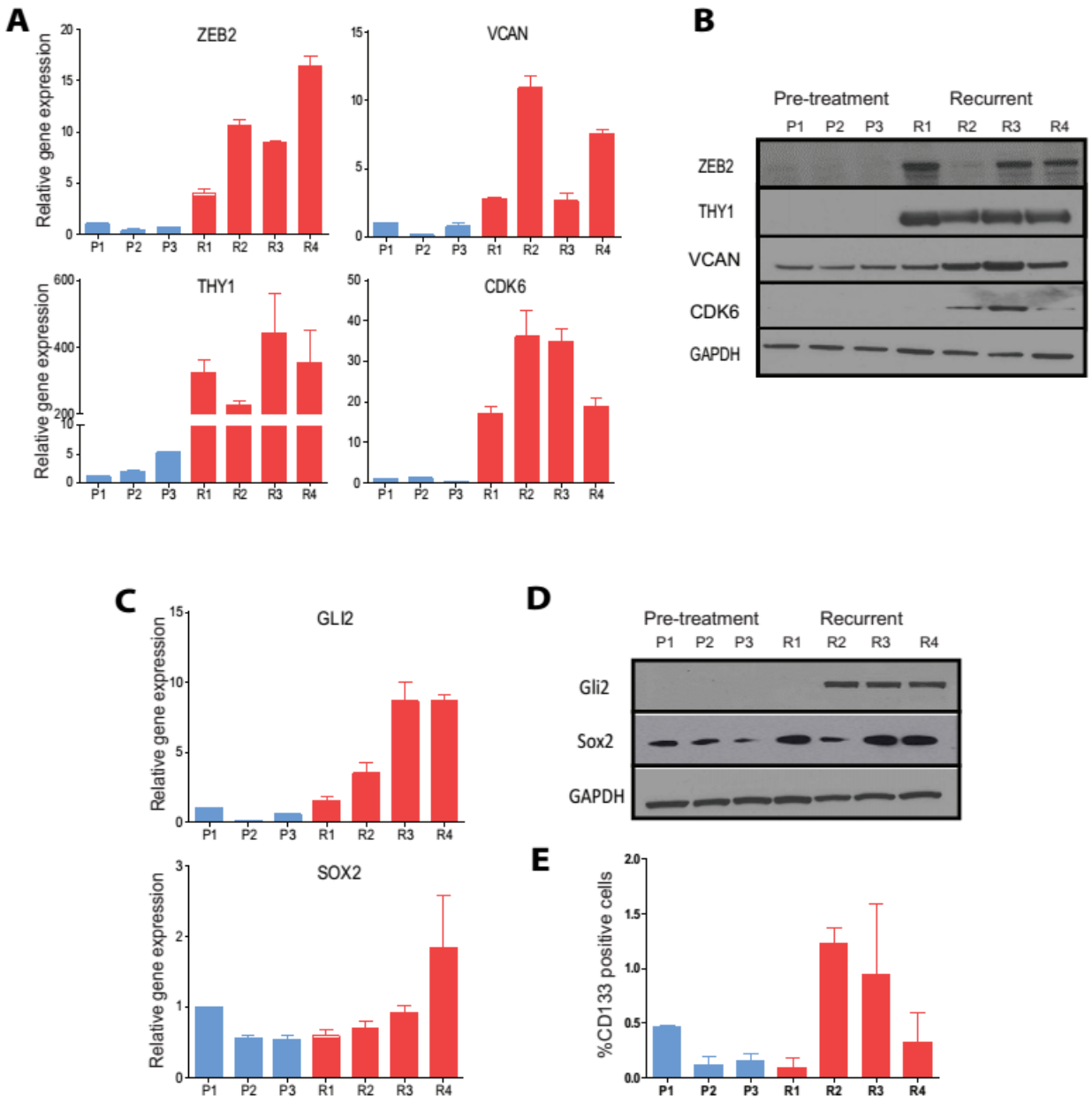

Figure 3.4. Mesenchymal and stem cell signature genes are enriched in recurrent tumor. (A)&(B) RT-qPCR and western blot of mesenchymal signature genes (ZEB2, VCAN, THY1 and CDK6) in pre-treatment and recurrent neurosphere cells. **(C)&(D)** RT-qPCR and western blot of stem cell genes (GLI2 and SOX2) in pre-treatment and recurrent neurosphere cells. **(E)** FACS analysis of CD133 expression in pre-treatment and recurrent neurosphere cells.

Figure 3.5

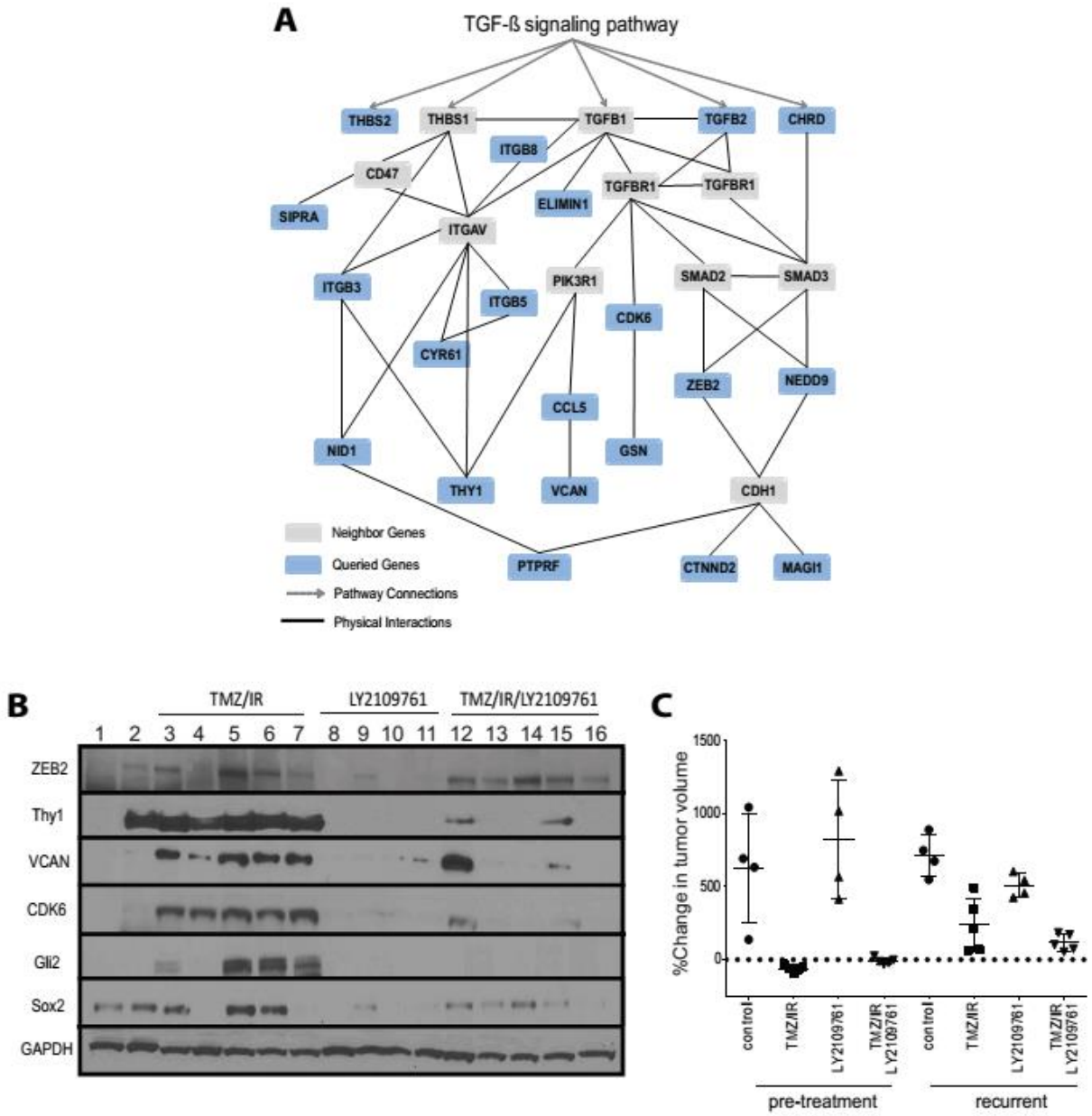

Figure 3.5. TGF-β signaling mediates expression of mesenchymal/stem cell markers and TMZ/IR resistance. (A) Pathway and protein interaction analysis of the TGF-β pathway in cell adhesion genes. **(B)** Western blot of mesenchymal/stem cell signature genes in recurrent tumors treated with TMZ/IR (Lane 3-7), a TGF-β inhibitor (LY2109761, Lane 8-11) or a combination of TMZ/IR and LY2109761 (Lane 12-16). Lane 1&2: pre-treatment and recurrent neurosphere cells without treatment. Pre-treatment and recurrent tumor cells were implanted into left and right flanks of immunedeficient mice, respectively. Animals were randomized into four groups: a untreated group, a TMZ/IR group where mice were treated with TMZ (5 days/week at 66mg/kg) and IR (5 days/ week at 2Gy) for two weeks followed by TMZ (3 days/week at 66mg/kg) every other week, a LY2109761 group where mice received 50mg/kg LY2109761 twice every day (5 days/week for the first two weeks followed by 3

days/week every other week), and a TMZ/IR/LY2109761 group where the animals were treated with a combination of the three aforementioned treatment modules. Tumor samples were collected at 6 weeks post treatment initiation. **(C)** Quantification of % change in tumor volume of pre-treatment and recurrent tumors in response to TMZ/IR, LY2109761 TMZ/IR/LY2109761. Tumor volumes were measured by caliper. Each dot denotes one tumor, and the horizontal line shows mean values of %change in tumor volume of each group.

Figure 3.6

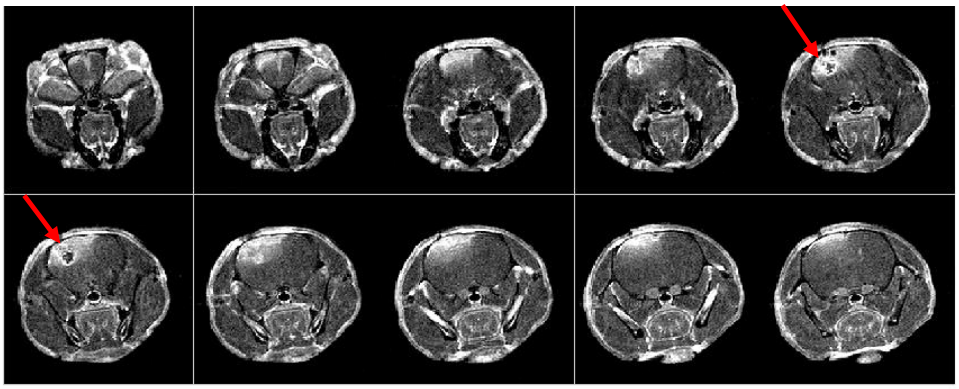

Figure 3.6 Representative images acquired post MRI-guided stereotactic biopsy. The MRI-guided stereotactic biopsy procedure was performed as described in section 3.2 when tumor sizes reached 20mm^3. T1W weighted Gadolinium-enhanced image sequences were acquired post biopsy sampling. Red arrows indicate the biopsy location. Slice thickness: 0.5mm.

Figure 3.7

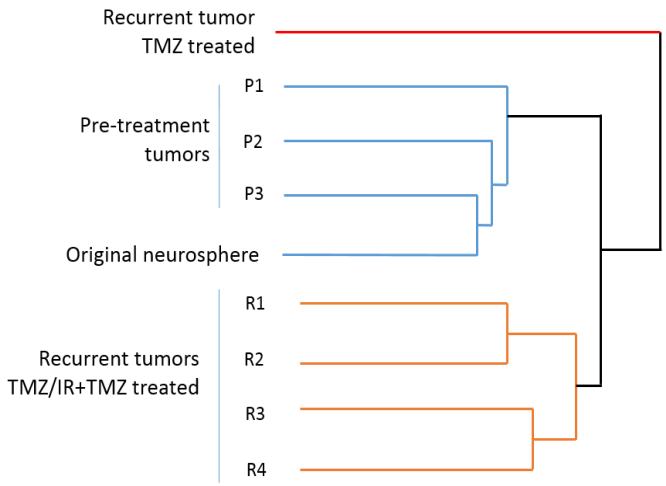

Figure 3.7 Unsupervised clustering analysis of gene expression in pre-treatment and recurrent tumors. Samples include original neurosphere cells derived from the GBM patient, pre-treatment tumor cells (P1, P2, P3), recurrent tumor cells treated with TMZ/IR+TMZ (R1, R2, R3, R4), and recurrent tumor cells treated with TMZ (recurrent tumor, TMZ treated).

Figure 3.8

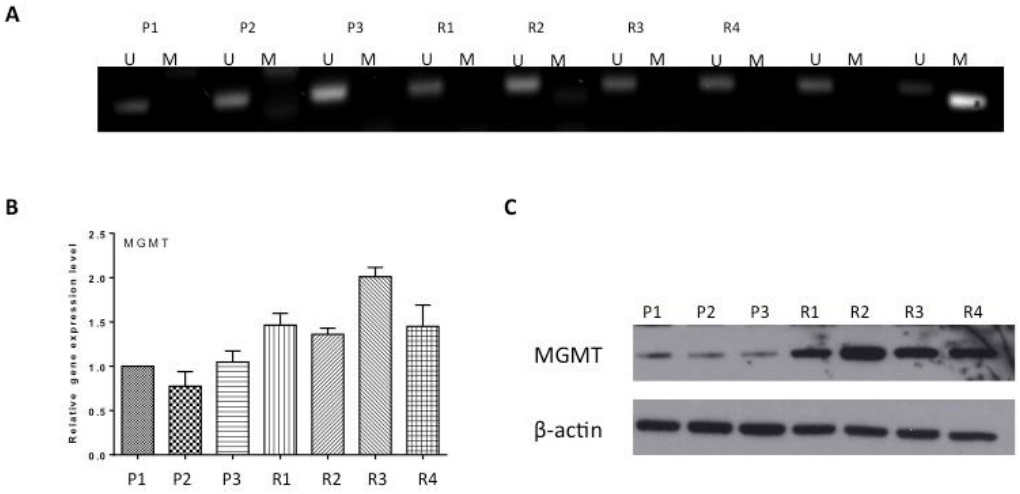

Figure 3.8 Expression of MGMT protein increases in recurrent tumor cells. (A) Methylation specific PCR of pre-treatment and recurrent samples and two neurosphere samples with charactreized MGMT status. **(B)** qRT-PCR of pre-treatment and recurrent samples. **(C)** Western blot of pre-treatment and recurrent samples.

3.5 References

1. Wen, P.Y. and S. Kesari, *Malignant gliomas in adults.* N Engl J Med, 2008. **359**(5): p. 492-507.
2. Stupp, R., et al., *Effects of radiotherapy with concomitant and adjuvant temozolomide versus radiotherapy alone on survival in glioblastoma in a randomised phase III study: 5-year analysis of the EORTC-NCIC trial.* Lancet Oncol, 2009. **10**(5): p. 459-66.
3. Stupp, R., et al., *Radiotherapy plus concomitant and adjuvant temozolomide for glioblastoma.* N Engl J Med, 2005. **352**(10): p. 987-96.
4. Keles, G.E., et al., *Volume of residual disease as a predictor of outcome in adult patients with recurrent supratentorial glioblastomas multiforme who are undergoing chemotherapy.* J Neurosurg, 2004. **100**(1): p. 41-6.
5. Lacroix, M., et al., *A multivariate analysis of 416 patients with glioblastoma multiforme: prognosis, extent of resection, and survival.* J Neurosurg, 2001. **95**(2): p. 190-8.
6. Sanai, N., et al., *An extent of resection threshold for newly diagnosed glioblastomas.* J Neurosurg, 2011. **115**(1): p. 3-8.
7. Ramirez, Y.P., et al., *Glioblastoma multiforme therapy and mechanisms of resistance.* Pharmaceuticals (Basel), 2013. **6**(12): p. 1475-506.
8. Carlson, B.L., et al., *Radiosensitizing Effects of Temozolomide Observed in Vivo Only in a Subset of O6-Methylguanine-DNA Methyltransferase Methylated Glioblastoma Multiforme Xenografts.* International Journal of Radiation Oncology Biology Physics, 2009. **75**(1): p. 212-219.
9. Kitange, G.J., et al., *Induction of MGMT expression is associated with temozolomide resistance in glioblastoma xenografts.* Neuro-Oncology, 2009. **11**(3): p. 281-291.
10. Park, C.K., et al., *The Changes in MGMT Promoter Methylation Status in Initial and Recurrent Glioblastomas.* Transl Oncol, 2012. **5**(5): p. 393-7.
11. Esteller, M., et al., *Inactivation of the DNA-repair gene MGMT and the clinical response of gliomas to alkylating agents.* N Engl J Med, 2000. **343**(19): p. 1350-4.
12. Colman, H., et al., *A multigene predictor of outcome in glioblastoma.* Neuro Oncol, 2010. **12**(1): p. 49-57.
13. Gravendeel, L.A., et al., *Intrinsic gene expression profiles of gliomas are a better predictor of survival than histology.* Cancer Res, 2009. **69**(23): p. 9065-72.
14. Cheng, W.Y., et al., *A multi-cancer mesenchymal transition gene expression signature is associated with prolonged time to recurrence in glioblastoma.* PLoS One, 2012. **7**(4): p. e34705.
15. DeCarvalho, A.C., et al., *Gliosarcoma Stem Cells Undergo Glial and Mesenchymal Differentiation In Vivo.* Stem Cells, 2010. **28**(2): p. 181-190.
16. Trapnell, C., L. Pachter, and S.L. Salzberg, *TopHat: discovering splice junctions with RNA-Seq.* Bioinformatics, 2009. **25**(9): p. 1105-1111.
17. Trapnell, C., et al., *Transcript assembly and quantification by RNA-Seq reveals unannotated transcripts and isoform switching during cell differentiation.* Nature Biotechnology, 2010. **28**(5): p. 511-U174.
18. Robinson, M.D., D.J. McCarthy, and G.K. Smyth, *edgeR: a Bioconductor package for differential expression analysis of digital gene expression data.* Bioinformatics, 2010. **26**(1): p. 139-140.

19. Robinson, M.D. and G.K. Smyth, *Moderated statistical tests for assessing differences in tag abundance.* Bioinformatics, 2007. **23**(21): p. 2881-2887.
20. Robinson, M.D. and G.K. Smyth, *Small-sample estimation of negative binomial dispersion, with applications to SAGE data.* Biostatistics, 2008. **9**(2): p. 321-332.
21. Zhou, X.B., H. Lindsay, and M.D. Robinson, *Robustly detecting differential expression in RNA sequencing data using observation weights.* Nucleic Acids Research, 2014. **42**(11).
22. Huang, D.W., B.T. Sherman, and R.A. Lempicki, *Systematic and integrative analysis of large gene lists using DAVID bioinformatics resources.* Nature Protocols, 2009. **4**(1): p. 44-57.
23. Huang, D.W., B.T. Sherman, and R.A. Lempicki, *Bioinformatics enrichment tools: paths toward the comprehensive functional analysis of large gene lists.* Nucleic Acids Research, 2009. **37**(1): p. 1-13.
24. Warde-Farley, D., et al., *The GeneMANIA prediction server: biological network integration for gene prioritization and predicting gene function.* Nucleic Acids Research, 2010. **38**: p. W214-W220.
25. Mao, P., et al., *Mesenchymal glioma stem cells are maintained by activated glycolytic metabolism involving aldehyde dehydrogenase 1A3.* Proc Natl Acad Sci U S A, 2013. **110**(21): p. 8644-9.
26. Bhat, K.P., et al., *Mesenchymal differentiation mediated by NF-kappaB promotes radiation resistance in glioblastoma.* Cancer Cell, 2013. **24**(3): p. 331-46.
27. Mani, S.A., et al., *The epithelial-mesenchymal transition generates cells with properties of stem cells.* Cell, 2008. **133**(4): p. 704-715.
28. Naka, K., et al., *TGF-beta-FOXO signalling maintains leukaemia-initiating cells in chronic myeloid leukaemia.* Nature, 2010. **463**(7281): p. 676-80.
29. Ikushima, H., et al., *Autocrine TGF-beta signaling maintains tumorigenicity of glioma-initiating cells through Sry-related HMG-box factors.* Cell Stem Cell, 2009. **5**(5): p. 504-14.
30. Anido, J., et al., *TGF-beta Receptor Inhibitors Target the CD44(high)/Id1(high) Glioma-Initiating Cell Population in Human Glioblastoma.* Cancer Cell, 2010. **18**(6): p. 655-668.
31. Lamouille, S., J. Xu, and R. Derynck, *Molecular mechanisms of epithelial-mesenchymal transition.* Nat Rev Mol Cell Biol, 2014. **15**(3): p. 178-96.
32. Lee, J., et al., *Tumor stem cells derived from glioblastomas cultured in bFGF and EGF more closely mirror the phenotype and genotype of primary tumors than do serum-cultured cell lines.* Cancer Cell, 2006. **9**(5): p. 391-403.
33. Kitange, G.J., et al., *Inhibition of histone deacetylation potentiates the evolution of acquired temozolomide resistance linked to MGMT upregulation in glioblastoma xenografts.* Clin Cancer Res, 2012. **18**(15): p. 4070-9.
34. Johannessen, T.C. and R. Bjerkvig, *Molecular mechanisms of temozolomide resistance in glioblastoma multiforme.* Expert Rev Anticancer Ther, 2012. **12**(5): p. 635-42.
35. Schmidmaier, R. and P. Baumann, *ANTI-ADHESION evolves to a promising therapeutic concept in oncology.* Curr Med Chem, 2008. **15**(10): p. 978-90.
36. Kalluri, R. and R.A. Weinberg, *The basics of epithelial-mesenchymal transition.* J Clin Invest, 2009. **119**(6): p. 1420-8.

37. Piao, Y., et al., *Acquired resistance to anti-VEGF therapy in glioblastoma is associated with a mesenchymal transition.* Clin Cancer Res, 2013. **19**(16): p. 4392-403.
38. Verhaak, R.G.W., et al., *Integrated Genomic Analysis Identifies Clinically Relevant Subtypes of Glioblastoma Characterized by Abnormalities in PDGFRA, IDH1, EGFR, and NF1.* Cancer Cell, 2010. **17**(1): p. 98-110.
39. Sayan, A.E., et al., *SIP1 protein protects cells from DNA damage-induced apoptosis and has independent prognostic value in bladder cancer.* Proceedings of the National Academy of Sciences of the United States of America, 2009. **106**(35): p. 14884-14889.
40. Zhang, P., et al., *ATM-mediated stabilization of ZEB1 promotes DNA damage response and radioresistance through CHK1.* Nat Cell Biol, 2014. **16**(9): p. 864-75.
41. Siebzehnrubl, F.A., et al., *The ZEB1 pathway links glioblastoma initiation, invasion and chemoresistance.* Embo Molecular Medicine, 2013. **5**(8): p. 1196-1212.
42. Polyak, K. and R.A. Weinberg, *Transitions between epithelial and mesenchymal states: acquisition of malignant and stem cell traits.* Nature Reviews Cancer, 2009. **9**(4): p. 265-273.
43. Lu, H., et al., *A breast cancer stem cell niche supported by juxtacrine signalling from monocytes and macrophages.* Nat Cell Biol, 2014. **16**(11): p. 1105-17.
44. Suva, M.L., et al., *Reconstructing and Reprogramming the Tumor-Propagating Potential of Glioblastoma Stem-like Cells.* Cell, 2014. **157**(3): p. 580-594.
45. Bao, S.D., et al., *Glioma stem cells promote radioresistance by preferential activation of the DNA damage response.* Nature, 2006. **444**(7120): p. 756-760.
46. Shipitsin, M., et al., *Molecular definition of breast tumor heterogeneity.* Cancer Cell, 2007. **11**(3): p. 259-273.

CHAPTER IV

Conclusion and Future Directions

4.1 Summary of thesis work

Therapeutic resistance is a major challenge in current clinical management of cancer. This thesis sought to dissect the mechanisms of therapeutic resistance by utilizing molecular imaging and integrated genomic analysis in clinically relevant mouse models. New therapeutic strategies are proposed to overcome therapeutic resistance by targeting key regulatory pathways in conjunction with chemotherapy and/or radiotherapy.

The first part of this thesis focused on understanding mechanisms of chemoresistance in ovarian endometrioid adenocarcinoma (OEA). Chemotherapy treatment induced activation of AKT signaling, which resulted in resistance to apoptosis. Inhibition of the AKT pathway enhanced the efficacy of chemotherapy in a genetically engineered mouse model of OEA, which warrants further clinical investigation of the combination of AKT inhibitors and chemotherapies.

Glioblastoma (GBM) is highly refractory to chemoradiotherapy while the resistance mechanism remains unclear. A patient derived xenograft mouse model was established to recapitulate the individual genomics and tumor relapses of GBM. RNA sequencing revealed the gene expression changes associated with chemoradioresistance, including upregulation of mesenchymal and stem cell genes as well as downregulation of apoptosis genes. Additionally, inhibition of the TGF-β signaling pathway, the core regulator of mesenchymal phenotype and cancer stem cells, partially reversed chemoradioresistance.

Overall, this thesis provides new insights of the AKT and TGF-β pathways in mediating therapeutic resistance in cancer. New combination therapy with AKT or TGF-β inhibitor and conventional chemoradiotherapy might benefit a subset of ovarian cancer and glioblastoma patients. While the findings presented here are derived from ovarian cancer and GBM, the discoveries and research methods can be applied to other types of cancer as well.

4.2 Signaling pathways and therapeutic resistance

As discussed in chapter I, targeted therapies have been shown to improve patients' outcomes by regulating essential oncogenic pathways. It also provides possibilities to overcome therapeutic resistance by targeting critical pathways in the development of resistance. In this thesis, the AKT and TGF-β pathways are proved to be the critical players in therapeutic resistance in ovarian cancer and GBM, respectively. Targeting either of the pathways improves the efficacy of chemotherapy and/or radiotherapy, which warrants further clinical investigation of both pathways in cancer patients.

4.2.1 The AKT pathway in chemoresistance in ovarian cancer

The second chapter of this thesis revealed the role of the AKT pathway in mediating chemoresistance in OEA through regulation of apoptosis. The AKT pathway regulates apoptosis via both direct and indirect mechanisms. For example, it can inactivate transcription factor FoxO family, thus inhibiting several pro-apoptotic factors. It can also directly phosphorylate and inactivate pro-apoptotic proteins such as BAD [1]. In the case of ovarian cancer, Abedini *et al.* showed that activation of the AKT pathway inhibited cisplatin-induced, p53-dependent FLIP ubiquitination and thus inhibited apoptosis, conferring chemoresistance in ovarian tumor cells [2]. The mechanism of AKT in modulating apoptosis seems to be context-dependent. Further research is required to elucidate the regulation axis from AKT to apoptosis in OEA.

Cisplatin treatment induced AKT activation, but the mechanism remains unclear. A precise balance of kinase and phosphatase regulates the phosphorylation status of AKT. DNA-PK and ATM has been shown to regulate AKT phosphorylation at Ser473 upon DNA damage [3, 4]. Since cisplatin

treatment causes DNA damage, AKT might be phosphorylated by DNA-PK or ATM in this scenario. A newly published article identified two additional phosphorylation sites (S477 and T479) at the extreme C-terminus of AKT1, which promoted phosphorylation of S473 to fully activate AKT. Interestingly, cyclin A2, which phosphorylates S477 and T479, is tightly regulated throughout the cell cycle. As cisplatin causes DNA damage and induces cell cycle arrest, cyclin A2 might accumulate and facilitate AKT phosphorylation [5]. Since the function of PTEN is compromised in this particular mouse model, it might also contribute to accumulation of phosphorylated AKT. Detailed research is needed to test this hypothesis.

OEA accounts for about 10% of ovarian carcinomas while 70-80% of ovarian carcinomas are high-grade serous ovarian cancer (HGS-OvCa). A comprehensive genomic analysis of 489 HGS-OvCa patients showed that 45% of HGS-OvCa patients harbor alterations in the PI3K/RAS pathway [6, 7], which suggests that the AKT pathway might also participate in tumorigenesis and chemotherapy response in HGS-OvCa. However, thorough research is required before we can generalize this knowledge, since OEA and HGS-OvCa have distinct genomic signatures as well. For example, mutations in CTNNB1 gene, which result in dysregulated Wnt signaling pathway, are observed in 16%–38% of OEA, but are not common in HGS-OvCa [8]. A genetically engineered mouse model of HGS-OvCa was recently established with Brca;Tp53;Pten defects that are found in human patients [9].This model could potentially be utilized to study chemoresistance in HGS-OvCa in the future.

Given the importance of the AKT pathway in mediating chemoresistance, over 50 drug candidates targeting the PI3K/AKT/mTOR pathway are under development at various stages. Those candidates include AKT inhibitors, PI3K inhibitors, mTOR inhibitors and pan-PI3K&mTOR inhibitors. Both monotherapies and combination therapies of chemotherapies/targeted therapies are being evaluated in clinical trials [10]. But, several challenges are present in preclinical studies as well as early clinical trials, such as activation of compensatory MAPK pathway and lack of effective patient stratification

strategies [11, 12]. Combination therapies and biomarkers are, at present, among the top research priorities to establish successful treatment strategies.

4.2.2 The TGF-β pathway in chemoradioresistance in GBM

In the third chapter of this thesis, the TGF-β pathway was shown to mediate chemoradioresistance by regulating expression of mesenchymal and stem cell genes. Yet the mechanistic relationship between mesenchymal/stem cells markers, TGF-β signaling and chemoradioresistance still remains to be fully explored.

Mesenchymal cells generally have enhanced migratory capacity, increased ECM elaboration, and elevated resistance to apoptosis [13]. The mesenchymal phenotype has been associated with resistance to targeted therapies and conventional therapies, although the mechanisms are not fully understood. The TGF-β pathway is a master regulator of epithelial to mesenchymal transition (EMT), which might promote mesenchymal phenotypes during development of therapeutic resistance. TGF-β signaling has been shown to regulate stem-like cells in various types of cancer, including breast cancer. Mani *et al.* showed that TGF-β signaling drove the generation of stem-like cells through EMT [14]. Later, it was shown that stem-like cells were enriched after chemotherapy, which was regulated by increased autocrine TGF-β signaling [15]. This data suggests that chemotherapy might be able to activate TGF-β signaling, which leads to mesenchymal transition and generation of stem-like cells. The population with mesenchymal and stem-like phenotype propagates resistance to chemoradiotherapy. In support of this hypothesis, our data has shown that TGF-β signaling regulated mesenchymal/stem cell genes and mediated therapeutic resistance in GBM. However, it is still unclear what mechanism triggers activation of TGF-β signaling.

Meanwhile, a growing body of evidence suggests that the TGF-β pathway regulates the DNA repair pathways, which might mediate chemoradioresistance [16]. ZEB1 and ZEB2 are two EMT master transcription factors that are regulated by the TGF-β pathway. ZEB2 has been shown to affect ATM/ATR functions upon DNA damage [17] while ZEB1 promotes

radioresistance in breast cancer by regulating the stability of CHK1 [18]. SMAD proteins, which are the major downstream signal mediators of TGF-β signaling pathway, form foci at DNA damage sites after exposure to radiation, indicating its direct involvement in DNA damage response [19, 20]. This might be mediated by ATM, and possibly by p53 as well [21, 22]. Inhibition of the TGF-β pathway resulted in decreased number of γH2AX foci, an indicator of DNA double strand break, and increased efficacy of radiation in mice bearing GBM [23]. Further research is required to understand whether chemoradioresistant cells have altered DNA damage capacity and whether it is regulated by the TGF-β pathway in our GBM model.

Overall, the TGF-β pathway is a promising target against chemoradioresistance. Various types of drug candidates against the TGF-β pathway are in different phases of clinical trials [24]. In the case of GBM, an antisense oligo against TGF-β ligand (rabedersen) showed survival benefit in recurrent or refractory high-grade glioma and anaplastic astrocytoma in three Phase I/II studies [25]. Even though controversies exist about the benefits of rabedersen, inhibition of the TGF-β pathway generally shows positive effect in cancer patients [24, 26, 27]. Currently, a small inhibitor against the TGF-β pathway from *Eli Lilly* is being tested in a clinical trial for newly diagnosed GBM patients in combination with standard chemoradiotherapy. This should shed light on the clinical benefits of TGF-β inhibitors in GBM patients in the near future. Additionally, patient stratification based on clinically applicable surrogates should also be taken into account to achieve optimal clinical outcomes. Drug resistance from single targeted therapy might also be an issue, which could be avoided by appropriate combination therapies.

To summarize, this thesis demonstrates that mechanisms of therapeutic resistance can be identified using state-of-the-art imaging and genomic technologies and that this information can be used to reverse resistance-dictating pathways through the appropriate use of targeted agents. The overall methodological approach as well as the specific knowledge related to the involvement of AKT and TGF-β pathways in tumor treatment resistance should be relevant to other types of cancer with similar genetic background as

well.

4.3 Tumor heterogeneity and therapeutic resistance

Recent studies have revealed extensive phenotypic and genetic heterogeneity between and within tumors, which confounds the research of therapeutic resistance. Tumors from different patients exhibit vastly different genetic alterations, pathological characters, and treatment response, which is defined as intertumor heterogeneity. Subpopulations of tumor cells in the same tumor might have distinct genetic and non-genetic profiles. This so-called intratumor heterogeneity might drive the evolution of tumors and emergence of therapeutic resistance [28]. While heterogeneity has great influence on therapeutic response, neither characters of heterogeneity have been fully addressed in previous research. This thesis tackled this problem by utilizing clinically relevant mouse models and systematic genomic analysis, which are discussed in details in the following section.

4.3.1 Intertumor heterogeneity

This thesis attempted to delineate the roles of intertumor heterogeneity in developing therapeutic resistance. In chapter III, we established a highly reproducible pipeline to study mechanisms of therapeutic resistance in GBM. Although we only focused on one patient, this system can be easily scaled up with other GBM patient samples. GBM is classified into four subtypes based on gene expression profiles, including mesenchymal, proneural, classical and neural subtypes [29]. Mesenchymal and proneural subtypes are the most prevalent subtypes in GBM, each of which accounts for 30~35% of the total cases [29, 30]. The proneural subtype often harbors mutations in IDH1 as well as concomitant amplification and overexpression of PDGFRA. The mesenchymal subtype is featured with NF1 mutations compared to other subtypes. In addition, both published data from patient cohorts and our data from animal studies showed that mesenchymal and proneural subtypes have different response to chemoradiotherapy [29]. Taken together, this data strongly suggests that therapeutic response and development of resistance might be driven by distinct molecular events in these two subtypes, which will be investigated in our lab.

The neurospheres used in this thesis were derived from a mesenchymal GBM case characterized by the TCGA. Gene expression analysis of all pre-treatment samples showed enrichment in mesenchymal gene signatures as defined by Verhaak *et al.*. Genetic profiling also revealed key genetic alterations in the mesenchymal subtype, such as NF1 deletion, p53 mutation, and EGFR amplification in all pre-treatment samples. This data shows that all the pre-treatment samples inherited and maintained the mesenchymal signatures present in the parental tumor.

We showed that mesenchymal associated genes were upregulated in recurrent tumors, which seems to be counterintuitive given that the original GBM case belong to the mesenchymal subtype. It might be due to the limitation of the computational classification system. Since the subtype signatures are defined by a computer algorithm, they might not represent the comprehensive gene spectrum of biological processes. Our data showed that the recurrent tumors maintained the key mesenchymal signatures in the pre-treatment tumors while gaining additional alterations in mesenchymal genes.

A recent study showed that transient radiation caused transition from proneural to mesenchymal subtype in a genetically engineered mouse model of GBM [31]. Other studies also showed that mesenchymal transition mediated radioresistance in proneural cancer stem cells [32, 33]. These studies raise an interesting possibility that different GBM subtypes might converge to the mesenchymal phenotype upon acquisition of therapeutic resistance. However, the caveat of these studies is that the transient radiation or *in vitro* system does not mirror the clinical settings. We will investigate this hypothesis with the experimental platform described in Chapter III.

In the next stage of our study, at least three individuals from mesenchymal and proneural subtypes will be used to illustrate the evolution of therapeutic resistance in the two major GBM subtypes.

4.3.2 Intratumor heterogeneity

Phenotypic and genetic heterogeneity exists among the cancer cells within the same tumor, which have been shown to drive therapeutic resistance in multiple types of cancer [34]. Glioma stem-like cells have been found resistant

to radiotherapy or chemotherapy either due to high DNA repair capacity or quiescent status [35, 36]. Single cell sequencing revealed that a subpopulation in primary GBM shared similar transcription profiles with cancer stem-like cells, which indicated that cancer stem-like cells might preexist in GBM prior to the treatment [37].

In this thesis, we showed that the expression of mesenchymal and stem cell genes are upregulated in recurrent tumors, but it remains unclear whether the cells expressing mesenchymal/stem cell genes are resistant to chemoradiotherapy and whether this population exists prior to treatment initiation. In order to address these questions experimentally, we choose THY1 (membrane protein) as a surrogate to isolate potential resistant population. THY1 is among the highest upregulated membrane proteins during EMT and cells with high expression of THY1 presented stem-like properties [38]. We plan to first identify and isolate THY1 positive (THY1+) and THY1 negative (THY1-) cells in both pre-treatment and recurrent tumor cells. Then we will examine the gene expression patterns and therapeutic response of THY1+/THY1- cells both *in vitro* and *in vivo,* which will be compared to pre-treatment and recurrent tumor samples as well. We hypothesize that the THY1+ population would show resistance to TMZ/IR and express high level of mesenchymal and stem cell markers. This hypothesis should potentially enable us to determine the origin of the resistant population as well as identify a new biomarker for treatment response to TMZ/IR.

4.4 Future directions

Therapeutic resistance is still a pervasive barrier in developing successful cancer therapies. This thesis is a pilot to develop a pipeline to optimize therapeutic paradigms in cancer. First, tumor heterogeneity was successfully recapitulated in both ovarian carcinoma and glioblastoma by leveraging the advantages of clinically relevant models. Second, mechanisms of therapeutic resistance were identified by both candidate-driven and discovery-driven research approaches. Third, treatment response was improved by targeting these essential regulatory pathways in therapeutic resistance. This thesis successfully proved the feasibility of this pipeline to develop novel therapeutic

combinations. The following section will focus on potential improvement in the future.

4.4.1 Maximizing the power of mouse models

This thesis dissected the mechanisms of therapeutic resistance in one individual GBM patient and one subtype of ovarian cancer. Given the heterogeneity within each cancer type, it is important to treat each tumor individually based on its own genetic profile. GEMMs and PDX used in this thesis provide the ideal platforms to mirror individual tumor in laboratories for mechanistic research, which bridge the clinical and laboratory demand.

While GEMMs and PDX are great model systems to recapitulate various types of cancer, both of them have some weaknesses. For PDX models, one major concern is the lack of a fully functional immune system. As the immune system plays an important role in therapeutic response, caution needs to be taken when evaluating results from PDX models. However, new methods are emerging to compensate this disadvantage in PDX models. For example, Wege *et al.* co-transplanted human hematopoietic stem cells (HSCs) and human breast cancer cells into neonatal NOD-scid IL2Rγ(null) mice. They observed that a humanized immune system formed in mice while tumor cells grew without evidence of rejection [39]. This study brings the hope of producing humanized PDX models in the future, which will grant high fidelity of recapitulating human cancer in PDX mice.

GEMMs, which have fully functional immune systems, face their own limitations. One drawback is that most of the current GEMMs rely on limited oncogenic alterations, which might not be sufficient to recapitulate the complexity of cancer genomes. CRISPR/Cas-mediated genome engineering provides a straightforward method to generate GEMMs with multiple genetic deletions in a timely manner. This can greatly facilitate future cancer modeling with GEMMs [40].

Besides providing a platform to study mechanisms of therapeutic resistance in individual patients, GEMMs and PDX models can also be utilized to evaluate the efficacy of personalized therapies. The challenge, however, is the duration

of this process. Co-clinical trial is an alternative to speed up the process. In 2011, a proof-of-principle study was carried out using patient derived xenograft models. Tumors from 14 patients with refractory advanced cancers were propagated in immunodeficient mice. 232 treatment regimens with 63 drugs were tested in those PDX mice and effective regimens were identified for 12 patients [41]. Another pilot study proved that GEMMs can be used to predict results of clinical trials as well as provide guidance for revising treatment regimen. In this particular case, the co-clinical trial challenged the patient stratification system based on a single genetic biomarker. It demonstrated that defects in additional tumor suppressors impaired the efficacy of targeted therapy and chemotherapy in GEMMs [42], which might explain the inconsistent response among the patients. It also identified new predictive genetic markers for resistance in patients for future trial designs. Overall, personalized clinical trials in mouse models will greatly improve the efficiency of therapeutic optimization and thus benefit cancer patients.

To summarize, the ideal scenario includes three steps: 1) each individual tumor is mirrored in a pre-clinical mouse model; 2) the drivers of therapeutic resistance are identified as targets for personalized medicine; 3) treatment regimens and schedules are optimized in mice before delivering to patients.

4.4.2 Cocktail therapy for chronic cancer management

This thesis showed that targeting master regulatory pathways of therapeutic resistance improves the efficacy of chemoradiotherapies. However, multiple mechanisms might contribute to chemoradioresistance, as demonstrated in the third chapter of this thesis. Meanwhile, failures of single targeted therapy in clinical trials prove that monotherapy is not sufficient to rescue chemoradioresistant patients. Even when some patients do respond to monotherapy, drug resistant clones quickly arise and contribute to tumor recurrence [43]. Therefore, it is critical to target multiple pathways of resistance simultaneously. This would maximize the cytotoxicity in tumor cells while minimizing the likelihood of emergence of new drug resistance.

In fact, the concept of combination therapy is not new in disease management. For example, HIV used to be a lethal disease due to the development of drug

resistance. Now the standard HIV treatment usually includes two or more drug classes targeting different anti-viral mechanisms, which minimizes the chances of selecting resistant clones and prolongs the time to acquire resistance mutations against multiple drugs. This combination therapy has generated significant clinical impact and turned the fatal disease into a chronic manageable condition [44].

It might not be that far away to bring this hypothesis to cancer clinical practice. First of all, a substantial number of targeted agents against critical therapeutic resistance pathways have already been developed and proven to be safe in patients. Those targeted therapies cover almost all the known mechanisms of therapeutic resistance, including DNA repair pathway, oncogenic pathways, apoptotic pathways, and so on. This provides multifarious possible combinations for each patient. Meanwhile, increasing number of drug candidates against new targets are in active pre-clinical or clinical development [45].

Secondly, it's becoming affordable and non-invasive to acquire whole genomic information from patients with advanced sequencing technology, which enables scientists and clinicians to interpret the comprehensive genomic alterations. This will optimize combination therapeutics in two ways. Firstly, it will allow utilization of one pathway as a biomarker instead of one single gene. Previous targeted therapies have usually relied on alterations of one single gene, which sometimes failed to stratify responders and non-responders. Take the PARP inhibitor trials as an example. PARP inhibitors target the compensatory pathway of BRCA1/2 in the DNA repair, which is predicted to cause cell death in BRCA1/2 deficient cells. However, some ovarian patients without BRCA1/2 mutations also showed response to PARP inhibitors. Genome sequencing and network analysis shows that about 50% patients with high-grade serous ovarian cancer have defects in homologous recombination pathways whereas only about 20% of the patients have defects in BRCA1/2 mutations, which might explain why patients without BRCA1/2 also responded to PARP inhibitors. Secondly, genomic profiling will identify all potential actionable pathways, which will maximize the efficacy of combined

therapy without overlapping or missing any targets. Moreover, liquid biopsies, including circulating tumor cells and circulating tumor DNA, have been shown to mirror genome alterations associated with therapy resistance in advance tumors. This non-invasive approach will generate comprehensive genomic evaluations of naïve patients to design initial treatment strategies, which might prevent occurrence of resistance. Moreover, it enables repeated and real-time analysis of tumor evolution during treatment, which can detect new therapeutic resistant clones and aid modification of treatment strategies to achieve the best outcome [46, 47].

It is very promising to use combination therapies to overcome drug resistance. However, a few issues still need to be addressed. One major challenge is to standardize genome interpretation and make it applicable for clinical practice. Although both patient genome information and drug resistance mechanisms are now available, it is still overwhelming and onerous to design effective combination therapy rationally. One promising solution is to construct computation models that integrate patient information, treatment response and mechanisms of therapeutic resistance, which can be used to predict the optimal treatment regimens for incoming patients. Attempts have been made to use mathematical modeling for drug resistance studies [48]. One recent study established a model with data from 20 patients treated with BRAF inhibitor, which can predict tumor response with genetic information and disease stages (metastasis) [49]. Another study modeled the response of resistant tumors to doxorubicin with experimental mice data, which can predict optimal treatment schedules to prevent tumor progression [50]. These pioneering studies demonstrated the power of computation modeling in therapeutic optimization, which should improve the efficiency of therapy designs in clinical settings.

Another concern of combination therapy is the cumulative toxicity. Although targeted therapies are generally less toxic compared to chemoradiotherapy, clinical trials still reveal some side effects in patients. This problem may become severe when several drugs are used simultaneously. Therefore, special attention is required during new drug development to minimize toxicity.

Economic and regulatory issues might also become obstacles in clinics, which will not be discussed in detail here.

4.4.3 Cancer treatment in the future

Figure 4.1 summarizes an optimized approach for the delivery of cancer treatment: in phase I, mechanistic knowledge of therapeutic resistance will be collected from a heterogeneous patient population. This can be achieved through experimental research as demonstrated in this thesis. In Phase II, patient information (including genetic and clinical information), treatment response phenotypes, and corresponding drug resistance mechanisms will be used to construct a computational model, which can stratify future cancer patients and predict the optimal therapies for each individual.

Figure 4.1

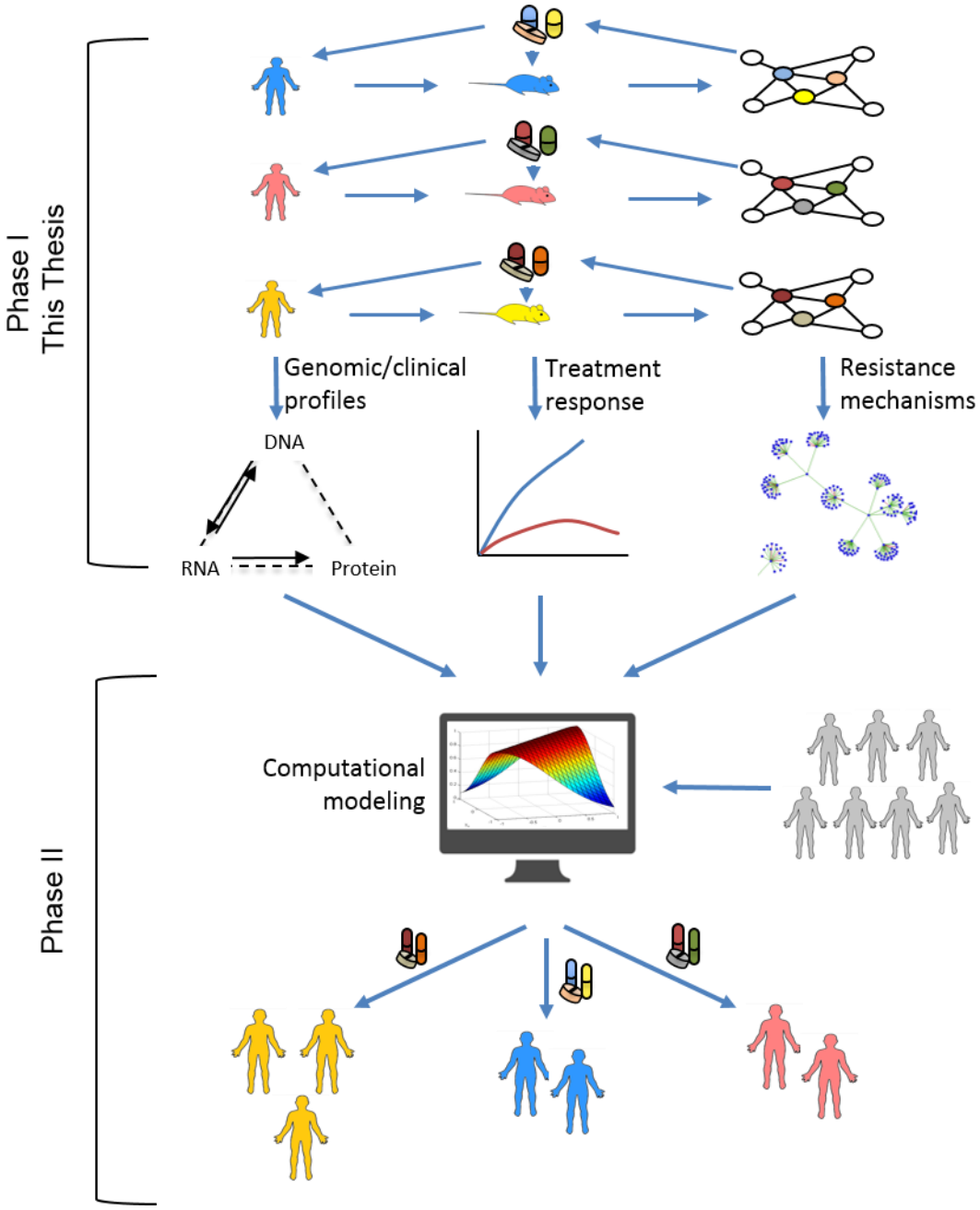

Figure 4.1 Future clinical management of cancer. In phase I, tumors from Individual patient will be mirrored in clinical relevant mouse models. Key regulatory pathways and optimal treatment regimens against therapeutic resistance will be identified through mechanistic studies in mice. In phase II, patient information, including genomic and clinical information, profiles of therapeutic response and key regulatory pathways will be integrated into computational modeling. Incoming patients will be stratified by the computer algorithm and receive optimal personalized medicine.

4.5 References

1. LoPiccolo, J., et al., *Targeting the PI3K/Akt/mTOR pathway: Effective combinations and clinical considerations.* Drug Resistance Updates, 2008. **11**(1-2): p. 32-50.
2. Abedini, M.R., et al., *Akt promotes chemoresistance in human ovarian cancer cells by modulating cisplatin-induced, p53-dependent ubiquitination of FLICE-like inhibitory protein.* Oncogene, 2010. **29**(1): p. 11-25.
3. Bozulic, L., et al., *PKB alpha/Akt1 acts downstream of DNA-PK in the DNA double-strand break response and promotes survival.* Molecular Cell, 2008. **30**(2): p. 203-213.
4. Viniegra, J.G., et al., *Full activation of PKB/Akt in response to insulin or ionizing radiation is mediated through ATM.* Journal of Biological Chemistry, 2005. **280**(6): p. 4029-4036.
5. Liu, P.D., et al., *Cell-cycle-regulated activation of Akt kinase by phosphorylation at its carboxyl terminus.* Nature, 2014. **508**(7497): p. 541-+.
6. McConechy, M.K., et al., *Ovarian and endometrial endometrioid carcinomas have distinct CTNNB1 and PTEN mutation profiles.* Modern Pathology, 2014. **27**(1): p. 128-134.
7. Bell, D., et al., *Integrated genomic analyses of ovarian carcinoma.* Nature, 2011. **474**(7353): p. 609-615.
8. Wu, R., et al., *Mouse model of human ovarian endometrioid adenocarcinoma based on somatic defects in the Wnt/beta-catenin and PI3K/Pten signaling pathways.* Cancer Cell, 2007. **11**(4): p. 321-333.
9. Perets, R., et al., *Transformation of the Fallopian Tube Secretory Epithelium Leads to High-Grade Serous Ovarian Cancer in Brca;Tp53;Pten Models.* Cancer Cell, 2013. **24**(6): p. 751-765.
10. Rodon, J., et al., *Development of PI3K inhibitors: lessons learned from early clinical trials.* Nature Reviews Clinical Oncology, 2013. **10**(3): p. 143-153.
11. Massacesi, C., et al., *Challenges in the clinical development of PI3K inhibitors.* Inositol Phospholipid Signaling in Physiology and Disease, 2013. **1280**: p. 19-23.
12. Shimizu, T., et al., *The Clinical Effect of the Dual-Targeting Strategy Involving PI3K/AKT/mTOR and RAS/MEK/ERK Pathways in Patients with Advanced Cancer.* Clinical Cancer Research, 2012. **18**(8): p. 2316-2325.
13. Kalluri, R. and R.A. Weinberg, *The basics of epithelial-mesenchymal transition.* J Clin Invest, 2009. **119**(6): p. 1420-8.
14. Mani, S.A., et al., *The epithelial-mesenchymal transition generates cells with properties of stem cells.* Cell, 2008. **133**(4): p. 704-715.
15. Bhola, N.E., et al., *TGF-beta inhibition enhances chemotherapy action against triple-negative breast cancer.* J Clin Invest, 2013. **123**(3): p. 1348-58.
16. Barcellos-Hoff, M.H. and F.A. Cucinotta, *New tricks for an old fox: Impact of TGF beta on the DNA damage response and genomic stability.* Science Signaling, 2014. **7**(341).

17. Sayan, A.E., et al., *SIP1 protein protects cells from DNA damage-induced apoptosis and has independent prognostic value in bladder cancer.* Proceedings of the National Academy of Sciences of the United States of America, 2009. **106**(35): p. 14884-14889.
18. Zhang, P., et al., *ATM-mediated stabilization of ZEB1 promotes DNA damage response and radioresistance through CHK1.* Nat Cell Biol, 2014. **16**(9): p. 864-75.
19. Wang, M.L., et al., *Novel Smad proteins localize to IR-induced double-strand breaks: interplay between TGF beta and ATM pathways.* Nucleic Acids Research, 2013. **41**(2): p. 933-942.
20. Shi, X.L., et al., *Study of interaction between Smad7 and DNA by single-molecule force spectroscopy.* Biochemical and Biophysical Research Communications, 2008. **377**(4): p. 1284-1287.
21. Cordenonsi, M., et al., *Links between tumor suppressors: p53 is required for TGF-beta gene responses by cooperating with Smads.* Cell, 2003. **113**(3): p. 301-314.
22. Park, S., et al., *Smad7 enhances ATM activity by facilitating the interaction between ATM and Mre11-Rad50-Nbs1 complex in DNA double-strand break repair.* Cell Mol Life Sci, 2014.
23. Hardee, M.E., et al., *Resistance of Glioblastoma-Initiating Cells to Radiation Mediated by the Tumor Microenvironment Can Be Abolished by Inhibiting Transforming Growth Factor-beta.* Cancer Research, 2012. **72**(16): p. 4119-4129.
24. Akhurst, R.J. and A. Hata, *Targeting the TGFbeta signalling pathway in disease.* Nat Rev Drug Discov, 2012. **11**(10): p. 790-811.
25. Hau, P., et al., *Inhibition of TGF-beta2 with AP 12009 in recurrent malignant gliomas: from preclinical to phase I/II studies.* Oligonucleotides, 2007. **17**(2): p. 201-12.
26. Chamberlain, M.C., *Convection-enhanced delivery of a transforming growth factor-beta2 inhibitor trabedersen for recurrent high-grade gliomas: efficacy real or imagined?, in reference to Bogdahn et al. (Neuro-Oncology 2011;13:132-142).* Neuro Oncol, 2011. **13**(5): p. 558-9; author reply 561-2.
27. Wick, W. and M. Weller, *Trabedersen to target transforming growth factor-beta: when the journey is not the reward, in reference to Bogdahn et al. (Neuro-Oncology 2011;13:132-142).* Neuro Oncol, 2011. **13**(5): p. 559-60; author reply 561-2.
28. Bedard, P.L., et al., *Tumour heterogeneity in the clinic.* Nature, 2013. **501**(7467): p. 355-364.
29. Verhaak, R.G.W., et al., *Integrated Genomic Analysis Identifies Clinically Relevant Subtypes of Glioblastoma Characterized by Abnormalities in PDGFRA, IDH1, EGFR, and NF1.* Cancer Cell, 2010. **17**(1): p. 98-110.
30. Lin, N., et al., *Prevalence and clinicopathologic characteristics of the molecular subtypes in malignant glioma: a multi-institutional analysis of 941 cases.* PLoS One, 2014. **9**(4): p. e94871.
31. Halliday, J., et al., *In vivo radiation response of proneural glioma characterized by protective p53 transcriptional program and proneural-mesenchymal shift.* Proceedings of the National Academy of Sciences of the United States of America, 2014. **111**(14): p. 5248-5253.

32. Bhat, K.P.L., et al., *Mesenchymal Differentiation Mediated by NF-kappa B Promotes Radiation Resistance in Glioblastoma.* Cancer Cell, 2013. **24**(3): p. 331-346.
33. Mao, P., et al., *Mesenchymal glioma stem cells are maintained by activated glycolytic metabolism involving aldehyde dehydrogenase 1A3.* Proceedings of the National Academy of Sciences of the United States of America, 2013. **110**(21): p. 8644-8649.
34. Marusyk, A., V. Almendro, and K. Polyak, *Intra-tumour heterogeneity: a looking glass for cancer?* Nature Reviews Cancer, 2012. **12**(5): p. 323-334.
35. Bao, S.D., et al., *Glioma stem cells promote radioresistance by preferential activation of the DNA damage response.* Nature, 2006. **444**(7120): p. 756-760.
36. Chen, J., et al., *A restricted cell population propagates glioblastoma growth after chemotherapy.* Nature, 2012. **488**(7412): p. 522-6.
37. Patel, A.P., et al., *Single-cell RNA-seq highlights intratumoral heterogeneity in primary glioblastoma.* Science, 2014. **344**(6190): p. 1396-401.
38. Lu, H., et al., *A breast cancer stem cell niche supported by juxtacrine signalling from monocytes and macrophages.* Nat Cell Biol, 2014. **16**(11): p. 1105-17.
39. Wege, A.K., et al., *Humanized tumor mice-A new model to study and manipulate the immune response in advanced cancer therapy.* International Journal of Cancer, 2011. **129**(9): p. 2194-2206.
40. Wang, H.Y., et al., *One-Step Generation of Mice Carrying Mutations in Multiple Genes by CRISPR/Cas-Mediated Genome Engineering.* Cell, 2013. **153**(4): p. 910-918.
41. Hidalgo, M., et al., *A Pilot Clinical Study of Treatment Guided by Personalized Tumorgrafts in Patients with Advanced Cancer.* Molecular Cancer Therapeutics, 2011. **10**(8): p. 1311-1316.
42. Chen, Z., et al., *A murine lung cancer co-clinical trial identifies genetic modifiers of therapeutic response.* Nature, 2012. **483**(7391): p. 613-617.
43. Rudin, C.M., et al., *Brief Report: Treatment of Medulloblastoma with Hedgehog Pathway Inhibitor GDC-0449.* New England Journal of Medicine, 2009. **361**(12): p. 1173-1178.
44. Broder, S., *The development of antiretroviral therapy and its impact on the HIV-1/AIDS pandemic.* Antiviral Res, 2010. **85**(1): p. 1-18.
45. Yap, T.A. and P. Workman, *Exploiting the cancer genome: strategies for the discovery and clinical development of targeted molecular therapeutics.* Annu Rev Pharmacol Toxicol, 2012. **52**: p. 549-73.
46. Murtaza, M., et al., *Non-invasive analysis of acquired resistance to cancer therapy by sequencing of plasma DNA.* Nature, 2013. **497**(7447): p. 108-12.
47. Hodgkinson, C.L., et al., *Tumorigenicity and genetic profiling of circulating tumor cells in small-cell lung cancer.* Nat Med, 2014. **20**(8): p. 897-903.
48. Lavi, O., M.M. Gottesman, and D. Levy, *The dynamics of drug resistance: A mathematical perspective.* Drug Resistance Updates, 2012. **15**(1-2): p. 90-97.

49. Bozic, I., et al., *Evolutionary dynamics of cancer in response to targeted combination therapy.* Elife, 2013. **2**.
50. Hadjiandreou, M.M. and G.D. Mitsis, *Mathematical Modeling of Tumor Growth, Drug-Resistance, Toxicity, and Optimal Therapy Design.* Ieee Transactions on Biomedical Engineering, 2014. **61**(2): p. 415-425.